SARS CORONAVIRUS PATHOGENESIS AND THERAPEUTIC TREATMENT DESIGN

Timothy Patrick Sheahan

A dissertation submitted to the faculty of the University of North Carolina at Chapel Hill in partial fulfillment of the requirements for the degree of Doctor of Philosophy in the Department of Microbiology and Immunology

Chapel Hill

2008

Approved by:

Ralph Baric, Ph.D.

Nancy Davis, Ph.D.

Mark Heise, Ph.D.

Raymond Pickles, Ph.D.

Lishan Su, Ph.D.

ABSTRACT

TIMOTHY P. SHEAHAN: SARS CORONAVIRUS PATHOGENESIS AND THERAPEUTIC TREATMENT DESIGN
(Under the direction of Dr. Ralph S. Baric)

Through the study of the viral pathogenesis, the mechanisms of disease can be elucidated providing specific targets for therapeutic intervention intended to prevent the development of disease. We conducted four studies to gain a better understanding of SARS-CoV disease pathogenesis and therapeutic design. We conducted two studies to investigate SARS-CoV evolution and adaptation to the human host. We have also investigated the importance of the innate immunity in protection from SARS-CoV disease. Lastly, we evaluated the protective efficacy of vaccination in senescent populations.

The prototypic civet SZ16 spike (S) gene was engineered into our epidemic strain infectious clone (icSARS) to create the recombinant icSZ16-S virus. A mutant of icSZ16-S (icSZ16-S K479N) was passaged on human airway epithelial cells (HAE) and resultant "evolved" viruses contained mutations in S that enhanced interactions with the receptor (hACE2) though adaptive mutations differed from those seen during the epidemic. icSARS grew equally well in cells expressing the civet or human receptor while icSZ16-S only grew within civet expressing cells. Dual species tropism is retained by the epidemic strain suggesting it evolved through repeated passage between human and civet hosts.

Mice deficient in MyD88 ($MyD88^{-/-}$), an adapter protein that mediates Toll-like receptor (TLR), IL-1R, and IL-18R signaling, are far more susceptible to mouse adapted SARS-CoV (rMA15) infection. Despite increased viral loads, the expression of multiple proinflammatory cytokines and chemokines within lung tissue was significantly reduced in $MyD88^{-/-}$ mice compared to wild-type mice suggesting that MyD88-mediated innate immune signaling and inflammatory cell recruitment to the lung are required for protection from lethal rMA15 infection.

We have developed a senescent BABL/c mouse model of SARS-CoV pathogenesis where infection with the mouse adapted SARS-CoV bearing a GD03 S glycoprotein (rMA15 GD03-S) mortality in senescent mice. We vaccinated senescent mice with Venezuelan equine encephalitis virus replicon

particles (VRP) expressing Urbani-S, GD03-S, SZ16-S, a pool of all three S expressing VRPs or control VRPs in a prime/boost regimen. After rMA15 GD03-S infection, all mice in the VRP HA and SZ16-S groups died while Urbani-S, GD03-S and Pool-S groups demonstrated 11, 29, 33% survival rates, respectively.

TABLE OF CONTENTS

LIST OF TABLES

Table

LIST OF FIGURES

Figure

Page

CHAPTER I

INTRODUCTION

The Global Disease Burden and Pathogenesis of Respiratory Infections. Fifteen million deaths each year are caused by infectious diseases throughout the globe(139). According to annual statistics published by the World Health Organization (WHO) in 2002, respiratory infections were the leading cause of mortality by infectious disease causing almost 4 million deaths world wide with a disproportionate amount of disease in children and the elderly (Fig. 1) (139, 229). Each year in the United States (U.S), respiratory tract infections cause over 500,000 hospitalizations and 4 million emergency department visits at an estimated combined annual cost of $14.6 billion(93). Viral respiratory tract infections (RTIs) caused by influenza A, respiratory syncytial virus (RSV), parainfluenza virus type 3 (PIV3), human metapneumovirus (hMPV) and human coronaviruses (OC43 and 229E) account for a considerable amount of this disease burden. For example, seasonal influenza is estimated to cause 500,000 deaths globally each year and 90% of influenza related deaths in the U.S. (~36,000/yr) occur in people over the age of 65(138, 202). While seasonal influenza is more damaging to elderly populations, RSV and PIV3 cause a significant amount of disease burden in children in the U.S. each year resulting causing 7 million cumulative cases (RSV 4 million/yr, PIV3 3 million/yr) and almost 140,000 cumulative hospitalizations (RSV = 113,000/yr, PIV = 29,000/yr)(112). In addition to the more common influenza, RSV and PIV RTIs, human coronaviruses cause approximately 10-15% of upper respiratory tract infections and hMPV causes 2-12% of all pediatric lower respiratory tract infections(97). Due to their ease of dispersion by the aerosol route, respiratory viruses can cause both epidemic and pandemic disease in immunologically naïve human populations. One of the most devastating infectious disease pandemics occurred during 1918-1920 when a zoonotic H1N1 influenza virus emerged to infect humans causing 20-50 million deaths world-wide(139). 1918 H1N1 was a newly emerging strain of influenza A and as a result, human populations did not have appropriate immune memory to adequately fight infection. In turn, the emergence of this

extremely virulent and transmissible virus into a immunologically naïve population contributed to the generation of the devastating pandemic. Since the 1918 pandemic occurred in a time when mass transportation and global air travel were not as widespread like they are today, the future emergence of pandemic influenza might have even more disastrous consequences. The SARS-CoV epidemic in 2003 provided us with a current example of the rapidity of the global spread of a novel respiratory virus in immunologically naïve human populations causing over 8000 cases (~10 % mortality rate) in 29 countries in 5 of the 7 continents(139). Moreover, the SARS-CoV epidemic serves as a current model of the rapidity of virus spread facilitated by air travel, mass transit and increased population density of today. Unfortunately, effective and approved vaccines and therapies for humans do not yet exist to prevent SARS-CoV, RSV, PIV and many other respiratory viral diseases. Though there is a vaccine for seasonal influenza, vaccine efficacy in humans varies with age and with antigenic identity between the vaccine and circulating strains(17, 18, 64, 83, 136). Since it is difficult to predict the identity of future emerging respiratory diseases, it is important that new vaccines or therapeutics have broad efficacy. Below, we review current models of SARS-CoV evolution, host range, and pathogenesis. We also review current models of SARS-CoV vaccination and passive immunization therapy focusing on efficacy in the immune senescent, SARS-CoV immunopotentiation, and efficacy against antigenically divergent strains.

Respiratory Virus Disease Pathogenesis. Infectious viral agents cause a wide array of diseases including cancer, destruction of immune system, arthritis and pneumonia(139, 140). Pathogenesis is defined as the factors that contribute to the development of disease. Virulence is defined by the capacity of a pathogen to produce disease where increasing virulence is most often results in increasing disease pathogenesis. The clinical presentation of viral disease is oftentimes the result of an unintended collaboration of direct viral effects on cell viability and function and host mediated immune pathogenesis where immune responses intended to eradicate invading pathogens also cause direct damage to the host. For example, the unchecked growth of pandemic influenza 1918 H1N1 in the lungs of immunologically naïve human population is thought to have instigated a massively dysregulated innate and adaptive immune response synergistically producing deadly disease(99). Through the study of the viral pathogenesis, the mechanisms of disease can be elucidated providing specific targets for therapeutic intervention intended to prevent the development of disease. Many successful therapies have been developed from knowledge of

viral pathogenesis like oseltimavir for influenza and the many antiretrovirals for HIV underscoring the importance and potential utility of viral pathogenesis research(117, 139).

A multitude of diseases can result from virus infection of the respiratory tract and the disease presentation of the infection can vary depending on the location of the infection. For example, infection of the upper respiratory tract (URT) with rhinovirus, human coronavirus 229E or OC43 produces common cold symptoms (nasal congestion, sneezing, pharyngitis, rhinorrhoea etc.) with more severe disease associated with high fever seen in children(97). In contrast, infection of the lower respiratory tract (LRT) with RSV, hMPV or influenza can cause bronchiolitis or pneumonia characterized by mild hypoxia (depressed blood oxygen saturation), tachypnea (increased respiratory rate), non-productive cough, and wheezing(97). In studies of community acquired pneumonia (pneumonia acquired outside of the hospital setting), virus infection was detected in 10-46% of cases and influenza A was the most commonly identified (4-19% of viruses detected)(54). Abnormalities in lung function and bilateral lung infiltrates visible on chest radiography are hallmarks of both viral pneumonia and conditions of more severe respiratory distress like acute lung injury (ALI) and acute respiratory distress syndrome (ARDS)(13, 97). In both pneumonia and ALI/ARDS, lung function is compromised by the inflammatory response which disrupts the alveolar-capillary units responsible for gas exchange(33, 97). Histopathologically, ALI is characterized by the formation of hyaline membranes, the loss of alveolar integrity resulting in their flooding with protein rich edema fluid, deactivation of surfactant by serum proteins and infiltration of alveolar space by inflammatory cells (macrophages, and neutrophils)(33). The degree of lung dysfunction and resultant depression in blood oxygen saturation allows for the differentiation between pneumonia (mild hypoxia), ALI (severe hypoxia) and ARDS (most severe hypoxia) where ALI/ARDS often requires mechanical ventilation and supplemental oxygen(33, 54, 97). Unfortunately, the exact mechanisms underlying the development of ARDS have not yet been elucidated(13). For the resolution of ALI, lung inflammation subsides while alveolar integrity is repaired, transcapillary water transport commences to remove fluid from the airway, and surfactant function is restored(33). In some cases, resolution of ALI is incomplete and inflammation continues, pulmonary edema is unresolved and alveolar fibrosis ensues causing permanent abnormalities in lung function and a reduction in the quality of life(33).

Coronavirus as Emerging Infectious Diseases. Zoonoses are defined as diseases that are transmitted from domestic or wild animals to humans(236). Many diseases of great human historical significance in the ancient and recent past like plague, smallpox, HIV, and influenza A emerged from wild or domestic animal populations to cause devastating human disease(4, 123, 143, 150, 209, 230, 236). In 2002, a novel coronavirus (SARS-CoV) emerged suddenly as the causative agent of Severe and Acute Respiratory Syndrome (SARS) and spread worldwide causing about 8000 cases and >700 deaths(29, 103, 173). Coronavirus belong to the order *Nidovirales* and within the past four years, newly emerging viruses of human relevance have been identified within several genogroups of the coronavirus family. The newly identified NL63 and HKU1 (genogroup I) and SARS-CoV (genogroup II) are newly emerging or newly recognized coronavirus that cause respiratory disease in humans with SARS being the most pathogenic of any known human coronavirus (Figure 2, Table 1) (48, 103, 173, 213, 233, 235). Coronavirus genogroups 1, 2 and 3 also contain viruses that cause disease in animals of economic and agricultural importance like avian infectious bronchitis virus (IBV, group 3), transmissible gastroenteritis virus (TGEV, group 1) and porcine epidemic diarrheal virus (PEDV, group 1) and bovine coronavirus (BCoV, group 2b) (Figure 2) (188). The ubiquity and diversity of coronavirus in nature coupled with innate virological factors such as a promiscuous RNA polymerase and high recombination rates make the generation of diverse and new coronavirus a reality(42, 161, 162, 248). In fact, human coronavirus OC43 (HCoV-OC43) provides us with an additional example to SARS-CoV where a zoonotic pathogen evolved to infect and cause disease in humans. Using a molecular clock approach, Vijgen et. al. suggest that BCov crossed the species barrier and evolved to infect humans in the late 1800s creating HCoV-OC43 (Table 1)(219). BCoV has also jumped into other ruminant species where a newly recognized water buffalo associated coronavirus (BuCoV) is thought to have emerged from BCoV (Table 1)(39). There is also evidence of the emergence of new coronavirus diseases resulting from evolution within the current natural host. For example, porcine respiratory virus (PRCV) causes respiratory disease in pigs and is thought to have evolved from a virus that causes gastroenteritis (TGEV) in the same host (Table 1)(216). Similarly, the gastroenteritis causing BCoV is thought to have mutated to become respiratory bovine coronavirus (RBCV) the causative agent of bovine shipping fever (Table 1)(74, 193). Up to and including the present time, we have been consistently provided with examples of newly emerging or recognized coronavirus and their associated diseases. Given

the trends of coronavirus emergence in the past, novel coronavirus emergence and/or discovery of novel coronavirus will most likely continue in the future.

Within live animal markets in China, a wide range of common and exotic food animals like bats and civets are sold live or as fresh meat for human consumption in part to improve health and sexual performance (28, 69, 236, 238). In Southern China, the consumption of exotic animals is especially prevalent during the winter months when most respiratory tract infections are highly prevalent(236). Since many zoonotic viral pathogens are shed in stool, densely housed birds and mammals shedding excreta in the wet marketplace creates an atmosphere for zoonotic virus transmission to human consumer populations(236). Most recently, wet markets in Southeast Asian have been associated with cultivating the cross species transmission of avian influenza H5N1 and the newly emerged SARS-CoV(69, 108, 236). Viruses similar to the epidemic strain were isolated from civets for sale within wet markets in China during the epidemic in 2003 and the reemergence of 2004(28, 69). Genome sequences of viruses isolated from bats, civets and humans suggest that viruses circulating in bats crossed the species barrier to infect civets who then served as an amplification host for yet another host range shift generating a human tropic virus(28, 69, 108, 122). In 2007, surveys of wild Asian leopard cats and Chinese ferret badgers revealed the presence of yet more novel and highly divergent coronavirus circulating in animals typically sold in wet markets in China(44). Since viruses similar to the epidemic strain of SARS-CoV are currently circulating in zoonotic pools, the future emergence of a SARS-CoV like virus may occur in the future. Therefore, it is imperative that we understand the pathogenic mechanisms of coronavirus lung diseases and that current vaccination and passive sero therapies be effective in protecting humans from infection by zoonotic SARS-CoV. Unfortunately, bat-SARS-CoV and the prototypic civet SARS-CoV strain, SZ16, have not yet been cultured *in vitro* hampering our ability to evaluate their epidemic potential and pathogenesis and their susceptibility to current therapeutic interventions.

SARS-CoV Virion and Genome Organization. Viruses within the family *Coronaviridae* have the largest RNA genomes of any virus known today(51). SARS-CoV is an enveloped RNA virus with a 29,727 base pair message sense RNA genome that is tightly associated with the viral nucleocapsid protein(103, 173). The SARS-CoV genome is organized in the classic coronavirus gene order of replicase, spike (S), envelope (E), membrane (M), and nucleocapsid (N) (listed in the 5' to 3' order) (Figure 3)(173).

Like other coronavirus, SARS-CoV has several virus specific open reading frames (ORFs) interspersed between the structural proteins in the 3' end of the genome (Figure 3)(173). The genomic RNA/nucleocapsid complex is contained within the viral envelope acquired by budding into the endoplasmic reticulum/golgi intermediate compartment (ERGIC)(35). At least five SARS-CoV structural proteins (S, E, M, 3a and 7a) are contained within the lipid belayed of the viral envelope (Figure 3)(154, 173, 181). When viewed by electron microscopy, the SARS-CoV virion is pleomorphic in shape with the club like protrusions of the spike protein emanating from the envelope giving the virion the classic crown appearance that contributed to the naming of the virus family (corona = latin for "crown")(103).

SARS Spike Glycoprotein as Critical Component of Species Specificity, Pathogenesis and Protective Immunity. Like gp160 of HIV, hemagglutinin of influenza, and glycoprotein of Ebola virus, the spike (S) glycoprotein protein of coronavirus is a class I viral fusion protein that mediates virus binding and fusion allowing the virus to enter the host cell(240). Like other class I fusion proteins, the SARS S glycoprotein contains two functional domains, S1 and S2, joined by a protease cleavage site(240). The S1 domain (17-756aa) contains the receptor binding domain (RBD) (318-510aa) while the S2 region (757-1225aa) contains the two heptad repeat (HR) regions that facilitate viral fusion and a transmembrane domain (1189-1227aa) that anchors spike to the viral envelope(Figure 4)(239). SARS-CoV is thought to gain entry into cells by the following sequence of events: binding to the cellular receptor ACE2, entry into the cell by endocytosis, and cleavage of the SARS-CoV S by cellular protease cathepsin-L causing a rearrangement of S1 and S2 subunits instigating viral and host membrane fusion depositing the viral genome/nucleocapsid complex into the cytoplasm where replication ensues (Figure 5C) (118, 120, 121, 184).

The coronavirus S glycoprotein is a critical component of species specificity which is also primary determinant of pathogenesis since a virus incapable of infection will most likely not cause disease (Figure 5A). Using reverse genetics, the substitution of the mouse hepatitis virus (MHV) S protein with the feline infectious peritonitis virus (FIPV) S protein alone was sufficient for the murine tropic virus to infect feline cells(107). In less extreme examples, host range of coronavirus can be modulated by few point mutations within the S glycoprotein which either focus within the RBD or in the fusogenic domain(34, 121, 137).

Though previous coronavirus dogma suggests that host range expansion is mediated by S1 region mutation, McRoy et al recently reported host range expansion of MHV can also be mediated by amino acid changes in the S2 region fusion machinery(137). A prime and pertinent example of a coronavirus host range shift due to mutations in the S1 region was seen during the evolution of the SARS-CoV epidemic strain, SARS Urbani. The SARS-CoV spike gene (S) sequences isolated from human cases during the early phase of the epidemic in 2002-2003 and during the reemergence of 2003-2004 are very similar to the SZ16 strain (Figure 6) (28, 69, 94). SZ16 was isolated from palm civets in live animal markets within the Guangdong region of China during the epidemic and its S protein differs from the epidemic strain, SARS Urbani, in 18 amino acids 16 of which reside in the S1 domain containing the RBD (Figure 6)(69). The crystal structure of the SARS-CoV RBD bound to the receptor ACE2 and biochemical experimentation have demonstrated critical amino acids (K479, T487) in the RBD of the civet SZ16 S inhibited its binding to the human ACE2 receptor (hACE2) thus providing a block in host range expansion and human pathogenesis (Figure 6) (119, 121). Using retrovirus pseudotyped with mutant or wild type versions of the zoonotic (SZ16) or epidemic strain (Urbani) S glycoprotein, Li et. al. demonstrated that K479 and T487 were critical residues inhibiting the binding of the civet spike to the human ACE2 receptor(122). Unfortunately, the pseudotype system is able to assess the efficiency of binding and entry but not virus growth kinetics. Using recombinant SARS-CoV bearing various zoonotic, intermediate and epidemic S glycoproteins in single step growth curve, data regarding binding, entry and growth can be elucidated (Figure 5B). Moreover, infection of cells expressing the civet (cACE2) or human versions (hACE2) of the SARS-CoV receptor with recombinant SARS-CoV S glycoprotein variants allows for the investigation of growth fitness and receptor usage in both the amplification and epidemic host. By assessing SARS S glycoprotein variant growth in cACE2 or hACE2 cell cultures, we deduced that the epidemic strain had retained growth fitness in cACE2 and hACE2 expressing cell cultures.

These data suggest that the epidemic strain evolved through repeated transmission from civet to human or human to civet. An alternative hypothesis is that civets repeatedly transmitted SARS-CoV like viruses to humans but virus, host and environmental conditions were not ripe for human to human spread. But at some point in time, a single introduction of a civet virus variant into the human population resulted in virus spread and evolution in humans while coincidently retaining growth fitness in the civet host.

Though it is difficult to prove that either one of these SARS-CoV evolutionary hypotheses is correct, both are supported by serological data of wet market workers, hospital workers and healthy clinic volunteers where SARS specific IgG was detected in 13%, 2.9% and 1.2%, respectively(2). It is important to note that the wet market workers, hospital workers and healthy volunteers that tested positive for SARS IgG did not present with SARS-CoV symptoms and if these populations are representative of the population in Guangdong (est. population 100 million), there were more than a million SARS-CoV cases in China that were not reported(2). Nevertheless, the molecular epidemiology, biochemical and serological data suggest that within wet markets in China, the interaction of infected civets and workers within the market ultimately gave rise to a SARS-CoV that could spread between humans thus beginning the early phases of the epidemic(2, 28, 119). Moreover, clinical and virological data isolated throughout the early, middle and late phases of the epidemic suggest that as the S glycoprotein adapted to the human host, the pathogenicity of the virus in humans increased (Figure 5)(2, 28, 69, 94, 121). Also, much of the variation seen in the S glycoprotein occurs within or in close proximity to the three known neutralizing epitopes suggesting that the adaptive immune response in humans played a role in driving SARS-CoV S evolution (Figure X)(171). These data suggest that virus host expansion, degree of pathogenicity and antigenicity/protective immunity can in part be mediated by the coronavirus S glycoprotein.

The SARS-CoV Receptor, Angiotensin I Converting Enzyme 2 (ACE2), in Virus Entry and Pathogenesis. Virus entry into a cell through the interactions between viral attachment proteins, cellular receptors and/or co-receptors is required for successful virus infection. Cellular proteins required for virus binding, entry, replication, assembly and egress oftentimes have diverse cellular functions as well(22, 80). The cellular receptor for SARS-CoV infection, angiotensin I converting enzyme 2 (ACE2), serves as a prime example of a cellular protein strictly required for the virus to gain entry into the host cell while also serving an important function in host physiology and perhaps viral pathogenesis and disease.

ACE2 and angiotensin I converting enzyme (ACE) are key regulators of the rennin-angiotensin system (RAS), which helps control cardiovascular function by maintaining the body's blood pressure and electrolyte balance(105, 145). ACE and ACE2 are metalloproteases with differing vasoactive peptide substrate specificities and as a result have disparate and antagonistic roles in maintaining physiologic homeostasis (Figure 7A)(105). ACE cleaves the peptide ANG I into ANG II which has vasoconstrictive

effects inducing hypertension while also inducing cell proliferation and fibrosis(105, 210). In contrast, ACE2 processes ANG I into ANG 1-9 and further processes ANG II into the peptide ANG 1-7 which acts as a vasodilator while also being anti-proliferative and apoptotic(47, 105, 203, 218). Current in vitro data suggests that ANG II ligation and signaling through angiotensin receptor 1a (AT1aR) can result in the production of proimflammatory cytokines (TNFα, IL-1β, IL-6, MCP-1 etc.), fibrosis, and cell proliferation(135). In vivo models of liver fibrosis or ALI support the above in vitro data suggesting that ANG II exacerbates pathology and this pathology is ameliorated by ACE2 related signals. In an acid aspiration model of ALI/ARDS, Imai et. al. demonstrated that ACE2 protected mice from injury while ACE, ANG II and AT1aR promoted disease pathology(89). Similarly, Herath et. al, demonstrated that ACE2 and ANG 1-7 counteracted the detrimental effects of ANG II in liver disease in rats(81). These data suggest a duality of RAS contributing to both homeostasis and immumopathology.

Within a year of discovering SARS-CoV, ACE2 was identified as the chief virus receptor utilized to gain entry into the host cell though other attachment factors have also been proposed(90, 120). A second human coronavirus, NL63, also uses ACE2 as a receptor for docking and entry(161). Isolation and expression of ACE2 molecules from various species such as mouse, civet and human in vitro have also helped elucidate important facets of epidemic and zoonotic SARS-CoV S and ACE2 interactions, virus host range expansion and the evolution of the epidemic strain(121). Perhaps the most interesting facet to the SARS-CoV and ACE2 relationship resides in the effect of virus infection on the local pulmonary disruption of RAS homeostasis. Within a mouse model of acute lung injury (ALI), Kuba et al demonstrated that SARS-CoV infection or the administration of SARS S alone depressed levels of ACE2 within the lung(104). Furthermore, the administration of SARS S recombinant protein exacerbated ALI induced by acid aspiration(104). It was proposed that SARS-CoV or SARS S decreased levels of ACE2 within the lung thereby removing a key regulator and processor of the proinflammatory ANG II peptide whose excess contributed to more severe disease (Figure 7B) (104). These data provide an interesting insight into possible RAS involvement in SARS-CoV pathogenesis and the progression of ALI to acute respiratory distress syndrome (ARDS) seen in more severe cases of SARS-CoV.

Transmission, Clinical Course and Immune Response to SARS-CoV Infection of Humans. The intrinsic transmissibility of an infectious agent in a susceptible population can be mathematically

defined as R_0 which represents the average number of new infections caused by an index case during their entire infectious period(45, 56). If R_0 is greater than 1, an infectious outbreak has the potential to establish an epidemic unless public health interventions are instituted that diminish R_0(45, 56). The estimates of R_0 during the global epidemic (R_0 = 0.77-7.7) of SARS-CoV vary widely over time since public health interventions were absent during the beginning of the epidemic and applied with success as the epidemic slowed(45, 127, 221). As compared to other highly infectious respiratory disease like measles (R_0 = 7-45) and pandemic Influenza (1978 H1N1 R_0 < 21), SARS-CoV is considered moderately transmissible(45, 56). SARS-CoV is thought to be transmitted by direct patient contact, airborne droplet nuclei, contact with fomites or urine/fecal contact with mucous membranes(152, 153). The time between exposure and onset of symptoms is approximately 6 days after which patients enter the acute febrile phase of SARS-CoV infection. The hallmark of the acute phase of infection is fever (>100 F°) coupled with chills, malaise and myalgia(19, 124, 152). During the acute phase of the infection patients develop a non-productive cough/shortness of breath (dyspnea) and bilateral pulmonary infiltrates are seen by chest radiography. Pulmonary lesions visible by radiography continue to worsen until 7 days after the onset of symptoms (AOS) after which most patients begin to improve. Approximately 30% of patients show clinical improvement after the first week of illness while the remaining 70% present with recurring fever and shortness of breath(152, 153). A case study of health care workers in Toronto (N = 14, age mean = 42yrs, age range 27-63yrs) provides a typical example of the course of SARS-CoV convalescence where a week after hospital discharge, all patients complained of dyspnea, weakness, lethargy and all suffered from significant weight loss (anorexia) from SARS-CoV disease(11). Three weeks after discharge, the Toronto healthcare worker cohort were no longer weak and continued to gain weight but still suffered from dyspnea (14/14 patients) and a few still presented with an abnormal chest x-ray (5/14 patients)(11). A case study in Hong Kong provides a detailed example of a non-convalescent cohort where lung damage continues to progress in a minority (20-30%) of patients where “diffuse ground glass” changes are seen in the chest X-ray typical of acute lung injury (ALI) and acute respiratory distress syndrome (ARDS) (152). ALI can progress to ARDS, which is characterized primarily by an acute onset, bilateral infiltrates on chest radiograph, hypoxemia, fever and leukopenia(13). Approximately 20% of SARS patients required intensive care unit (ICU) treatment due to ARDS symptoms and a majority of those admitted to the ICU

require mechanical ventilation and oxygen support(19, 152). Though overall mortality rates of the global SARS-CoV epidemic approached 8%, the mortality rates for patients over the age of 65 ranged from approximately 25-55% as a result of comorbidities and immune senescence(19, 116, 124, 152).

Chest x-ray, serology and virological data suggest direct involvement of the adaptive immune response in viral clearance. A detailed virological/immunological longitudinal analysis was performed on a cohort of SARS patients in Hong Kong(152). Five days AOS, nasopharyngeal aspirates contained between 3 and 7 $\log_{10}$ genomes/ml of SARS-CoV and by day 10 the range tightened to 5-7 $\log_{10}$ genomes/ml. In most patients SARS-CoV specific IgG seroconversion begins near day 10 AOS (mean = 20 days AOS) after which virus titers begin to fall. Interestingly, 40% of the cohort (n=75) did not seroconvert until 24 days AOS but 93% had serconverted by day 29 AOS. Even after seroconversion viral genomes were detected in nasopharyngeal aspirate (47%), stool (67%) and urine (21%) as far as 21 days AOS. Of note, many patients in the Hong Kong cohort were treated with corticosteroids and these drugs may have delayed the onset of seroconversion. In an animal model of coronavirus lung infection (PRCV) with similar pathologies to SARS-CoV, the administration of corticosteroids alleviated signs of PRCV pneumonia early (2 dpi) though exacerbated later stages of disease (4, 10, 21 dpi) probably due to the lack of a cell mediated response that created an environment for extended virus lung replication(92). In another Hong Kong SARS cohort, seroconversion was detected as early as 4 days AOS with a median seroconversion occurring at 15 days AOS(113). Nevertheless, these data suggest that as the adaptive immune response mounts, viral load is depressed paving the way for convalescence.

The primary target organs and cells of SARS-CoV infection of humans remains controversial. Several thorough pathological studies of post mortem tissues from SARS-CoV infection have identified the ciliated epithelial cells within the lung as the primary target of virus infection though virus antigen has also been found in macrophages (Mø), dendritic cells (DCs), T cells, B cells, NK cells, and putative lung stem/progenitor CD34+Oct-4+ cells (26, 68, 88, 144, 206, 245). Unfortunately, the in situ hybridization utilized in these pathological studies was unable to differentiate between active viral infection and uptake of virus by passive cellular means like phagocytosis. Several in vitro studies have demonstrated that human Mø and DCs were unable to support active virus replication in vitro and instead instigated cell activation leading to upregulation of MHC II and secretion of inflammatory cytokines(27, 111, 207). In

support of gross lung pathology seen by x-ray, microscopic evaluation of SARS-CoV lung pathology has repeatedly been described in various cohorts as showing various phases of exudative and proliferative acute lung injury (ALI)(68, 88, 144, 206). Typical SARS-CoV lung pathology is characterized by inflammatory cell infiltration, pulmonary edema, hyaline membrane formation, mild to moderate fibrosis, alveolar epithelial hyperplasia, and alveolar/epithelial cell desquamination (i.e. sloughing)(68, 88, 206).

The Role of the Innate Immune Response in the Pathogenesis of SARS-CoV infection of Humans, Non-Human Primates and Rodents. The innate immune response is thought to provide the first line of host defense against invading pathogens. Specialized membrane bound or cytosolic pathogen recognition receptors (PRRs) such as Toll-Like Receptors (TLRs), RIG-I/Mda5, and Nod-like receptors (NLRs) sense pathogen-associated molecular patterns (PAMPs) and initialize the innate immune inflammatory response by activating the transcription of various proinflammatory genes (Figure 8)(147, 175). These PRRs are very specific in their pathogen component recognition (e.g. double stranded RNA, CpG DNA, LPS etc.) and the type of immune response generated as a result of activation(147, 175). TLRs, NODs, RIG-I and Mda5 have been shown to be expressed within lung epithelial cells as well as in the more "professional" environmental sensing cells like conventional/plasmacytoid dendritic cells (cDCs/pDCs) and macrophages (Mø)(25, 96, 134, 211).

Important insights into the mechanisms of the innate inflammatory response of SARS-CoV infection has been gleaned from several clinical, in vitro and in vivo animal model studies yet a clear and concise model of this innate response and its relation to viral pathogenesis remains to be elucidated. Inconsistencies in experimental protocol, clinical treatment, cell type infected in vitro, and possible species specific effects within various animal models have created a confusing and complicated body of data making the generation of a comprehensive model of SARS-CoV pathogenesis difficult. Nevertheless, concordant data between experimental systems has provided the coronavirus field with a great body of useful information and those data are summarized below.

A thorough evaluation of inflammatory gene expression in SARS-CoV patient peripheral blood mononuclear cell (PBMC) was performed by both Cameron et al and Regunathan et al. but described disparate conclusions. Cameron et al concluded that a robust type I INF response was observed early in the progression of disease and was predicted to be essential for viral clearance and convalescence(21). In

addition to a strong INF response, genes typically induced by INF like CCL2 (MCP-1) and CXCL10 (IP-10) were also upregulated in patients at early times during SARS-CoV disease(21). Interestingly, Cameron and collaborators present data that suggests that the cytokine storm that serves to protect convalescent SARS-CoV patients can progress in an unchecked manner in severe cases contributing more severe disease and to the development of an inadequate adaptive immune response(21). Reghunathan and collaborators also sampled SARS patient PBMCs for microarray analysis but did not find type I INF induced in their samples and instead found upregulation of several other tissue inflammation/remodeling, homeostasis and cell cycle genes(166). Compounding the fact that Reghunathan did not discuss virological data and failed to mention when over the course of SARS-CoV disease these samples were extracted, the sample size (n = 10) was small in comparison to the Cameron et al cohort (n = 50)(21, 166). Of note, many cohorts of SARS patients, including the Cameron cohort discussed above, were treated with immunosuppressive corticosteroids making the resulting immunological and virological data more difficult to interpret and evaluate(192).

Since human clinical SARS data is complicated by host genetic variation, disease exacerbating comorbidities, age variation, and variable drug treatment regimens, animal models provide a more homogenous and controlled environment within which to ask questions related to the involvement of the host innate response to SARS-CoV infection. In non-human primate (NHP, cynmolgous macaque) infection with SARS-CoV, Haagmans et al demonstrated the prophylactic administration of pegylated INFα controlled virus replication and lessened disease pathology(70). Concordantly, transcriptional profiles of NHP infected lung tissue suggest that INFα, β, λ, γ and also IP-10, MCP-1, IL-6 and IL-8 genes were all upregulated in SARS-CoV infected NHPs(36). Since NHPs do not succumb to infection, it is proposed that the inflammatory response to virus infection described above aids in the control and clearance of this acute infection.

The development of mouse models that recapitulate components of human disease have been invaluable in viral pathogenesis research. BALB/c and C57BL/6 strains of mice support virus SARS-CoV replication in the lung and experience lung pathologies similar to those seen in human cases of SARS(169, 172). Glass et al demonstrated SARS-CoV was cleared with similar kinetics in WT C57BL/6 mice or strains that lacked that T, B and NK cells suggesting that the innate immune response alone is sufficient for

viral clearance(62). Like gene expression data from human samples, MCP-1, MIP1-α, and IP-10 are all upregulated in the lung during SARS-CoV infection of C57BL/6 mice suggesting a role for these chemokines in protection(62). In support of Glass et al, Hogan et al demonstrated that STAT1, a key modulator INF α/β, λ, γ signaling, was required for the resolution of SARS infection, once again implicating the importance of the innate response in the clearance of SARS-CoV(84). The induction of INF in mice seems to be dependent on mouse strain where BALB/c mice induce type I INF following SARS-CoV infection as measured by microarray (Rockx et al manuscript in preparation) and ELISA while the induction of INF is undetectable in C57BL/6 mice(Sheahan et al published data)(168). These immunologic and pathologic discrepancies between mouse strains are unfortunate caveats of animal models of viral disease. Moreover, no animal model of SARS-CoV pathogenesis to date has fully recapitulated both the acute and extended immunopathological aspects SARS-CoV disease. Nevertheless, mouse models of SARS-CoV pathogenesis faithfully recapitulate many aspects of acute human disease like virus replication, the induction of inflammatory cytokines, migration of immune cells into pulmonary tissues, virus and immune cell mediated lung pathology, and weight loss. Also, unlike human and NHP in vivo models, transgenic "knock out" mice provide the opportunity to evaluate the role of single genes in viral pathogenesis.

Perhaps the most simplified models within which to study SARS-CoV pathogenesis are in vitro models. Though in vitro models are less complicated than in vivo models, the resultant data and relevance to SARS-CoV pathogenesis is hotly debated. There is a seeming incongruity between in vivo human, primate and mouse data where the induction of INF is observed while the in vitro infection of various primary or immortalized interferon competent cell types fail to induce or produce INF. These in vitro experiments are further complicated by the notion that several viral genes have been implicated as active INF antagonists(57, 100, 257). The in vitro data regarding SARS-CoV innate immune activation is reviewed below.

The infection of interferon competent primary human airway epithelial cells (HAE) with SARS-CoV does not result in the induction or secretion of INF but does result in the secretion of inflammatory chemokines IL-6, MCP-1 and IP-10 (Sims unpublished data)(57). Pathological evaluation of lung tissue from lethal SARS-CoV and in vitro data suggests that airway epithelial cells are the primary target for

SARS-CoV infection yet do not induce INF in vitro(185, 206, 245). In NHP studies by Haagmans and colleagues, it was demonstrated that epithelial cells adjacent to infected epithelial cells stained positive for INFβ suggesting a possible bystander activation effect. It may be that viral INF antagonists suppress the antiviral sensing network in the infected cell but eventually neighboring cells are activated through the sensing of viral proteins or genomic RNA released into the extracellular milleu as a result of viral induced cell lysis.

Several studies focusing on infection of professional antigen presenting cells like dendritic cells and macrophages have also produced controversial data. Most studies utilize human PBMC derived macrophages or DCs where CD14+ cells are isolated and differentiated in the presence of cytokines (Mø = GM-CSF, DC = IL-4, GM-CSF) in vitro after which the cell populations resemble "macrophages" and "dendritic cells" by cell surface staining profiles(27, 57, 111). When SARS-CoV is added to these Mø and DC populations, a productive infection does not ensue, INF is not induced but several other inflammatory cytokines are induced and secreted (MIP1-α, IP-10, MCP-1)(27, 57, 111). A possible explanation for the disparity between the in vitro and in vivo data regarding INF induction in SARS-CoV infection is presented by Cervantes-Barragan and colleagues where they show key differences in conventional (cDC) and plasmacytoid dendritic cell (pDC) populations in response to SARS-CoV infection(25). pDCs differ from cDCs in their surface characteristics (cDC = CD11c+, B220-, pDC = B220+, CD11c-low, PDCA-1+) and function where pDCs are the major source of INFα in both humans and mice(10, 23, 25, 183). Unlike most investigators who artificially differentiate Mø and DC from CD14+ precursor cells isolated from PBMCs, Cervantes-Barragan and colleagues isolated cDC and pDC populations directly from human blood and were subsequently incubated with SARS-CoV and demonstrated that unlike cDC, pDC induced INFβ transcription and produced large amounts of INFα protein in the cell media(25). In the assessment of both pDC and cDC populations side by side, Cervantes-Barragan provide a possible explanation as to why previous studies of SARS-CoV infection of dendritic cells failed to induce INF especially since the differentiation protocol used by Law, Tseng, and Cheung result in the differentiation of a more cDC like cell(25, 27, 111, 207). Cervantes-Barragan also utilized in vitro differentiated mouse cDC and pDC that were used in mouse hepatitis virus experiments (MHV). Interestingly, the cytokine used by Cervantes-Barragan to generate cDC (GM-CSF only) from CD14+ cells was used by other investigators to create Mø

though the generation of the pDC using Flt3-L was not employed by either Law, Tseng or Cheung(25, 27, 111, 207). Though the work of Cervantes-Barragan helps clarify some of the discrepancies seen in studies the innate immune response to SARS-CoV, the body of work is deficient in demonstrating the generation of infectious virus through infection of cDC's or suggesting a mechanism of SARS-CoV binding and entry since ACE2 expression in cDC's was not addressed(25, 27, 111, 207). Nevertheless, it will be interesting to see if future mouse/NHP studies definitively demonstrate a role for pDC's in SARS-CoV pathogenesis.

The Effects of Immunosenescence in Innate and Acquired Immunity. The general deterioration of the immune system regarded as "immunosenescence" is found in both short and long lived species and this phenomena occurs as a function of age relative to life expectancy rather than chronological time(61). Describing the complex process of immunosenescence as a simple deterioration is not completely accurate as certain processes decline, others remain static and some are even enhanced with age(55, 61). Though the memory immune response may be unperturbed in the aged, the ability to mount effective primary immune responses to new antigens declines with age(61). The inability to mount effective primary immune responses in the aged may affect susceptibility to infectious disease by new pathogens and vaccine efficacy may be limited. The potential deficiencies of the immunosenescent innate and adaptive immune system that may enhance viral pathogenesis are reviewed below.

Immunosenescence in Innate Immunity. In the context of virus infection or vaccination, the innate immune system plays an integral role in the generation of the initial inflammatory response thought to be essential for the generation of an adaptive immune response of appropriate quality, quantity and longevity(160). Macrophages (Mø), neutrophils (Nø), and dendritic cells (DCs) are phagocytic cells that drive the innate immune response providing both effector functions that mediate pathogen clearance and antigen (Ag) presentation that begins the adaptive immune response(176). Ag acquisition and recognition by phagocytes is thought to be the first step in the innate immune activation cascade. Residing on the cell membranes and within the cytosol are specialized receptors called pathogen recognition receptors (PRRs) that recognize molecular signatures of invading pathogens and signal to begin the inflammatory response(147, 175). In vitro and in vivo murine studies of Mø and DC activation and cytokine secretion have produced conflicting results where levels of PRR expression and activation are similar in young and aged animals but the magnitude of cytokine secretion in aged mice is reported as both similar and

dissimilar as compared to young mice(7). Similarly conflicting results have been reported in the examination of PRR gene expression and cytokine secretion in monocyte derived DCs from young and aged human donors. Some studies suggest a functional equivalency in both PRR gene expression and cytokine secretion in young and aged DCs while others report discrepancies in cytokine secretion in response to PRR stimulation in the aged with decreased IL-12 but increased IL-6 and TNF-α(6, 7, 40). Basal levels of the Mø recruiting IL-8 are depressed in the elderly but LPS stimulation of senescent Mø results in increased induction of IL-8 as compared to young controls and may contribute to increased pulmonary inflammation seen in the elderly(31). Recent studies suggest a decline in the phagocytic and pinocytic abilities of DC and Mø impairing antigen capture and sensing which affects the induction of the inflammatory response and the activation of the adaptive immune response(6). Also, several studies suggest that DC migration to lymph nodes is impaired in the aged hampering efficient adaptive immune activation(6, 32, 126). Lastly, non-phagocytic innate natural killer cells (NK) migration and cytotoxic capabilities to not seem to be hampered with ageing(102). Taken together, current data suggests that multiple levels of the innate immune system may be compromised in the immunosenescent. Deficiencies or delay in APC pathogen sensing could allow for unchecked replication of invading pathogens which may contribute to more severe disease. Moreover, since APC and T cell interaction drives the adaptive immune response, APC dysfunction could affect the kinetics and quality of the cell mediated immune response contributing to more severe disease.

Immunosenescence in Adaptive Immunity. Like the innate immune compartment, the adaptive immune compartment experiences various functional deficiencies with ageing. In general, primary adaptive immune responses are generated by the presentation of antigen by antigen presenting cells (APCs) on MHC class II to the cognate T cell receptor (TCR, CD3) on naive CD4+ helper cells (Th)(129). For efficient Th cell activation, a second costimulatory signal between APC surface molecules (CD40, CD80, CD86) and CD28 on the T cell must occur(212). Depending on the antigen and mechanism of APC activation, a third signal (Th1 = IL-12, Th2 IL-4, IL-12) then triggers differentiation into either Th1 or Th2 cells which each have unique helper functions(129). In response to intracellular pathogens, Th1 cells produce IL-2, IL-12, IL-15 and INFγ to mediate activation of cognate cytotoxic CD8 T cells and the generation of IgG2a antibody(61, 160). In response to extracellular pathogens like helminthes, Th2 cells

produce IL-4, IL-5, and IL-10 and promote a B cell mediated response inducing IgG1, IgE and IgA(61, 160). With ageing, there is a general and preferential shift from a Th1 to a Th2 type of immune response with an associated decrease in INFγ and increase in IL-4 production(61). Due to Th1 to Th2 skewing with age, elderly individuals may have a more difficult time generating a Th1 response that is necessary to combat viral infection contributing to the development of severe viral disease.

The T cell compartment plays a pivotal role in the development of the cell mediated response to an invading pathogen while also driving the development of immune memory for future protection from similar pathogens(129). While the relative percentage of T cell subsets remains static over time, the absolute numbers of T cells decrease with age(61). Due to thymic involution, the numbers of naive T cells in circulation decrease while the memory pool increases in size hampering immune responses to novel antigens(67). Besides decreasing in frequency with immunosenescence, naïve T cells in aged individuals secrete lower amounts of IL-2 as compared to young cells after Ag stimulation by APCs. Decreased IL-2 output from newly activated Th cells results in diminished clonal expansion and reduced activation suggesting that Th effector cell differentiation is incomplete(77). Interestingly, Haynes et. al. have demonstrated that these defects in Th expansion and activation can be overcome in vitro when exogenous IL-2 is provided(76). Reduced activation of senescent Th cells has been shown to dramatically alter cognate helper function hampering B cell expansion and differentiation thereby reducing IgG production(50). The reduction in B cell activation by Th cells was not due to age related effects on Th cell migration and Eaton et. al suggest a reduction in the expression of CD154 (CD40L), the ligand for the B cell CD40 molecule, causes a reduction B cell proliferation and antibody production(50).

The CTL response is thought to be important for the clearance of intracellular viral pathogens and unfortunately both primary and memory CTL responses are affected by immunosenescence(77). Repeated challenge of the immune system through persistent viral infection with CMV can result in more than 10% of their CTLs targeted against a single CMV epitope(215). CTL activation in the immunosenescent is also affected through the loss of CD28 expression (CD28null) which is necessary for efficient T cell activation. In people over the age of 50 or 65, up to 70% and 95% of CD8 T cells are CD28null, respectively(212). With a significant portion of CTLs exhibiting a CD28null phenotype and a certain percentage targeted to chronic viral antigen, the CTL compartment in the immunosenescent is compromised and may affect the

pathogenesis of intracellular pathogens. Since CTLs have been implicated in clearance of influenza and West Nile virus infection, defects in the CTL compartment may contribute to the more severe disease seen in the elderly(1, 15, 142, 182).

Vaccination and Passive Immunization to Protect Against SARS-CoV Disease. It is clear that vaccination and passive immunization technologies are among the most important public health interventions in the past 200 years contributing to the complete eradication of small pox(132, 157). Though vaccination campaigns have eradicated polio and measles in developed nations, those diseases and other vaccine preventable diseases continue to plague developing nations(226-228). Rapidly and newly emerging infectious diseases like SARS-CoV provide unpredictable scenarios for the of field vaccinology where diseases never before seen in human populations arise and spread rapidly while reagents necessary for vaccine development do not yet exist. As seen with SARS-CoV epidemic, isolation of the virus allowed for the rapid generation of "killed", DNA and viral vectored vaccines within a year of the start of the epidemic(196, 199). Like vaccination, the practice of passive immunization to prevent infection or curtail established disease was first shown by Robert Koch in the late 1800s where he demonstrated that sheep antisera against diptheria toxin could protect against death in humans(132). More recently, technologies like phage display and memory B cell immortalization have been developed to produce sufficient quantities of human monoclonal antibodies (hu-mABs) directed against specific viral antigens(132). These technologies allowed for the rapid development of neutralizing hu-mABs directed against SARS-CoV within a year of the beginning of the epidemic(196). We will discuss the problems associated with SARS-CoV vaccination and passive immunization therapies which fall into three categories that include a) SARS-CoV antigenic variation and therapy efficacy b) the complications of immunosenescence and SARS-CoV vaccine efficacy c) SARS-CoV vaccine immunopotentiation of lung pathology.

SARS-CoV antigenic variation and therapy efficacy. The body of work attributed to SARS-CoV vaccine development is astounding though many studies are limited to assessment of the immune response and fail to evaluate the vaccine platform of interest through the more powerful and pertinent SARS-CoV virus challenge(12, 91, 128, 251). Inactivated whole virus and vectored SARS-CoV vaccine trials in a number of different animals models have demonstrated that the SARS-CoV spike glycoprotein

(S) is the critical component of protective immunity and the passive transfer of SARS-CoV S specific sera is sufficient to provide protection from infection and disease by a homologous SARS-CoV strain(20, 41, 78, 95, 163, 190, 194, 224, 241, 253, 254). However, current animal models universally display a very acute SARS-CoV like disease(30, 41, 70, 71, 167, 169, 170, 195). As such, these models may under represent the importance of the cell mediated and humoral responses in controlling more prolonged infection and pathogenesis as seen in human cases of SARS-CoV. In fact, the development of a SARS-CoV animal model that recapitulates both acute and prolonged infection with the development of adaptive immunity would greatly benefit the study of SARS-CoV pathogenesis and SARS-CoV vaccine development. Nevertheless, these acute animal models of SARS-CoV infection are currently the most effective systems within which to assess vaccine and passive immunization efficacy.

Animal models to assess vaccine and passive immunization therapy efficacy against divergent SARS-CoV antigens. Since the epidemic strain may no longer exist in nature, vaccination with epidemic strain antigens followed by challenge with the epidemic strain may not be the most biologically and medically relevant design. Due to the complications of designing a vaccine against future emergence of SARS-CoV whose antigenic identity is unknown, several difficult questions arise in the development of effective SARS-CoV therapies: Which SARS-CoV antigen or pool of antigens will provide the greatest degree of cross protection if the vaccination is to prevent disease from future emergence of SARS-CoV? Similarly, which cross neutralizing epitopes should be targeted by passive immunization therapies in order to effectively treat future emergence of SARS-CoV? Lastly, which SARS-CoV strain(s) should be employed as challenge virus to assess vaccine efficacy? We can begin to answer these questions within current animal models of SARS-CoV pathogenesis.

In 2006, Deming et al demonstrated that a Venezuelan equine encephalitis virus replicon particle expressing SARS Urbani S (VRP-S) vaccine provided complete protection from replication of a SARS-CoV bearing a zoonotic heterologous GD03 S but protection was variable in senescent mice(41). Due to the lack of significant morbidity and mortality in the SARS-CoV replication models, previous vaccine studies were unable to assess protection from disease or death and could only speculate that diminishing virus replication would diminish disease. Nevertheless, heterogeneity between antigen and challenge virus provides a more stringent, thorough, biologically and medically relevant model within which to assess

vaccine efficacy. Therefore, employing an antigenically diverse panel of SARS-CoV antigens for vaccination coupled with the use of a similarly diverse lethal challenge virus panel may represent the most pertinent and relevant strategy to assess vaccine efficacy (Table 2). In 2007, Subbarao et al created a mouse adapted SARS-CoV (MA15) through repeated passage of SARS Urbani in BALB/c mice(167). Our laboratory created a molecular clone of MA15 (rMA15) by introducing the six amino acid changes found in MA15 into our infections clone for SARS Urbani (icSARS)(167). When administered intranasally to BALB/c mice of most any age, rMA15 causes significant weight loss (~20 % of starting weight) most likely resulting from an acute infection of the lung resulting in almost 100% mortality(167). The robustness of the MA15 lethal BALB/c would allow for the assessment of vaccines to induce protection from not only replication but also disease and mortality.

Similar to vaccination, the most successful hu-mABs for passive immunization against SARS-CoV should broadly neutralize all current and future SARS-CoV strains. One of the first hu-mABs developed against SARS-CoV, 80R, was effective in neutralizing pseudovirus bearing epidemic (Tor2) and civet (SZ3) S proteins but was not as effective against pseudovirus bearing the civet-like GD03 S in vitro(197). Using hu-mAB m396, Zhu et al reported complete neutralization of SARS Urbani and SARS-CoV bearing GD03 S (icGD03-S) but was less effective at neutralizing the SARS-CoV bearing the SZ16-K479N S (icSZ16-S K479N, 4 log reduction in virus lung titer as compared to control hu-mAB) in passive transfer experiments in young BALB/c mice(256). In contrast to the m396 antibody, Zhu et al also reported complete protection from virus replication (day 2 post infection) against SARS Urbani, icGD03-S and icSZ16-S K479N using a similar doses of hu-mAB S230.15(256). Rockx et al also demonstrated the cross reactivity and potent neutralizing ability of the S230.15 and another novel hu-mAB(S227.14) in passive transfer studies in mice(171). 230.15 and 227.14 effectively neutralized SARS Urbani and recombinant SARS-CoV bearing the early epidemic phase GZ02 S though were both less efficacious against recombinant SARS-CoV bearing the civet HC/SZ/61/03 S glycoprotein (2 log reduction in virus lung titers on day 2 post infection as compared to control Ab)(171). Though S230.15 and S227.14 did not protect against virus replication in HC/SZ/61/03 challenged mice, both antibodies protected Urbani, GZ02 and HC/SZ/61/03 infected mice from clinical signs of disease(171). These data highlight the importance of using more than one strain of SARS-CoV when evaluating SARS-CoV therapies since the hu-mABs

discussed above provided varying degrees of protection from replication depending the SARS-CoV S variant that was employed in the in vitro or in vivo assay. Also, these data suggest that the complete abrogation of replication may not be necessary to protect from clinical signs of SARS-CoV disease.

SARS-CoV vaccine efficacy in senescent populations. As mentioned above, the immunosenescence that occurs with ageing can hamper both the innate and adaptive immune responses whose collaboration is necessary for efficient vaccination. The SARS-CoV epidemic was particularly harsh on immune senescent populations where mortality ranged between 25-55% in people over the age of 65(19, 116, 124, 152). If a SARS-CoV like virus were to reemerge in the future, it is imperative that current vaccination strategies be successful in the most vulnerable populations. Unfortunately, the successful vaccination of elderly populations is a difficult and unpredictable task due to immunosenescence(17, 18, 50, 53, 64, 65, 67, 77, 151, 212, 215). Much of this research related to vaccination of the immunosenescent was been performed with influenza. Current models predict influenza vaccine efficacy in elderly populations ranges from 17-53% while the vaccine in young adults is 70-90% effective and the reason for the discrepancy seems to be a result of senescent immune system malfunction on multiple levels(64). Defects in antigen presentation, T cell activation and cytokine secretion affect the generation of effective adaptive immune system helper (T helper or Th) cells and effector (B cells and cytotoxic T cells) cells resulting in diminished vaccine efficacy(50, 53, 58, 64, 65, 77, 136, 212, 223). Current research suggest that the some defects of the senescent immune system can be overcome through administration of cytokines (IL-2) or adjuvants (MF59, CpG DNA) during vaccination that effectively activate APCs/Th cells thereby increasing the probability of generating appropriate effector cells required for successful vaccination(75, 76, 83, 160, 201). Since influenza, West Nile Virus and SARS-CoV infection all produce disproportionately more disease in the elderly, the development of successful vaccine strategies in the elderly has a broad public health application(1, 116, 142).

Like in humans, the infection of aged mice with SARS Urbani results in more severe disease as compared to similar infection of young adult mice. In senescent mice, both virus replication and lung pathology is enhanced but virus is eventually cleared suggesting that components of the aged immune system are less effective at controlling virus replication. Though the senescent mouse model does not fully recapitulate SARS-CoV acute and extended cell mediated pathogenesis seen in humans, it serves as a

useful model to study the effects of immunosenescence on vaccine efficacy. Using VRP vectors expressing the Urbani S glycoprotein, Deming et al demonstrated complete protection of young adult mice from replication of a heterologous challenge virus bearing the GD03 S glycoprotein though protection in similarly vaccinated senescent mice was variable(41). Not surprisingly, high titers of Urbani and GD03 neutralizing antibody were found in young vaccinated mice while most senescent animals had very low Urbani specific neutralization titers and most GD03 titers below the limit of detection(41). Using vesicular stomatitis virus vectors expressing Urbani S (rVSV-S), Vogel et. al. obtained similar results in aged mice where neutralization titers in vaccinated aged mice were low and did not provide protection from replication upon homologous SARS Urbani challenge(220). Similar to what is seen in humans, these data suggest that vaccination of young mice induces a robust and cross protective IgG response while the IgG response in aged animals is depressed in both magnitude and cross reactivity.

SARS-CoV vaccine immunopotentiation. Effective vaccination induces specific protective immunity that confers protection from future disease. Unfortunately, vaccination can sometimes exacerbate disease upon natural infection with the pathogen the vaccine was designed to protect against. This phenomena where the vaccine induced "protective" immune response upon challenge promotes rather than protects from disease is called "immunopotentiation" of disease(225). Both measles (MV) and RSV are paramyxovirus respiratory pathogens that cause significant morbidity and mortality in infants that might be prevented through the development of effective vaccines (158, 214). In the 1960s, two infamous examples of immunopotentiation of disease surfaced with formalin inactivated MV (FI-MV) and RSV (FI-RSV) vaccines(158, 214). Infants with no prior exposure to RSV were vaccinated with the FI-RSV vaccine, developed virus specific antibody but were not protected from subsequent natural RSV infection(49). In fact, FI-RSV vaccinated children infected with RSV suffered from enhanced RSV disease requiring hospitalization and a few children died from infection(49). The pathological hallmark of FI-RSV immunopotentiation was lung and peripheral eosinophelia which is absent during the natural course of RSV infection(49, 214). Similar to FI-RSV, protective immunity waned in infants shortly after vaccination with FI-MV and subsequent natural measles infection resulted in more severe disease with eosinophelia uncharacteristic of natural measles infection(158). Due to these severe vaccine associated disease complications, both vaccines were withdrawn and work began to understand the biology of these flawed

vaccines. Within mouse and non-human primate animal models, both FI-RSV and FI-MV were found to induce an atypical Th2 adaptive immune response not seen in natural infection(37, 49, 158, 214). The effects of the Th2 responses generated by FI-RSV and FI-MV differ. FI-RSV vaccination induces a Th2 allergic immune response with T cells secreting cytokines (IL-13, IL-5) that upregulate the production of the potent eosinophil chemotactic molecule eotaxin(37, 49, 214). Natural infection of vaccinated individuals is thought to have been exacerbated by this atypical allergic immune response in the lung(37, 49, 214). Interestingly, similar results are achieved in macaques using formalin inactivated human metapneumovirus vaccines (FI-hMPV) followed by hMPV challenge(38). With FI-MV vaccination, non-human primate models suggest the associated allergic Th2 response generated after MV challenge recruits eosinophils to sites of virus replication with disease pathology in part mediated by immune complex deposition(158).

Vaccine induced immunopotentiation has also been observed in coronavirus with vaccinia virus vectored feline infectious peritonitis virus (FIPV) vaccines. Vennema et. al. observed that vaccination with recombinant vaccinia virus expressing FIPV S (vFS) induced short lived immunity in kittens(217). When challenged, vFS immunized animals suffered from much more severe disease than those receiving a control vaccine. vFS vaccine induced immunopotentiation was suspected to be a result of antibody dependent enhancement (ADE) of virus infection where subneutralizing antibody coating FIPV virions allowed for the entry and productive infection of cells (e.g. macrophages) not normally targeted during natural infection.

Vaccine induced immunopotentiation of disease has also been shown with vectored vaccines expressing SARS-CoV N. Deming et. al. demonstrated that mice vaccinated with VRP based vaccines expressing the SARS-CoV N gene were not protected from infection and developed enhanced lung immunopathology upon challenge with eosinophelia not seen in control mice(41). These data suggest that the N protein not only does not provide protection from disease in these acute replication models, it also promotes enhanced disease pathogenesis in the lung. The evaluation of several formalin inactivated SARS-CoV vaccines suggest these vaccines primarily induce a Th2 response while natural SARS-CoV infection of humans induces primarily a Th1 response(190, 208, 232). Given the data from both FI-RSV and FI-MV vaccination where the alteration of the natural Th response induced more severe disease upon challenge,

caution should be taken in developing vectored vaccines containing SARS-CoV N or formalin inactivated SARS-CoV vaccines which may promote rather than prevent disease.

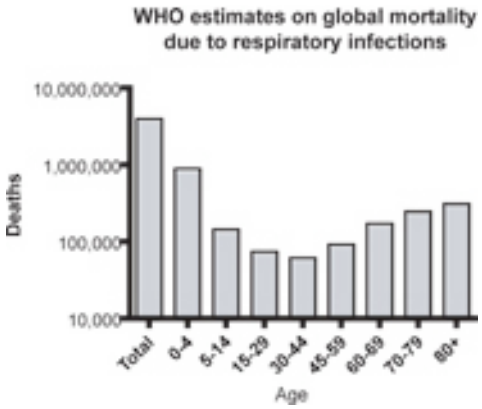

Figure 1: World Health Organization (WHO) on global mortality due to respiratory infections by age group.

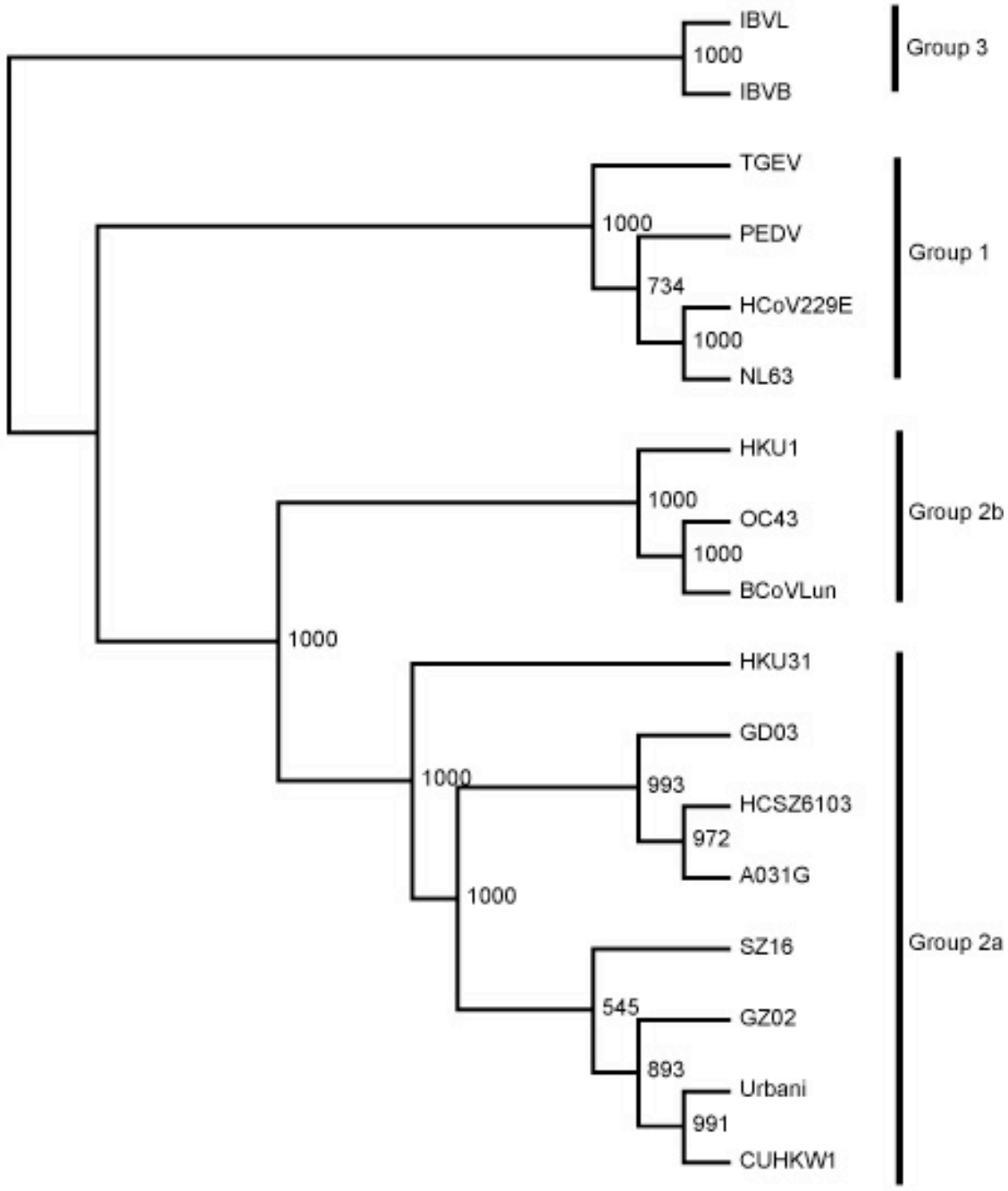

Figure 2: Neighbor joining tree created from coronavirus S gene amino acid sequences. Numbers represent bootstrap values based on 1000 bootstrap replicates.

Table 1: Examples of past and newly emerging/discovered coronavirus.

Virus Name	Genogroup	Host	Disease	Host range expansion	New disease	Newly discovered or emerging virus
Sever acute respiratory syndrome coronavirus (SARS-CoV)	2a	Human	Respiratory disease	X		X
Human coronavirus OC43 (OC43)	2	Human	Respiratory disease	X		
Buffalo associated coronavirus (BuCoV)	2b	Buffalo	Gastroenteritis	X		
Respiratory bovine coronavirus (RBCV)	2b	Cows	Respiratory disease		X	
Porcine respiratory virus (PRCV)	1	Pig	Respiratory disease		X	
Human coronavirus NL63 (NL63)	1	Human	Respiratory disease	?		X
Human coronavirus HKU1 (HKU1)	2	Human	Respiratory disease	?		X

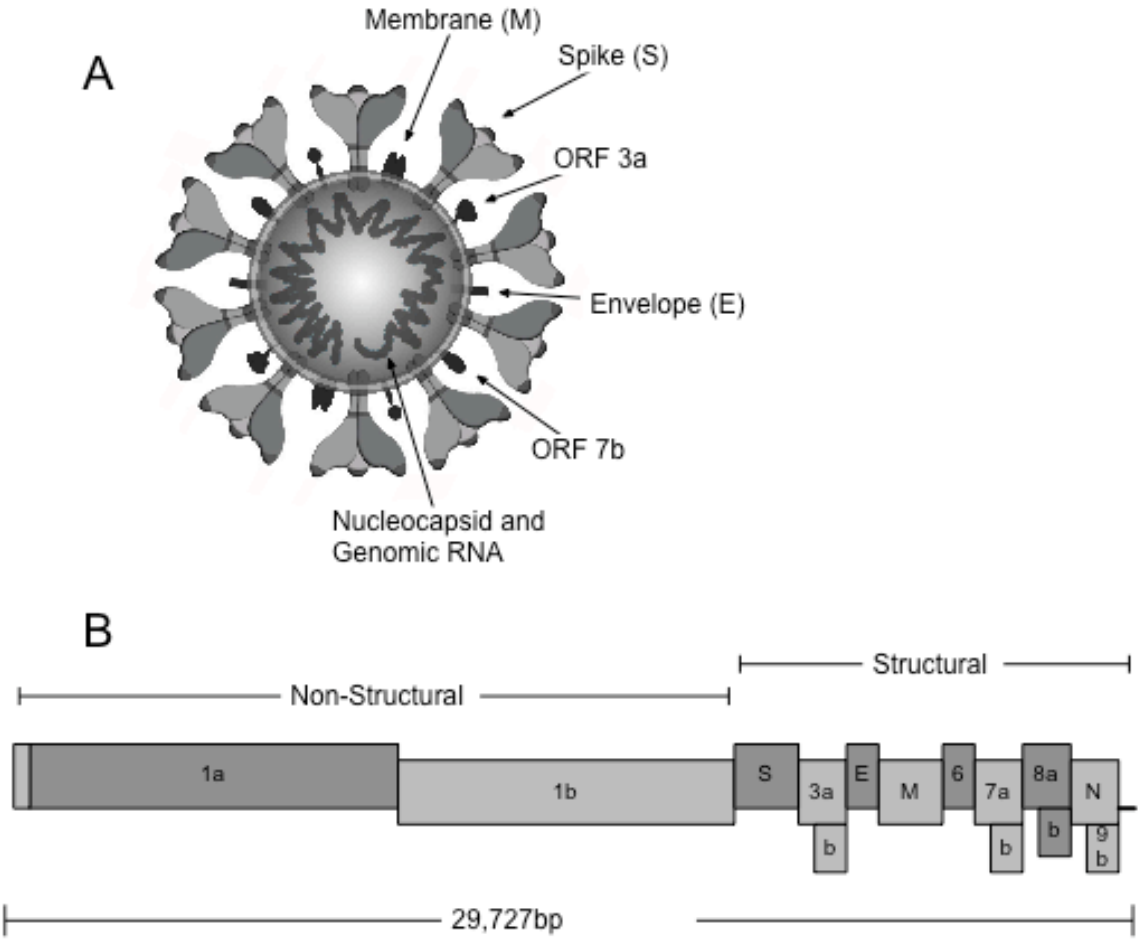

Figure 3: Schematics of SARS-CoV virion and genome organization. (A) Schematic of the SARS-CoV virion. The virus genome is associated with the nucleocapsid protein and is contained within a lipid bilayer containing at least five structural proteins (membrane (M), spike (S), envelope (E), ORF 3a, and ORF 7a). (B) Schematic of the SARS-CoV genome organization. The SARS-CoV genome is 29,727bp of positive sense RNA. The first two thirds of the genome contains genes encoding non-structural proteins while the last third contains genes encoding structural genes. The SARS-CoV genome is layed out in the classic coronavirus gene order 5'-non-structural genes, S, E, M, and N-3' with group specific open reading frames interspersed between the structural genes.

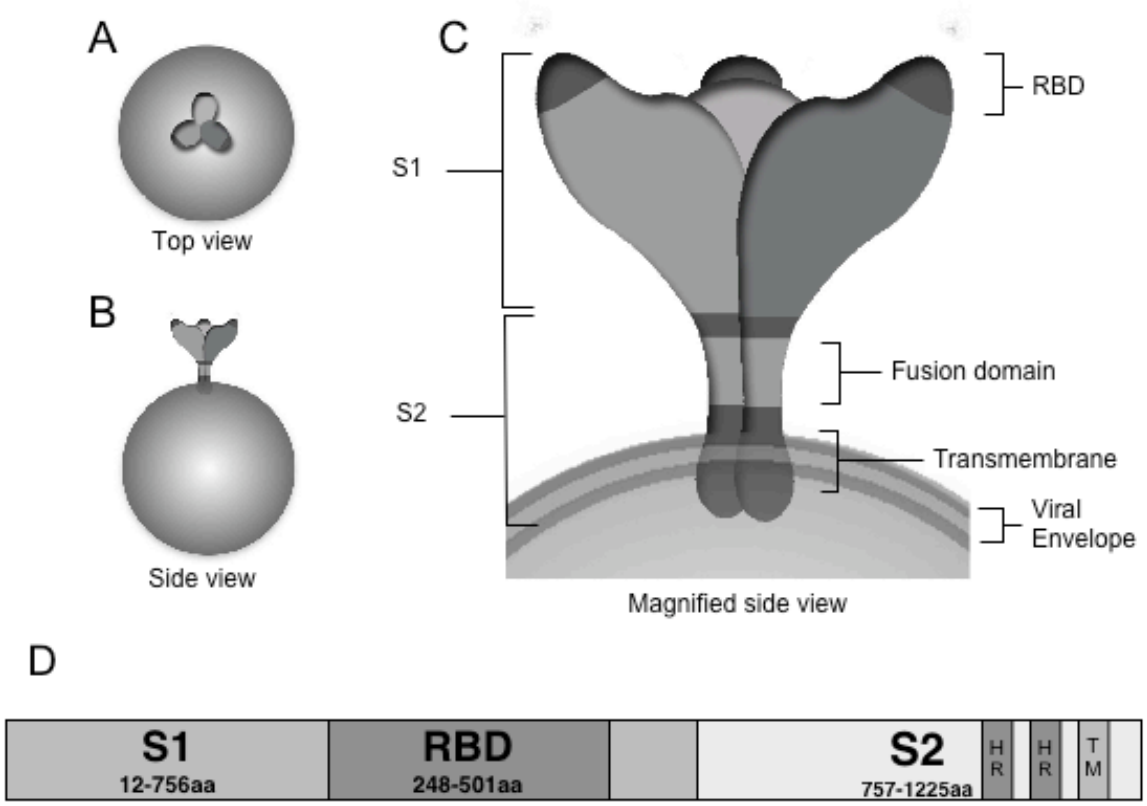

Figure 4:Schematics of the SARS Spike (S) glycoprotein domain organization. Like gp160 of HIV, hemagglutinin of influenza, F protein of paramyxovirus, and glycoprotein of Ebola virus, the spike (S) glycoprotein protein of coronavirus is a class I viral fusion protein that mediates virus binding and fusion allowing the virus to enter the host cell. (A) Above view of S protein trimers situated in the viral envelope. (B) Side view of S protein trimer situated in the viral envelope. (B) Close up side view of S trimer situated within the viral envelope. Putative locations of the receptor binding domain (RBD), S1, S2, fusion and transmembrane domains are noted. (D) Linear layout (N-terminal to C-terminal) of the S protein domains. Like other class I fusion proteins, the SARS S glycoprotein contains two functional domains, S1 and S2, joined by a protease cleavage site. The S1 domain (17-756aa) contains the receptor binding domain (RBD) (318-510aa) while the S2 region (757-1225aa) contains the two heptad repeat (HR) regions that facilitate viral fusion and a transmembrane domain (1189-1227aa) that anchors spike to the viral envelope.

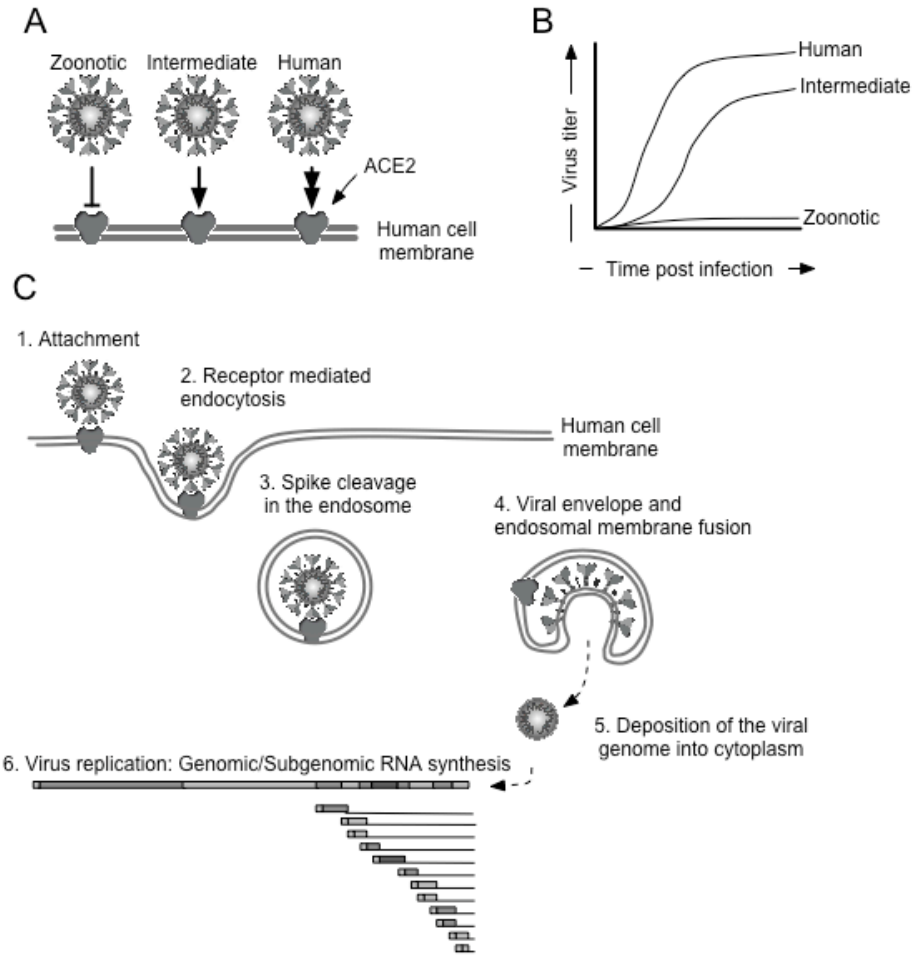

Figure 5: SARS-CoV S protein interactions with the human receptor angiotensin I converting enzyme 2 (hACE2) mediate entry into the host cell. (A) The coronavirus S glycoprotein is a critical component of species specificity which is primary determinant of pathogenesis since a virus incapable of infection will most likely not cause disease. SARS-CoV S and ACE2 interactions affect efficiency of virus entry and infection where zoonotic viruses are incapable of binding hACE2, intermediate SARS-CoV are moderately capable of binding hACE2 and human epidemic strains are very capable of binding hACE2. These differences in binding efficiency affect infection efficiency and pathogenesis. (B) An example of a one step growth curve examining zoonotic, intermediate and human tropic SARS-CoV replication kinetics within cells expressing hACE2. Cell cultures are infected at a high multiplicity of infection (MOI) and cell media is sampled over time to monitor virus growth. Since the cells are infected with a high MOI, only one cycle of virus growth is seen in the time allotted. These experiments provide data regarding binding, entry and replication efficiency. As virus titers of human tropic strains are superior to intermediate strains at early times post infection suggesting the human tropic strains appear to gain entry more quickly while zoonotic virus cannot gain entry and does not grow. Since the slopes of the human and intermediate curves are similar, this indicates that these viruses replicate at similar rates. Even though human and intermediate strains seem to replicate at similar rates, human tropic viruses achieve titers superior to those of the intermediate strains. Since human tropic S binding is to hACE2 is the most efficient, more cells are infected as compared to intermediate strains and as a result, more progeny virus is produced. (C) SARS-CoV is thought to gain entry into cells by the following sequence of events 1. Binding to the cellular receptor ACE2 2. Entry into the cell by endocytosis 3. Cleavage of the SARS-CoV S by cellular protease cathepsin-L causing a rearrangement of S1 and S2 subunits 4. Viral and host membrane fusion depositing the viral genome into the cytoplasm 5. Virus genomic and subgenomic replication ensues.

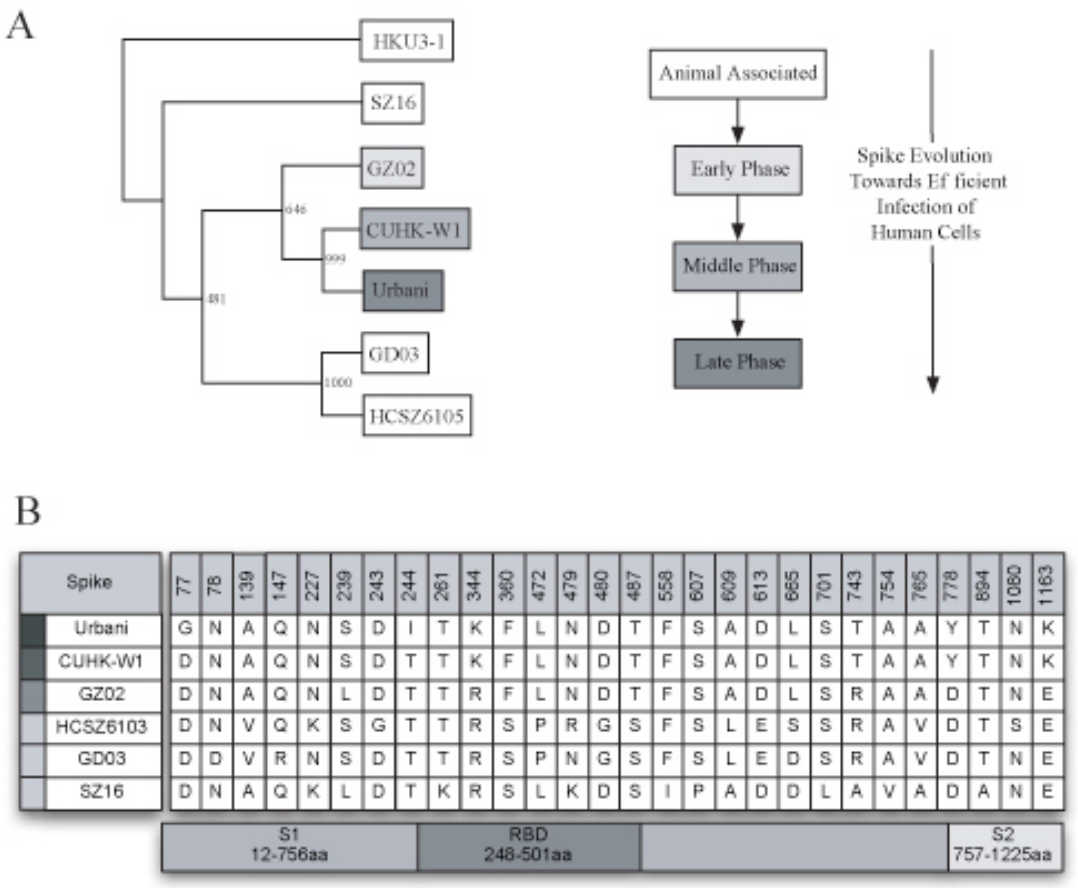

Spike	77	78	139	147	227	239	243	244	261	344	360	472	479	480	487	558	607	609	613	665	701	743	754	765	778	894	1080	1163
Urbani	G	N	A	Q	N	S	D	I	T	K	F	L	N	D	T	F	S	A	D	L	S	T	A	A	Y	T	N	K
CUHK-W1	D	N	A	Q	N	S	D	T	T	K	F	L	N	D	T	F	S	A	D	L	S	T	A	A	Y	T	N	K
GZ02	D	N	A	Q	N	L	D	T	T	R	F	L	N	D	T	F	S	A	D	L	S	R	A	A	D	T	N	E
HCSZ6103	D	N	V	Q	K	S	G	T	T	R	S	P	R	G	S	F	S	L	E	S	S	R	A	V	D	T	S	E
GD03	D	D	V	R	N	S	D	T	T	R	S	P	N	G	S	F	S	L	E	D	S	R	A	V	D	T	N	E
SZ16	D	N	A	Q	K	L	D	T	K	R	S	L	K	D	S	I	P	A	D	D	L	A	V	A	D	A	N	E

Figure 6: Phylogenetic relationships of zoonotic and epidemic SARS-CoV. (A) Neighbor joining tree constructed from nucleotide sequences of various SARS-CoV S genes. The degrees of gray color indicate evolutionary relationships between zoonotic virus (white), early (light gray), middle (medium gray) and late (dark gray) phases of the epidemic. Numbers represent bootstrap values based on 1000 bootstrap replicates. (B) Spike amino acid differences between Urbani (late phase), CUHK-W1 (middle phase), GZ02 (early phase), HC/SZ/61/03 (zoonotic phase), GD03 (zoonotic phase) and SZ16 (zoonotic phase) viruses.

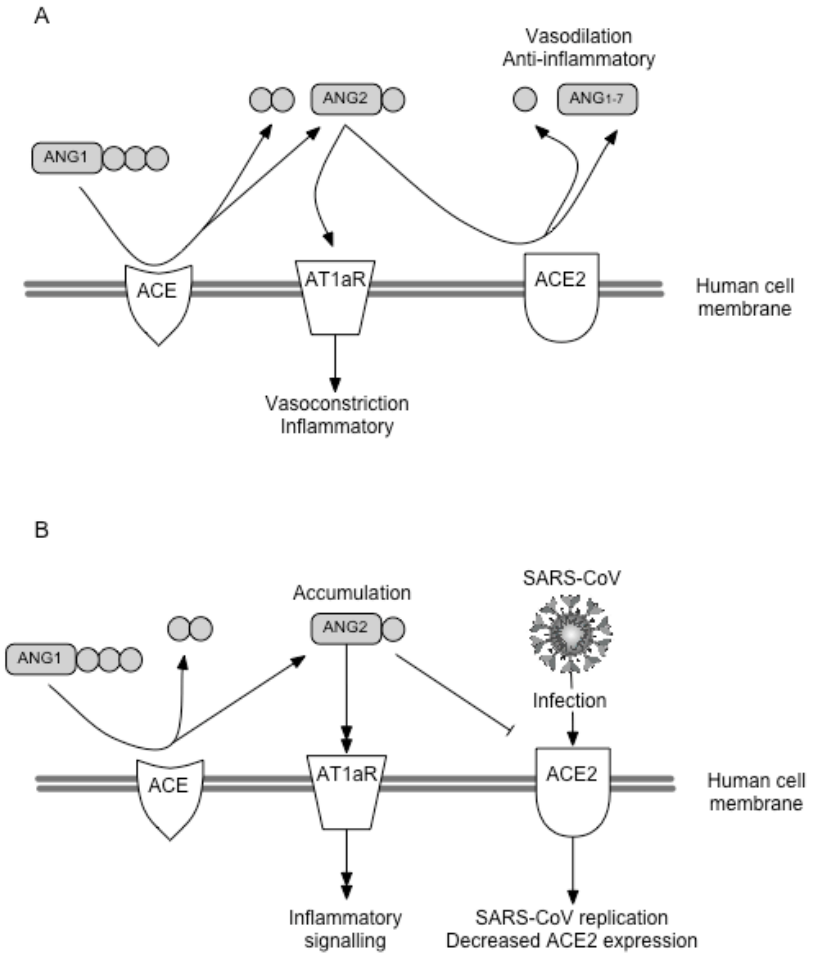

Figure 7: The SARS-CoV receptor, angiotensin I Converting Enzyme 2 (ACE2), in virus entry and pathogenesis. (A) ACE2 and angiotensin I converting enzyme (ACE) are key regulators of the rennin-angiotensin system (RAS), which helps control cardiovascular function by maintaining the body's blood pressure and electrolyte balance. ACE and ACE2 are metalloproteases with differing vasoactive peptide substrate specificities and as a result have disparate and antagonistic roles in maintaining physiologic homeostasis. ACE cleaves the peptide ANG I into ANG II which has vasoconstrictive effects inducing hypertension while also inducing cell proliferation and fibrosis. In contrast, ACE2 processes ANG I into ANG 1-9 and further processes ANG II into the peptide ANG 1-7 which acts as a vasodilator while also being anti-proliferative and apoptotic. Current in vitro data suggests that ANG II ligation and signaling through angiotensin receptor 1a (AT1aR) can result in the production of proimflammatory cytokines (TNFα, IL-1β, IL-6, MCP-1 etc.), fibrosis, and cell proliferation. (B) Infection of the lung by SARS-CoV disrupts of RAS homeostasis. SARS-CoV infection or the administration of SARS S alone depresses levels of ACE2 within the lung. Furthermore, the administration of SARS S recombinant protein exacerbated ALI induced by acid aspiration. Current data suggests that SARS-CoV infection or SARS S protein decreases levels of ACE2 within the lung thereby removing a key regulator and processor of the proinflammatory ANG II peptide whose excess contributes to more severe disease. These data provide an interesting insight into possible RAS involvement in SARS-CoV pathogenesis and the progression of ALI to acute respiratory distress syndrome (ARDS) seen in more severe cases of SARS-CoV.

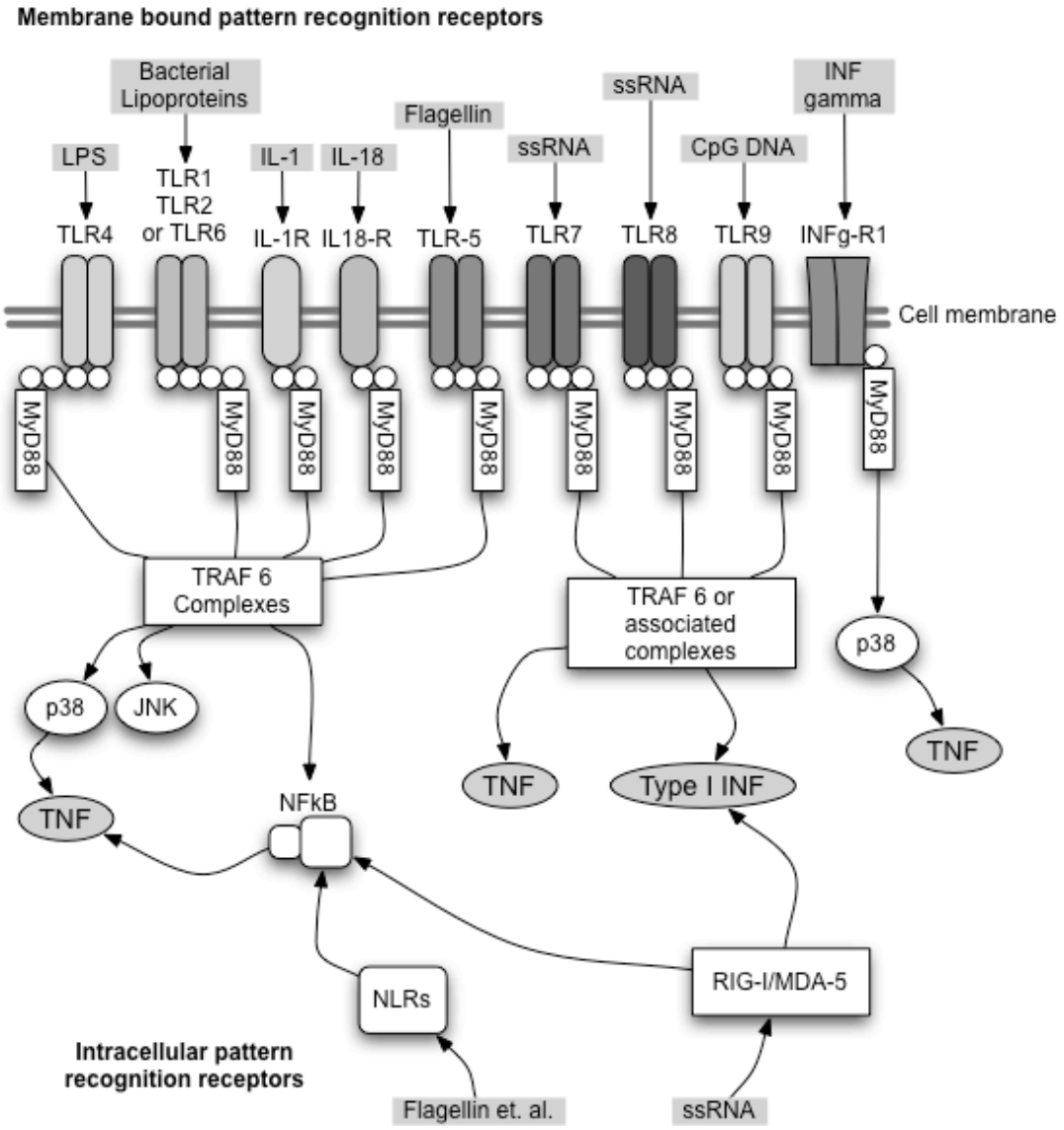

Figure 8: Schematic of membrane bound and cytosolic pathogen recognition receptors. The innate immune response is thought to provide the first line of host defense against invading pathogens. Specialized membrane bound or cytosolic pathogen recognition receptors (PRRs) such as Toll-Like Receptors (TLRs), RIG-I/Mda5, and Nod-like receptors (NLRs) sense pathogen-associated molecular patterns (PAMPs) and initialize the innate immune inflammatory response by activating the transcription of various proinflammatory genes. These PRRs are very specific in their pathogen component recognition (e.g. double stranded RNA, CpG DNA, LPS etc.) and the type of immune response generated as a result of activation. TLRs, NODs, RIG-I and Mda5 have been shown to be expressed within lung epithelial cells as well as in the more "professional" environmental sensing cells like conventional/plasmacytoid dendritic cells (cDCs/pDCs) and macrophages (Mø).

Table 2: A panel of antigenically divergent recombinant SARS-CoV bearing various S glycoproteins for the assessment of vaccine efficacy.

Recombinant Virus Name	Description	Spike AA Δs from Urbani	Pathogenic Phenotype in Young BALB/c	Pathogenic Phenotype in Senescent BALB/c
icSARS	Molecular clone of the epidemic strain SARS Urbani	0	No weight loss, high titer virus replication in lung	Moderate weight loss, more virus replication than in young
icCHUK-W1	icSARS bearing a middle epimdemic phase virus spike	3	No weight loss, high titer virus replication in lung	Little weight loss,similar virus replication than in young
icGZ02	icSARS bearing an early epidemic phase virus spike	6	No weight loss, high titer virus replication in lung	Lethal, more virus replication in lung than in young
icHC/SZ/61/03	icSARS bearing a zoonotic SARS-CoV spike isolated from a palm civet	21	No weight loss, high titer virus replication in lung	Lethal, similar virus replication in lung than in young
icA031G	icSARS bearing a zoonotic SARS-CoV spike isolated from a racoon dog	23	No weight loss, high titer virus replication in lung	Moderate weight loss, similar virus replication than in young
icGD03	icSARS bearing a zoonotic SARS-CoV spike isolated from a sporadic human case	18	No weight loss, high titer virus replication in lung	Little weight loss, similar virus replication than in young
icSZ16-S K479N	icSARS bearing a zoonotic SARS-CoV spike isolated from palm civet mutated at residue 479	17	No weight loss, high titer virus replication in lung	Little weight loss, similar virus replication than in young
rMA15	Molecular clone of the mouse adapted SARS-CoV	1	Lethal, high titer virus replication in lung	Lethal, more virus replication in lung than in young
rMA15-GD03	rMA15 bearing the GD03 spike	19	Moderate weight loss, high titer virus replication in lung	Lethal, more virus replication in lung than in young

Since the epidemic strain may not exist in nature, vaccination with epidemic strain antigens followed by challenge with the epidemic strain may represent a biologically irrelevant design. Unfortunately, a difficult choice is presented in choosing SARS-CoV vaccine antigens in hopes of preventing disease by future emergents whose antigenic identity is unknown. Therefore, employing an antigenically diverse panel SARS-CoV antigens for vaccination coupled with the use of an similarly diverse lethal challenge virus panel may represent the most pertinent and relevant strategy to assess vaccine efficacy.

CHAPTER II

MECHANISMS OF ZOONOTIC SARS-CoV HOST RANGE EXPANSION IN HUMAN AIRWAY EPITHELIUM

Abstract

In 2002, SARS Coronavirus (SARS-CoV) emerged and caused over 8000 human cases and greater than 700 deaths worldwide. Zoonotic SARS-CoV likely evolved to infect humans by a series of transmission events between humans and animals for sale in China. Using synthetic biology, we engineered the spike protein (S) from a civet strain, SZ16, into our epidemic strain infectious clone creating the chimeric virus, icSZ16-S, which was infectious but yielded progeny viruses incapable of propagating *in vitro*. After introducing a K479N mutation within the S receptor binding domain (RBD) of SZ16, the recombinant virus (icSZ16-S K479N) replicated in Vero cells but was severely debilitated in growth. The *in vitro* evolution of icSZ16-S K479N on human airway epithelial cells (HAE) produced two viruses (icSZ16-S K479N D8 and D22) with enhanced growth on HAE and on DBT cells expressing the SARS-CoV receptor (hACE2). icSZ16-S K479N D8 (D8) and D22 (D22) virus RBDs contained mutations in ACE2 contact residues Y442F and L472F that remodeled S interactions with hACE2. Further, these viruses were neutralized by a human monoclonal antibody (mAb), S230.15, while the parent icSZ16-S K479N strain was eight times more resistant. These data suggest that human adaptation of zoonotic SARS-CoV strains may select for some variants that are highly susceptible to select mABs that bind to the RBD. Epidemic, icSZ16-S K479N and D22 viruses replicate similarly in the BALB/c mouse lung highlighting the potential use of these zoonotic spike SARS-CoV to assess vaccine or sero therapy efficacy *in vivo*.

Introduction

Emerging viral diseases such as HIV, Ebola, Influenza H5N1, West Nile and Dengue virus have had a profound impact on global public health(139). In 2002, a novel coronavirus (SARS-CoV) emerged suddenly as the causative agent of Severe and Acute Respiratory Syndrome (SARS) and spread worldwide

causing about 8000 cases and >700 deaths(29, 103, 173). SARS-CoV most likely evolved from viruses circulating within the Chinese horseshoe bat and other bat species that are believed to be the natural animal reservoirs(108). Within live animal markets in the Guangdong region of China, it is hypothesized that close cohabitation of bats and palm civets allowed for subsequent cross species transmission and amplification of bat strains in civets (69, 108). Palm civets then served as an intermediate host for subsequent viral evolution of strains that could infect and transmit between humans(108). Clinical data suggests that the sporadic early human SARS-CoV infections were significantly less pathogenic and that a progressive series of adaptive mutations were necessary for increased human to human transmission and the expanding phases of the epidemic(28, 69, 173). Despite initial reports that civet strains SZ16 and SZ3 could be propagated in cell culture, subsequent studies have indicated that these viruses could not be successfully maintained in culture thereby hampering our understanding of their pathogenicity and mechanisms of cross species transmission in humans(110).

Within the past four years, multiple newly emerging coronaviruses of human relevance have been identified highlighting the emerging disease potential of the coronavirus family(161, 173, 213, 235). SARS-CoV and human coronavirus HKU1 are newly emerging members of coronavirus genogroup II and both cause pneumonic disease in humans with SARS-CoV being the most pathogenic of the known human coronaviruses(48, 103, 173, 233, 235). Viruses related to the SARS-CoV epidemic strain have recently been found in Chinese horseshoe bats during surveillance of wild animals in Hong Kong(108). Since viruses similar to the epidemic strain have been found circulating within zoonotic pools, there is the potential for yet another reemergence(108). Moreover, a promiscuous RNA-dependent RNA polymerase coupled with high frequency recombination rates make the evolution of future human coronavirus pathogens a real possibility(42, 162, 248).

The coronavirus spike glycoprotein (S) is a key determinant of host specificity and elucidating the molecular mechanisms of viral host expansion may help us understand the events that rendered SARS-CoV pathogenic to humans(94, 122). Virus sequence data isolated throughout the course of the epidemic suggests that S gene was under heavy positive selection during the early phase of the epidemic but eventually stabilized as the epidemic progressed(28). The S protein is 1225 amino acids in length and can be divided into two main functional domains S1 and S2. The S1 region (17-756aa) contains the receptor

binding domain (RBD) (318-510aa) while the S2 region (757-1225aa) contains the two heptad repeat regions responsible for viral fusion and a transmembrane domain (1189-1227aa) that anchors S to the viral envelope. SARS-CoV entry into the host cell is mediated by a receptor, angiotensin I converting enzyme-2 (ACE2), and perhaps other coreceptors(90, 120). ACE2 has been detected on the apical surfaces of ciliated cells within the lung epithia as well as in kidney and colon(72). After S and receptor binding, the virus enters the cell by receptor mediated endocytosis. Cleavage of the SARS-CoV S by cathepsin L within the endosome is required for SARS-CoV infection and precedes fusion(184).

Sequences isolated throughout the initial epidemic in 2002-2003 and during the reemergence of 2003-2004 chronicle the mutations in S that may have allowed for host expansion. During the epidemic and reemergence, the early 2003 SARS-CoV animal isolate, SZ16, and the 2004 reemergent human isolate, GD03, were among the most divergent viruses isolated from civets and humans, respectively. SARS-CoV SZ16 was identified from palm civets in live animal markets within the Guangdong region of China during the epidemic and its S protein differs from the epidemic strain, SARS Urbani, in 18 amino acids 16 of which reside in the S1 domain. Using pseudotyped viruses, recent work has shown that mutation of residue 479 within the SZ16 RBD was sufficient to allow for the host range expansion of zoonotic SARS-CoV spike bearing pseudovirus to infect human cells(119, 122).

In this study, we describe the synthetic construction and characterization of a SARS-CoV chimera bearing a zoonotic SZ16 S protein. Importantly, we find that the mutations acquired during the *in vitro* evolution of a zoonotic S bearing recombinant virus in human airway epithelial cells (HAE) can vary from those that occurred during the epidemic highlighting the adaptive plasticity of the zoonotic S protein. Also, these data suggest that HAE can be used as a model to evaluate the possible avenues of SARS-CoV zoonotic S evolution towards efficient infection of human cells. Lastly, recombinant viruses bearing zoonotic S proteins replicated efficiently in mice, and will serve as a valuable tool in assessing the efficacy of vaccines and therapies.

Materials and Methods

Viruses and Cells. The recombinant epidemic strain virus "icSARS" (AY278741), icSZ16-S (AY304488) and icSZ16-S K479N, icSZ16-S K479N D8, and icSZ16-S K479N D22 were propagated on Vero E6 cells as described(249). Virus stocks used throughout this study were grown and titered by plaque assay in Vero

E6 cells as described(249). Vero E6 and delayed brain tumor (DBT) cells were grown in MEM (Invitrogen, Carlsbad, CA) supplemented with 10% FCII (Hyclone, South Logan, UT) and gentamycin/kanamycin (UNC Tissue Culture Facility). Mink lung epithelial cells (Mv1lu) were grown in DMEM (Invitrogen, Carlsbad, CA) supplemented with 10% FCII (Hyclone, South Logan, UT) and gentamycin/kanamycin (UNC Tissue Culture Facility). Human tracheobronchial epithelial cells (HAE) were obtained from airway tissues harvested from patients undergoing elective surgery under UNC Institutional Review Board-approved protocols by the UNC Cystic Fibrosis (CF) Center Tissue Culture Core. Briefly, primary cells were expanded on plastic to generate passage 1 cells and plated at a density of 250k cells per well on permeable Transwell-Col (T-Col, 12mm diameter) supports (59, 156). HAE cultures were generated by provision of an air-liquid interface for 4-6 weeks to form well-differentiated, polarized cultures that resemble *in vivo* pseudo-stratified mucociliary epithelium (156). All virus work was performed in a Class II biological safety cabinet in a certified biosafety level 3 laboratory containing redundant exhaust fans while wearing Tyvek suits and PAPRs as described(247).

Construction of Chimeric SARS-CoV bearing the SZ16 spike protein "icSZ16-S". The Baric laboratory's infectious clone for the epidemic strain is divided into six subgenomic cDNA clones (A–F) that span the SARS-CoV genome. The first two thirds of the S gene is located within the icSARS E fragment (21492-24056) and the last third is located within the icSARS F fragment (nt 24057–25259). A synthetic DNA containing SZ16 nucleotides 21541-24056 was purchased from Blue Heron Technology (Bothell, WA). The fragment was digested with AgeI and XbaI (NEB, Ipswich, MA), and cloned into the existing icSARS-E pSMART plasmid, replacing the Urbani S glycoprotein with the SZ16 variant sequence to create icSZ16-E pSMART. Within the SARS-F fragment, the two remaining coding changes of the SZ16 S were introduced via PCR and the class II restriction enzyme AarI. Briefly, three amplicons A, B, and C were generated by PCR using Expand High Fidelity Polymerase (Roche, Indianapolis, IN). Primer pairs are as follows: Amplicon A (PasIF 5'-CTGTTTTCCCTGGGATCGC-3', AarIM1NR 5'-NNNNNNCACCTGCTTTTGGGCAACTCCAATGCC -3') Amplicon B (AarIM1NF 5'-NNNNNNCACCTGCAGTTGCCCAAAATGTTCTCTATGAGAAC -3', AarIM2NR 5'-NNNNNNCACCTGCATTTCTTCTTGAATGTTGACGACAGAAG-3'), and Amplicon C (AarIM2NF 5' NNNNNNCACCTGCTCAAGAAGAAATTGACCGCCTC-3', BamHIR 5'-

CATAAATTGGATCCATTGCTGG-3'). A, B, and C amplicons were digested with AarI for 1.5hr at 37˚C (Fermentas, Burlington, Ontario, Canada), gel purified and ligated to create the fragment ABC. ABC ligation products were gel purified and TA cloned into TOPO-XL (Invitrogen, Carlsbad, CA) to create pTOPO-XL ABC. The pTOPO-XL ABC subclones were sequence confirmed. pTOPO-XL ABC was BamHI digested at 37˚C for 1hr releasing a 2059nt fragment containing the icSZ16 F-fragment S sequence. icSARS F-pSMART was digested with BamHI at 37˚C for 1hr excising the epidemic strain S sequence while releasing a 5749bp vector fragment. The 2059bp SZ16 insert and the 5749bp vector fragments were gel purified using a QIAquick gel purification kit (Qiagen, Valencia, CA) and ligated (NEB, Ipswich, MA) to create icSZ16 F-pSMART.

Construction of Chimeric icSZ16-S K479N mutant. The icSZ16-E pSMART sequence for S residue 479 was mutated from lysine (AAA) to an asparagine (AAT) using overlap PCR. Amplicon A (NcoIF 5'-TGTTTCTAAACCCATGGGTACACAG-3', SZ16479R5'- CCATAATCATTTAATGGCCAATAAC-3') and Amplicon B (SZ16479NF 5'- GTTATTGGCCATTAAATGATTATGG-3', XbaIR 5'-GGGCCCTCTAGAGATCGAGC-3') were generated using Expand High Fidelity Polymerase (Roche, Indianapolis, IN). To join the fragments, Amplicons A (1010bp) and B (1153bp) were used as template in overlapping PCR with primers NcoIF and XbaIR. The final AB amplicon was purified using a Qiagen PCR purification kit (Qiagen, Valencia, CA) and digested with NcoI and XbaI (NEB, Ipswich, MA) for 1 hour at 37˚C. The digested amplicon (2.2KB) was gel purified using a QIAquick gel purification kit (Qiagen, Valencia, CA), ligated to the 5.3KB NcoI/XbaI fragment of icSARS SZ16-E pSMART and sequence verified.

Isolation of Recombinant Viruses. From the ligation of appropriate infectious clone fragments, icSZ16-S or icSZ16-S K479N full-length chimeric cDNA was generated, full-length transcripts were synthesized and mixed with polyadenylated N gene transcripts and then electroporated into cells as previously described(247). Clarified supernatants from the icSZ16-S or icSZ16-K479N electroporations were passaged onto naive Vero E6 cells to confirm the presence of replicating virus. If CPE was not detected, viruses were passaged every 48 hours on Vero E6 cells until cytopathology was observed. With icSZ16-S K479N, mild CPE was observed at passage 3 (p3) and more robust CPE was seen by passage 6 (p6). P3 and p6 icSZ16-S K479N viruses were plaque-purified in Vero E6 cells. The S, 3a, E, and M genes of the

recombinant viruses were sequence verified, and stocks were grown in T75 flasks and stored at -80˚C for future use.

RT-PCR to detect subgenomic leader containing transcripts. RT-PCR to detect subgenomic leader containing transcripts was performed to demonstrate viral replication. RNA from virus infected cells was isolated using TRIzol reagent (Invitrogen, Carlsbad, CA) according to protocol. 1-5µg of total RNA was used to generate cDNA by Superscript II (Invitrogen, Carlsbad, CA) using random hexamer primers (Invitrogen, Carlsbad, CA). cDNA was then used as template for PCR using Taq polymerase (NEB, Ipswich, MA) with a leader forward (CTCTTGTAGATCTGTTCTCTAAACGAAC) and reverse primer in the M gene (TTACTGTACTAGCAAAGCAATATTGTCG). Detection of GAPDH (GAPDHF 5'-CATGGGGAAGGTGAAGGTCG-3', GAPDHR 5'-TTGATGGTACATGACAAGGTGC-3') messages by RT-PCR was done as a positive control. PCR reactions were separated by gel electrophoresis on 1.8% agarose TAE gels and visualized by ethidium bromide staining.

***In vitro* evolution of icSARS SZ16 K479N in human airway epithelial cell cultures for 22 days.** Human airway epithelial cell cultures (HAE) were created as described(185). Cultures were infected with 10^5 pfu of icSARS-S K479N in a 200ul volume. After a 2hr infection, the inoculum was removed, the cells were washed briefly with DPBS, and then maintained for 4 days. After 4 days of infection, the apical surfaces of the cultures were rinsed and supernatants were placed onto the apical surface of fresh cultures for 1 hr, washed and maintained for another four days. Apical washes were then plaque purified to isolate icSZ16-S K479N D8 virus. 200µl of day 8 supernatants were used to infect naive HAE cultures as described above and the cultures were passaged two additional times at 4 day intervals and then 3 times every 48 hrs to preferentially enrich for more efficiently replicating virus variants. After 22 days of selection for efficient growth in HAE, the apical surfaces were rinsed and supernatants were plaque purified to isolate icSZ16-S K479N D22 virus. Plaques were expanded on 60mm dishes and RNA was isolated using TRIzol (Invitrogen Carlsbad, CA). Amplicons spanning from S, 3a, E and M genes were generated by RT-PCR and directly sequenced.

Generation of hACE2 expressing DBT cells. Plasmid encoding an N-terminal myc tagged human angiotensin I converting enzyme-2 (hACE2) was kindly donated by M. Farzan at Harvard Medical School. The hACE2 gene was amplified by PCR using Expand High Fidelity polymerase (Roche, Indianapolis, IN)

(ACE2For 5'-CACCATGTCAAGCTCTTCCTGGCTCC-3', ACE2Rev 5'-CTAAAAGGAGGTCTGAACATCATCAGTG-3'). Amplicons were gel purified using the QIAquick gel purification kit (Qiagen, Valencia, CA) and cloned into pcDNA3.1/V5-His (Invitrogen, Calrsbad, CA) according to protocol to create pcDNA3.1/V5-His hACE2. The ACE2 gene plasmid was sequence verified. Delayed brain tumor cells (DBT) cells were transfected with 4µg of pcDNA3.1/V5-His hACE2 using the Fugene reagent (Roche, Indianapolis, IN). After 24 hours, cells were placed under drug selection using 700µg/ml of G418 (Invitrogen, Carlsbad, CA) in complete growth media and remained under drug selection throughout all experiments. Cells were passaged 4 times, sorted for high ACE2 expression by flow cytometry, and then expanded under drug selection before use.

Growth curve analysis in HAE, Vero E6, DBT hACE2, or DBT cells. HAE cells were infected with $4.4x10^4$pfu of the recombinant epidemic strain icSARS, icSZ16-S K479N p3, icSZ16-S K479N D8, or icSZ16-S K479N D22 for 2 hours at 37˚C after which the inoculum was removed and apical surface rinsed with DPBS. At times 0, 6, 12, 24, 36, 48 and 72 hr post infection, the apical surface of the HAE was rinsed with 200µl DPBS and the samples stored at -80˚C until titration by plaque assay. Vero E6 and DBT hACE2 were infected with icSARS, icSZ16-S K479N p3, icSZ16-S K479N p6, icSZ16-S K479N D8, or icSZ16-S K479N D22 at an MOI of 0.01 for 1hr at 37˚C after which the inoculum was removed, the monolayer was rinsed with DPBS, and growth media was added. DBT cells were infected in a similar manner and with the same panel of viruses as the Vero E6 and DBT hACE2 except icSZ16-S K479N p3 was excluded from the experiment. Cell media was sampled at 0, 6, 12, 24 and 36 hours post infection (hpi) and samples were stored at -80˚C until titered by plaque assay(247). Growth curve data presented are representative of two separate experiments.

Immunohistochemistry of HAE infected cells. To detect SARS-CoV antigens in HAE, infected or mock infected cultures were fixed in 4% paraformaldehyde (PFA) for 24 hours, transferred to 70% ethanol and prepared as paraffin-embedded histological sections by the UNC CF Center Morphology and Morphometrics Core. After deparaffinzation, histological sections were incubated for 1 hour in PBS containing 3% bovine serum albumin (BSA). Primary antibodies directed against SARS N or tubulin were applied at a 1:100 dilution in PBS with 1% BSA overnight and detected with FITC or Texas Red secondary antibodies (Jackson ImmunoResearch). Immunofluorescence was visualized with a Leica Leitz DMIRB

inverted fluorescence microscope equipped with a cooled-color charge coupled digital camera (MicroPublisher, Q-Imaging). A tri-color filter cube set (GFP/Texas Red/DAPI) was used to show the morphology of the tissue section (by combining low level autofluorescence levels across the 3 filters) thus aiding determination of fluorescent antibody localization to specific regions of the cells.

Plaque reduction neutralization assay (PRNT). Neutralizing titers were determined by plaque reduction neutralization titer assay (PRNT) (172). 24hr prior to infection, 6-well plates were seeded with $5x10^5$ Vero E6/well. A human monoclonal antibody (mAb), S230.15, directed against the SARS-CoV RBD and an isotype control antibody directed against cholera toxin, D2.2, were kindly provided by A. Lanzavecchia. mAbs were serially diluted two-fold, and incubated with 100 pfu of either icSARS, icSZ16-S K479N p6, icSZ16-S K479N D8 or icSZ16-S K479N D22 for 1 hour at 37ºC. Virus and antibodies were then added to 6-well plates of Vero E6 cells in duplicate and incubated at 37˚C for 1 hour after which the cells were overlayed with 3ml of 0.8% agarose in media. Plates were incubated for 48 hours at 37ºC, stained with neutral red for 3 hours and plaques were counted. The percentage of neutralization was calculated as: 1-(number of plaques with antibody/number of plaques without antibody) x 100%.

Infection of 6wk old and senescent BALB/c mice. Six week old (Charles River, Wilmington, MA) or twelve month old female BALB/c mice were anaesthetized with a ketamine and xylazine mixture administered intraperitoneally in a 50µl volume. Each mouse was inoculated with $1x10^5$pfu/50µl of icSARS, icSZ16-S K479N p6, or icSZ16-S K479N D22 intranasally (n=10/virus in six week old animals, n=12/virus in twelve month old animals) and weight was monitored daily for four days post infection. On days two and four, three mice per group were sacrificed by isofluorane overdose and the lungs were removed for virus titer. One half of the lung was frozen at -80˚C until titration by plaque assay. Lungs were weighed, homogenized and PBS added to generate a 20% solution. The solution was then clarified by centrifugation and serially diluted for use in a standard plaque assay in Vero E6 cells(247).

Phylogenetic Analysis of SARS-CoV spikes and Computer Modeling. Nucleotide and protein sequence alignments of Urbani (GenBank Accession no. AY27841), HKU3 (GenBank Accession no. DQ022305), HC/SZ/61/03 (GenBank Accession no. AY515512), SZ16 (GenBank Accession no. AY304488), GD03 (GenBank Accession no. AY525636), GZ02 (GenBank Accession no. AY390556), and CUHK-W1 (GenBank Accession no. AY278554) were created using ClustalXv1.83(164). A neighbor joining tree was

generated from the ClustalX nucleotide sequence alignment, bootstrapped 1000 times, and exported into TreeView to create neighbor joining tree graphics(149). The numbers at each node represent the corresponding bootstrap value.

The crystal structure coordinates of SARS-CoV RBD interacting with the hACE2 receptor (PDB code 2AJF) were used as a template to generate each set of mutations using the Rosetta Design web server (http://rosettadesign.med.unc.edu/)(119). In each case, the SARS-CoV RBD structure was analyzed using the molecular modeling tool, MacPyMol (DeLano Scientific), to determine which amino acids were proximal to the amino acid(s) being targeted for replacement. Briefly, each amino acid to be altered was highlighted and all other amino acids within an interaction distance of 5 angstroms were identified. Using the Rosetta Design website, the amino acid replacements were incorporated and all amino acids within the 5 angstrom interaction distance were relaxed to allow the program to repack the side chains to an optimal energetic state. This process was repeated with each mutation and series of mutations. Ten models were generated for each set of mutations, and the best model, based on lowest energy score, was selected and further evaluated using Mac Pymol.

Results

Construction and characterization of icSZ16-S and icSZ16-S K479N viruses. Public genetic databases and synthetic biology were harnessed to rapidly translate electronic S gene sequence information into S gene DNA fragments. The SZ16 virus was isolated in live animal markets in China and its sequence was published in 2003. When comparing nucleotide sequences of S proteins isolated over the course of the epidemic, the SZ16 S is similar to viruses isolated from Chinese horseshoe bats (HKU3) and to the evolved human adapted strains (Figure 1A). The SZ16 S differs from the epidemic strain in 18 amino acid positions, 16 of which reside in the S1 region and may well represent the progenitor strains for the 2003 human epidemic. Much of the SZ16 sequence variability maps in and around the three known neutralizing epitopes marked as regions A, B, and C (Figure 1B) suggesting that human monoclonal antibodies derived from human SARS-CoV infections might be less efficacious against SZ16 early civet isolates. As the SZ16 virus could not be successfully maintained in culture, we used synthetic biology and reverse genetics to molecularly resurrect a recombinant and genetically modifiable SARS-CoV bearing the SZ16 S glycoprotein (icSZ16-S) (Figure 1C).

Although icSZ16-S recombinant virus infection was not evident by cytopathology-based assays or by plaque assay, RT-PCR confirmed the presence of virus replication within the electroporated cell culture by detecting subgenomic leader containing transcripts for ORFs 3a, E, and M (Figure 2A). The transfer of icSZ16-S supernatants from the electroporated cell culture to naïve Vero E6 or a mink lung epithelial cell (Mv1Lu) cultures did not result in productive infection as leader containing transcripts were not detected (Figure 2B). As a positive control, we passaged icSARS supernatants to Vero E6 and Mv1Lu cultures and both infections resulted in detectable wild type virus replication by RT-PCR (Figure 2B).

Since the icSZ16-S genomic RNA was capable of replicating in Vero E6 cells but progeny virions were incapable of re-infection and amplification, we hypothesized that infection was blocked due to inefficient S glycoprotein and ACE2 receptor interaction. In 2005, Li et al crystallized the RBD of SARS-CoV bound to ACE2 and proposed that residues 479 and 487 of the civet S inhibited efficient usage of the human ACE2 receptor(119). Using site directed mutagenesis, we changed residue 479 of the SZ16 S from lysine to the more human tropic asparagine (K479N), constructed and recovered the recombinant virus (icSZ16-S K479N). Unlike icSZ16-S virus, icSZ16-S K479N infection could be passed in Vero E6 cell cultures by the transfer of supernatants to naive cell cultures (Figure 2C) providing direct support for the hypothesis that SZ16 infection of human and/or primate cells is blocked by civet S residue at position 479.

***In vitro* evolution of icSZ16-S K479N virus in primary human airway epithelial cell cultures (HAE)**. Zoonotic reintroductions represent the most likely mechanism for reemergence of epidemic SARS-CoV strains in human populations. The SZ16 S K479N mutation permitted binding and entry into primate cells but our preliminary data suggested that infections of HAE were inefficient (data not shown). To select for civet viruses with enhanced growth in HAE, cultures were apically infected with icSZ16-S K479N, maintained and passaged for a total of 22 days. The virus isolated after 8 days in culture, icSZ16-S K479N D8 (D8), contained one mutation from tyrosine to phenylalanine at position 442 within the RBD (Y442F). The virus recovered after 22 days in culture, icSZ16-S K479N D22 (D22), contained the Y442F mutation as well as an additional mutation within the RBD from leucine to phenylalanine at position 472 (L472F). No other coding mutations were found in the S, 3a, E, or M genes. Interestingly, both 442 and 472 are contact residues between S and ACE2 according to the reported crystal structure (119).

Evolved D8 and D22 viruses exhibit growth kinetics similar to the epidemic strain in various cell types. The growth fitness of icSARS, icSZ16-S K479N p3 and the HAE evolved D8 and D22 viruses were assessed on HAE, Vero E6, murine DBT cells stably expressing hACE2 and on nonpermissive murine DBT cells. HAE cultures were infected with $4.4x10^4$pfu virus for 2 hours, rinsed and apical wash samples were taken over 72 hours post infection (hpi) to monitor virus growth. The epidemic strain, icSARS, grew to peak titers approaching 10^7pfu/ml by 72 hpi (Figure 3A). icSZ16-S K479N p3 grew poorly in the HAE cultures with peak titers only approaching 10^3pfu/ml (Figure 3A). As compared to the epidemic strain, the D22 virus grew with similar growth kinetics at early time points but peak titers were reduced by about 1 log and approached ~10^6pfu/ml by 72 hpi (Figure 3A). The D8 virus' growth lagged at early time points but recovered to grow to peak titers similar to that of the D22 virus (Figure 3A). In Vero E6 cells, the epidemic strain and the D22 virus reached peak titers of 10^7pfu/ml 24hpi while icSZ16-S K479N D8, icSZ16-S K479N p3, and icSZ16-S K479N p6 grew to 10^5pfu/ml (Figure 3B).

To model the SARS S and hACE interactions within the primary HAE cells and to prove that these mutations were influencing docking and entry via hACE2, we constructed DBT cells that stably express hACE2. In comparison to HAE, viral growth kinetics were more rapid in DBT-hACE2 although the overall trends in growth among viruses were more or less conserved. In DBT-hACE2 cells, icSARS replicated to peak titers of 10^7pfu/ml by 24hpi and then diminished over time to 10^6pfu/ml by 36hpi (Figure 3C). Similar to the HAE model, early growth of the D22 virus was more rapid than the D8 virus in DBT-hACE2, but the D8 virus never matched the D22 virus growth even after 36 hrs post infection (Figure 3C). Similar to the HAE, the icSZ16-S K479N p3 and the icSZ16-S K479N p6 viruses replicated poorly in DBT-hACE2 cells reaching titers of only 10^3pfu/ml by 36hpi (Figure 3C). DBT cells did not support the replication of any of the viruses within our panel supporting the hypothesis that the expression of ACE2 within DBT-hACE2 cells is required for the growth of all viruses within our panel (Figure 3D).

Immunohistochemistry of infected HAE. Host range expansion of other coronaviruses resulted in a change in cell tropism that was oftentimes associated with a change in receptor usage (34, 137). To determine the types of cells were infected by our panel of virus in HAE, infected cultures were fixed and sectioned for histological staining of SARS-CoV nucleocapsid antigen and tubulin for the staining of cilia. SARS N antigen was not detected in mock infected cultures though cilia on the apical surface of ciliated

epithelial cells are stained brightly (Figure 4A). SARS N antigen is readily detected within the ACE2 expressing ciliated cells of icSARS (Figure 4B) and D22 (Figure 4D) infected cell cultures but is only sporadically detected in icSZ16-S K479N p6 (Figure 4C) infected cell cultures. Nevertheless, the HAE evolved D22 and parent zoonotic icSZ16-D K479N viruses encode ciliated cell tropisms that were similar to that seen in late phase epidemic strains.

Plaque reduction neutralization assay using human monoclonal antibody S230.15. Future outbreaks of SARS-CoV would most likely emerge from pools of zoonotic virus and it is imperative that vaccination or sero therapies be effective against both past and future emergent zoonotic strains. S230.15 is a human monoclonal antibody (mAb) that is broadly neutralizing through the binding to the RBD though the specific location of the epitope is unknown(205, 256). The epidemic strain and the evolved D8 and D22 viruses are equally neutralized by S230.15 (PRNT50 0.0625µg/ml) while the icSZ16-S K479N is eight times more resistant (PRNT50 0.5µg/ml) (Figure 5). Since icSZ16-S K479N and the evolved D8 virus only differ in one amino acid within the S protein, these data suggest that the S230.15 epitope resides near residue 442. Moreover, these data suggest that as SZ16-like zoonotic SARS-CoV adapt to the hACE2 receptor in the human airway, they may become more susceptible to S230.15 neutralization, especially if they evolve mutations at residue 442. As an isotype control, an irrelevant cholera toxin specific antibody (D2.2) was used in a PRNT assay with the mutant virus panel and none of the viruses were neutralized at any concentration of antibody (Data not shown).

icSZ16-S K479N and D22 virus replicate in lungs of young BALB/c mice but do not cause clinical signs in young or senescent BALB/c mice. Since the epidemic strain may no longer exist in nature and future epidemic SARS-CoV strains would most likely evolve from zoonotic pools of virus, it is prudent to employ an antigenically divergent panel of zoonotic challenge viruses to assess therapeutic efficacy and cross reactivity. To this end, it is imperative that challenge virus behave similarly in current animal models used to assess vaccine efficacy. Infection of young BALB/c mice with SARS Urbani typically does not cause clinical signs(41, 169). Young mice that were either mock infected or infected with icSARS, icSZ16-S K479N or D22 viruses did not lose weight or present with other clinical signs (Figure 6A). Clinical outcomes in senescent mice infected with icSZ16-S K479N or D22 mirrored that of young mice with senescent mice losing little to no weight following infection (data not shown). The icSZ16-S K479N

and D22 viruses replicated in the lungs of young BALB/c mice to similar titers as the epidemic strain on day two post infection (pi) (~$3x10^6$pfu/g) (Figure 6B). By day 4 pi, the titers of the SZ16 lineage viruses were about 1 log lower than the epidemic strain suggesting that the civet viruses might be cleared more rapidly (Figure 6B).

Rosetta Design modeling of S RBD and ACE2 interactions. Rosetta design was used to model hACE2's interactions with the RBDs of SZ16, SZ16 K479N, D8 and D22 viruses. In contrast to the epidemic strain N479 residue, the SZ16 K479 residue appears to electrostatically clash with ACE2 binding partners K31 and H34. After a point mutation (K479N) is introduced in the civet S RBD, the repulsive forces of the civet K479 are eradicated allowing for S and ACE2 binding(Figure 7A, B and C). The Urbani RBD residues 442 and 479 are predicted to have single hACE2 binding partners (442 interacts with H34, 479 interacts with K31) (Figure 7A). Though residues 442 and 479 of the SZ16 K479N RBD are identical to Urbani, residues 442 and 479 are predicted to compete for hACE2 binding partners H34 and 442 is also predicted to interact with H34 and K31 of hACE2 (Figure 7C). The difference in binding efficiencies of seemingly similar Urbani and K479N RBD is likely due to subtle alterations of the RBD hydrogen-bonding network created by mutations at the peripheral RBD residue 487. Residue S487 of SZ16 K479N RBD binds to one ACE2 residue while T487 of Urbani binds to three residues of ACE2 thereby enhancing S and ACE2 binding interactions (Figure 7C). The Rosetta Design model predicts that the Y442F mutation within the D8 S protein creates an RBD architecture similar to that of SARS Urbani where S residue F442 and N479 have singular and unique hACE2 binding partners (442 binds K31 of hACE2 and 479 binds H34 of hACE2) while retaining the S487 and Y41 interaction and hydrogen bonding network (Figure 7C and D). Finally, while the D8 L472 residue is predicted to have only two potential ACE2 binding partners (L79 and M82), the L472F mutation of the D22 S protein is predicted to increase the numbers of possible binding partners of ACE2 to three residues (L79, M82 and Y83) thereby strengthening S binding (Figures 7D and E).

Discussion

Past and present sporadic reemergence of Chikungunya, Ebola, and Nipah viruses highlight the severe pathogenic and epidemic potential of zoonotic viruses and the identification of the animal reservoir host is often elusive(85, 115, 125, 204, 222). Live animal markets in China and elsewhere have been

proven to be an important factor in cultivating food borne illnesses and cross species transmission of SARS-CoV, avian influenzas and other pathogens(143, 243, 244). Within the live animal markets of China, dense human and animal populations mix creating an environment ripe for the exchange of virus from animal to human and from human to animal. During the SARS-CoV epidemic, the Himalayan palm civet was identified as a principle source of the SARS-CoV zoonosis though 1,107 civets on farms that supplied the markets tested negative suggesting that the civets were infected within the markets(94). Moreover, sequence analysis of bat and civet associated SARS-CoV has provided more definitive evidence that bat associated SARS-CoV jumped the species barrier to infect civets and that bat and civet viruses are similar yet distinct from late phase epidemic strain isolates(28, 69, 108, 133, 159, 173).

After the identification of ACE2 as the cellular receptor for SARS-CoV, several investigators have defined the molecular determinants of virus and receptor interactions that allowed for epidemic SARS-CoV host expansion. Prior to this report, key residues in the civet S gene responsible for changes in host range were identified using SARS-CoV S pseudotyped retrovirus, but these results had not yet been not confirmed in the context of wild-type SARS-CoV infection *in vivo* or *in vitro*. In support of data from Li et al, we demonstrate that the civet spiked icSZ16-S virus was capable of a single round of replication following transfection of full length genomic RNA but was incapable of infecting naive Vero E6 cells in subsequent rounds of infection(119). However, introduction of a single amino acid mutation (K479N) in the icSZ16-S virus S allowed for low level spread and passage in Vero E6 cells. Both icSZ16-S K479N p3 and p6 viruses grew similarly in Vero and DBT-hACE2 cells suggesting that the slight differences in their ability to cause CPE did not affect virus binding, entry or replication fitness during the time observed and at the MOI used in our assays. Though we did not use icSZ16-S K479N p6 in our HAE growth studies, we would expect both p3 and p6 isolates to perform similarly since their growth kinetics in Vero and DBT-hACE2 cells were similar. Importantly, the K479N mutation did not result in a virus capable of efficient replication in HAE or DBT-hACE2 cells, supporting the argument that additional mutations are required to enhance the SZ16 S interaction with the human ACE2 receptor. The differences seen in icSZ16-S K479N growth in HAE and Vero E6 cells highlight the strength and relevance of the HAE model of the human airway. Even though the contact residues of primate and human ACE2 are predicted to be similar, the differences in icSZ16-S K479N growth in HAE and Vero E6 cells suggest that differences in primate and

human ACE2 proteins (89% similar on the amino acid level) may affect binding efficiency or that the abundance of mucous and a unique extracellular matrix on the surface of HAE differentially antagonizes virus entry. Thus, in order to study and model S protein and hACE2 interactions, HAE or DBT-hACE2 cells should be used as a more relevant alternative to Vero E6 cells. Importantly, expression of hACE2 in a nonpermissive DBT cell line rendered these cells permissive for icSARS, icSZ16-S K479N, D8, and D22 virus infection strongly supporting earlier hypotheses that ACE2 is the principle receptor required for docking and entry of both human and zoonotic strains(122).

In both canine parvovirus (CPV) and 1918 Spanish influenza H1N1, point mutations in viral structural proteins responsible for binding to the host cell were sufficient to catalyze host range expansion(86, 191). In 1978, two mutations in the capsid protein of feline parvovirus evolved that were sufficient to catalyze host expansion causing severe canine infection and a worldwide epidemic in CPV naïve canine populations(86, 150). In 1918, the zoonotic H1N1 influenza virus acquired two mutations in HA changing the preferential binding from the avian to the human sialic acid receptor. When the HA mutations were coupled with a few additional mutations in the genome, a human pandemic ensued with estimated deaths of 20-40 million(150, 191). Similar to CPV and H1N1 viruses, analyses of zoonotic and human SARS- CoV S sequences show a logical progression in S protein mutations that most likely fostered host range expansion and increased human pathogenesis(94). Of the 14 amino acids of S that contact 18 amino acids of ACE2, mutations at positions K479N or S487T have been shown to be equally essential for civet S adaptation to human ACE2(119). The K479N mutation removed an electrostatic clash, allowing the S RBD to interact with human ACE2, while S487T appears to have subtly remodeled the RBD through hydrogen bonding differences that optimized hACE2 binding. Considering our *in vitro* evolution data and sequence data from the SARS epidemic, we hypothesize that at least two independent mutational pathways can optimize hACE2 binding. The first was observed during the epidemic, where the S487T mutation optimized binding as described above. The second route occurred during our *in vitro* evolution, whereby the Y442F optimized hACE2 binding in the presence of the S487 variant.

ACE2 expressing ciliated epithelial cells in the airway are targets for SARS-CoV infection in humans, primate and rodent models making the HAE an important *in vitro* system to study molecular mechanisms of animal S adaptation to the human host(70, 71, 144, 168, 169). Since the icSZ16-S virus

could not be propagated in Vero E6 cells, we introduced the K479N point mutation in the virus S that was sufficient to allow multiple rounds of replication of the civet-spiked icSZ16-S K479N virus in cell culture. Passage of the icSZ16-S K479N recombinant virus in HAE resulted in the emergence of S variants that could replicate more efficiently. Surprisingly, S487T was not selected with the passage of SZ16 K479N but new mutations evolved within contact residues of the D8 and D22 virus RBDs (Y442F and L472F) that enhanced virus infection of HAE, Vero E6, and DBT-hACE2 cells. To rule out non-receptor specific cell culture adaptations that enhance entry into cells *in vitro*, we infected DBT cells and did not see evidence of virus growth with any of the viruses tested. Moreover, our immunohistochemistry of HAE infected cell cultures (Figure 4) suggests that *in vitro* evolved viruses and the epidemic strain infect similar cell types providing further support that non-receptor specific entry adaptations had not occurred in our model. Recent passage of a related coronavirus, mouse hepatitis virus (MHV), in cell lines resulted in variants with expanded host range due to the acquisition of a common non-receptor specific cell culture adaptation using heparin sulfate for virus entry into cells(34). Most recently, McRoy et al demonstrated that passage of MHV in cell lines resulted in expanded host range through mutations within the fusion peptide and heptad repeats demonstrating that host range can be governed by changes in spike fusogenicity(137). From sequence analysis, we concluded that the *in vitro* evolved mutations of icSZ16-S K479N had not created a heparin consensus binding site (XBXBBX) and that our adaptive mutations were constrained to the RBD.

To determine the potential impact of the mutations acquired during HAE passage, we used Rosetta Design to generate structural models of the SZ16, K479N, K479N D8 or K479N D22 RBDs, and then superimposed these models onto the existing crystal structure of the SARS Urbani RBD bound to hACE2 (PDB Accession no. 2AJF), (Figure 7A). Similar to Li et al, we observed that residue K479 of the SZ16 S inhibited binding to hACE2 by sterically clashing with residues K31 and H34 (Figure 7B). After the K479N mutation, the electrostatic repulsion at residue 479 is eradicated but Rosetta Design predicts that local remodeling within the RBD creates cross reactions whereby residues 442 and 479 of the K479N RBD compete with each other for interaction with partners H34, K31 and D32 of ACE2 (Figure 7C). It appears that Y442 could interact with all three hACE2 residues while N479 is only predicted to interact with H34 of hACE2. We predict that this network of competing interactions reduces the avidity between the K479N RBD and the hACE2 receptor by misaligning other key residues in the RBD. Of note, the only difference in

the receptor binding domains of SZ16 K47N and Urbani occurs at position 487. The fact that SZ16 K479N is compromised in growth compared to Urbani suggests that the hydrogen bonding differences between S487 of SZ16 K47N and Thr487 of Urbani influence the receptor interaction. During the 2003 epidemic, S487T likely evolved to eliminate this putative inhibitory effect. Interestingly, the D8 Y442F mutation also restores an optimal RBD by allowing for favorable amino acid packing that recreated an RBD architecture similar to that of wild type (Figure 7A and 7D). In this case, the D8 RBD residues 442 and 479 have distinct and unique interaction partners in hACE2, which likely restores avidity to near wild type levels, and may explain why D8 virus grows more efficiently than icSZ16-S K479N virus in cells expressing hACE2 (Figure 3C and 7D). Thus, at least two independent routes of evolution could increase S RBD and human ACE2 interactions. Leucine 472 of the icSZ16-S K479N and the D8 RBD interacts with L79 and M82 of ACE2. The D22 virus RBD is mutated at position 472 from leucine to phenylalanine, which Rosetta Design predicts will induce strong hydrophobic interactions between F472 and partners L79, M82 and Y83 of ACE2 (Figure 7E). The D22 virus F472 mutation likely strengthens the binding interface of the D22 virus over the D8 strain, which may explain why the D22 virus has a growth advantage over the D8 virus in HAE, Vero E6 and DBT-hACE2 cells. Of note, it is possible that these viruses acquired replication enhancing mutations in structural or non-structural genes that we did not sequence. Nevertheless, these data demonstrate the plasticity of the RBD-ACE2 interface site and its ability to subtly remodel the RBD and hACE2 binding interface to promote efficient entry and growth. Clearly, multiple genetic pathways likely exist to allow for zoonotic SARS-CoV host range expansion and it will be interesting to determine if other contact interface point mutations can enhance zoonotic virus infection of HAE cultures.

Since viruses similar to the epidemic strain are currently circulating in bats in China, we may see yet another emergence of human SARS-CoV from zoonotic pools of virus. Therefore, it is imperative that current vaccination and passive sero therapies be effective against all known SARS-CoV zoonotic strains and their human adapted progeny. Previous work by Deming et al has highlighted the value of using zoonotic strains as challenge virus to assess vaccine efficacy(41). Deming et al demonstrated that sera from animals vaccinated with epidemic strain antigen were not as effective in neutralizing the zoonotic icGD03-S virus as compared to the epidemic strain(41). Within this study, we demonstrated that two zoonotic spiked viruses, icSZ16-S K479N and icSZ16-K479N D22, grew to peak titers in the mouse lung

similar to that of the epidemic strain two days post infection. In contrast to recombinant SARS-CoV bearing early human (GZ02) or civet (HC/SZ/61/03) S proteins that were extremely pathogenic in aged animals, icSZ16-S K479N and icSZ16-S K479N D22 caused little to no disease in either young or senescent BALB/c mice(172). Although the SZ16 and HC/SZ/61/03 viruses are both of civet origin, their S proteins differ by 18 amino acids(69, 246). The 7 month period of time in between the isolation of SZ16 (May 2003) and HC/SZ/61/03(December 2003) isolation may help explain their sequence differences(69, 246). Zoonotic SARS-CoV infection of humans is typically less severe than infection with human strains, but it is possible that the sequence differences between the SZ16 and the HC/SZ/61/03 S alter the structure of the S proteins such that the viruses bearing the HC/SZ/61/03 S are lethal in mice while our SZ16 lineage viruses are attenuated(28, 69, 110, 121, 172, 189). Nevertheless, icSZ16-S K479N and D22 viruses grow to similar levels as the epidemic strain in mice, and could be useful as challenge viruses to assess the efficacy of vaccines or sero therapies. The human monoclonal antibody, S230.15, binds within the RBD although the specific epitope has yet to be defined(205, 256). Recent data by Zhu et al have shown monoclonal antibodies S230.15 and to a lesser extent m396 are potent and cross neutralizing antibodies against human and zoonotic SARS-CoV isolates(205, 256). We have demonstrated that the "evolved" D8 and D22 viruses were equally susceptible to neutralization by the human monoclonal antibody S230.15 while the icSZ16-S K479N was eight times more resistant. In this instance, these data suggest that as zoonotic virus adaptation to the human ACE2 receptor may enhance susceptibility to neutralization by S230.15. Since there was a dramatic difference in neutralization between icSZ16-S K479N and icSZ16-S K479N D8, these data suggested that the epitope of S230.15 is in close proximity to residue 442 of the S protein or was affected by structural changes associated with mutation of residue 442. Future efforts to revive the divergent wild type icSZ16-S virus *in vitro* will be especially helpful at mapping the S230.15 epitope since it is possible that the K479N mutation may contribute to enhanced S230.15 binding. Even though S230.15 is less effective at neutralizing icSZ16-S K479N *in vitro*, recently published passive transfer studies in mice have shown that the S230.15 antibody is extremely potent and broad neutralizing *in vivo* where replication of SARS Urbani, icGD03-S and icSZ16-S K479N were not detected in the mouse lung(256). These data highlight the power and utility of zoonotic strains in assessing the efficacy of passive sero therapy both *in vitro* and *in vivo*.

In conclusion, synthetic biology has been employed to rapidly construct and assemble a completely synthetic and infectious 5.3KB bacteriophage, poliovirus, 1918 influenza virus and a panel of SARS viruses bearing animal and human S glycoproteins(24, 41, 172, 186, 209). We provide yet another example of the utility of synthetic biology by resurrecting the civet SZ16 S. We have shown that a single point mutation (K479N) in the SZ16 S facilitates host range expansion but additional mutations must occur for robust infection of human cells. Mutation of residue 479 (K479N) and 487 (S487T) occurred during the early phase of the SARS-CoV epidemic to help facilitate host range expansion. Though we did not generate a mutant SZ16 S containing S487T, previous studies have shown that the inclusion of either 479 or 487 in pseudotype virus bearing the civet S allowed for infection of human cells but this approach provides little information on growth efficiency and spread. Through our *in vitro* evolution of the icSZ16-S K479N virus, we discovered a novel evolutionary path by which SARS-CoV S can interface with hACE2 to allow for efficient infection of human cells. When comparing S mutations acquired during our *in vitro* evolution to mutations that occurred during the evolution of the epidemic strain, the plasticity of the SARS-CoV S protein becomes starkly apparent. Through the use of HAE cultures, synthetic biology, reverse genetics and animal models, we have created a system to isolate and characterize novel genetic pathways of zoonotic SARS-CoV S adaptation to the human ACE2 receptor. We have also generated antigenically divergent SARS-CoV zoonotic strains that might be useful in assessing SARS-CoV vaccine or sero therapy efficacy. Since future emergence of SARS-CoV will most likely evolve from zoonotic pools of virus, it is imperative that current vaccination and passive sero therapies be effective against zoonotic virus, epidemic strain virus and all of the evolutionary permutations in between.

Acknowledgements We would like to thank Dr. Michael Farzan at Harvard Medical School for kindly providing the hACE2 expression plasmid. We would also like to thank Antonio Lanzevecchia at the Institute for Research in Biomedicine, Bellinzona, Switzerland for graciously provided mABs S230.15 and D2.2. We would also like to thank Boyd Yount for superb technical assistance and expert cloning advice. This work was supported by research grants (R01 AI059136 and AI059443) to RSB from the National Institutes of Health, Division of Allergy and Infectious Diseases.

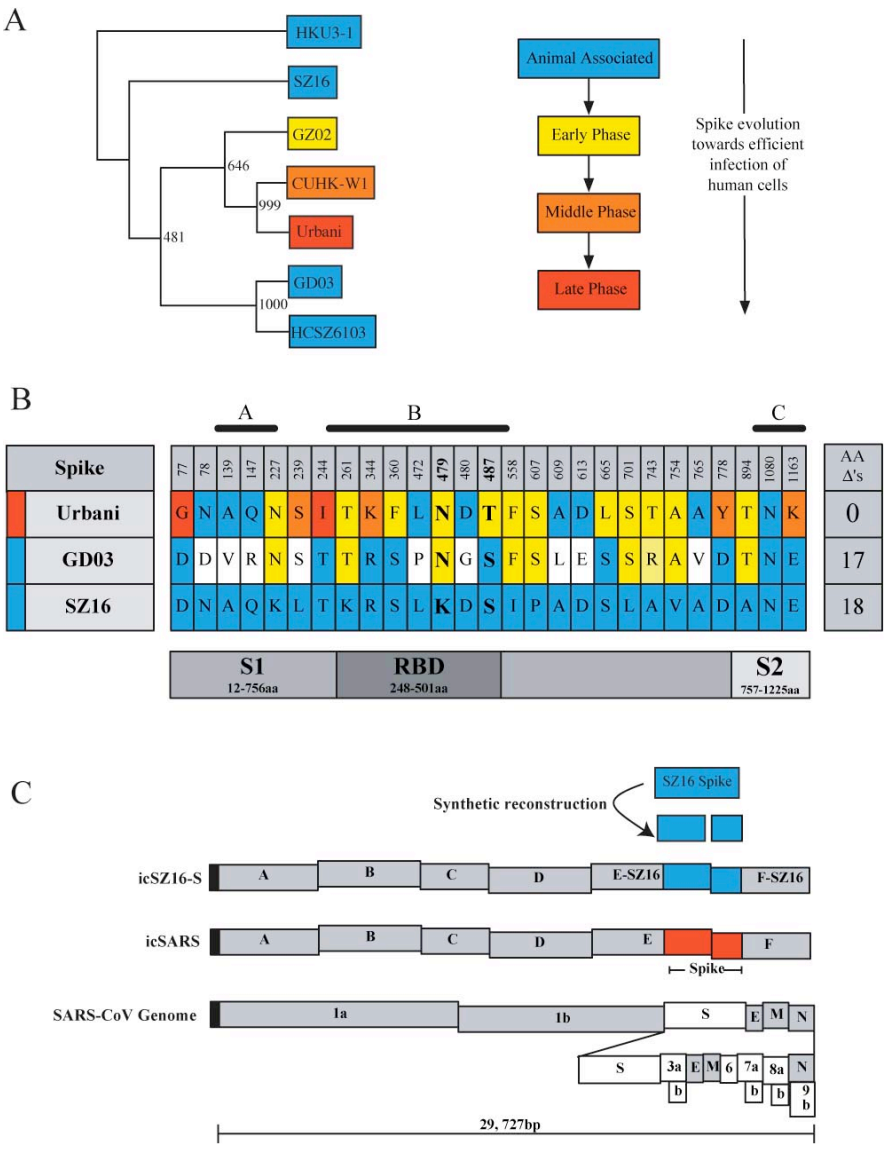

Figure 1: Phylogenetic relationships of zoonotic SARS-CoV and construction of zoonotic spike chimeras within the SARS-CoV infectious clone. Colors in panels A, B, and C denote the phase of the SARS-CoV epidemic at which the viruses or amino acid residues evolved. Blue = animal associated, yellow = early phase, orange = middle phase, and red = late phase. (A) Neighbor joining tree constructed from nucleotide sequences of various SARS-CoV S genes. Numbers represent bootstrap values based on 1000 bootstrap replicates. (B) Spike amino acid differences between Urbani, GD03 and SZ16. Known neutralizing epitopes are denoted as "A", "B" and "C". (C) Schematic of infectious clone fragments A-F and the SARS-CoV genes contained therein. Using synthetic biology and site directed mutagenesis, we reconstructed the SZ16 S that was then inserted into our infectious clone replacing the epidemic strain S.

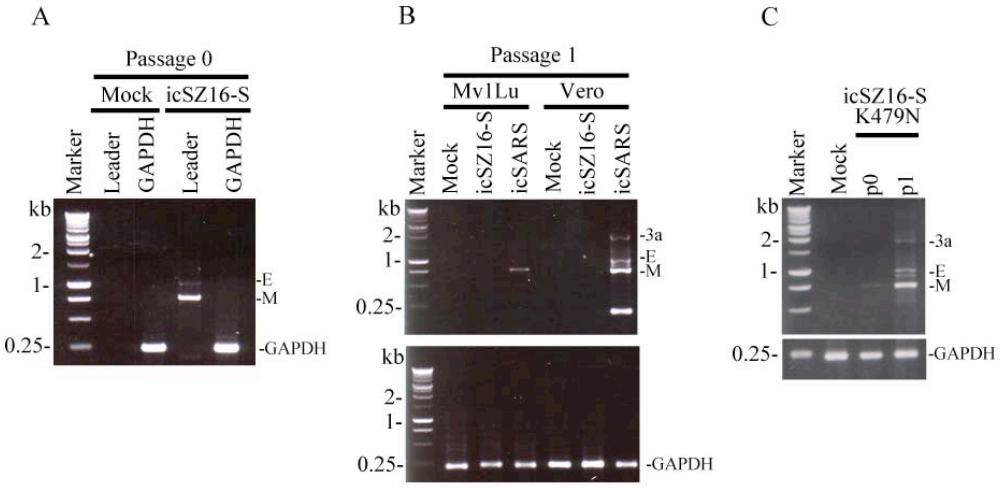

Figure 2: SARS-CoV SZ16 spike chimera, icSZ16-S, replicates in Vero E6 cells but infection cannot be passed in culture until a point mutation (K479N) is introduced within the receptor binding domain. The expected sizes of the target RT-PCR products are as follows: 3a (1796bp), E (949bp), M (666bp) and GAPDH (235bp). (A) RT-PCR for leader containing transcripts detects actively replicating genomic RNA. RT-PCR using RNA extracted from Vero E6 cells transfected with genomic icSZ16-S RNA (Passage 0) detects transcripts for the E and M gene of icSZ16-S. (B) Transfer of icSZ16-S supernatants from passage 0 to naïve Vero E6 or mink lung epithelial (Mv1Lu) cells does not result in a productive infection. As a positive control Vero E6 and Mv1Lu cells were successfully infected with epidemic strain supernatants as replication was detected by the presence of leader containing transcripts. (C) In contrast to wild-type icSZ16-S, a point mutation (K479N) in the icSZ16-S spike allows for passage of icSZ16-S K479N virus in Vero E6 cells.

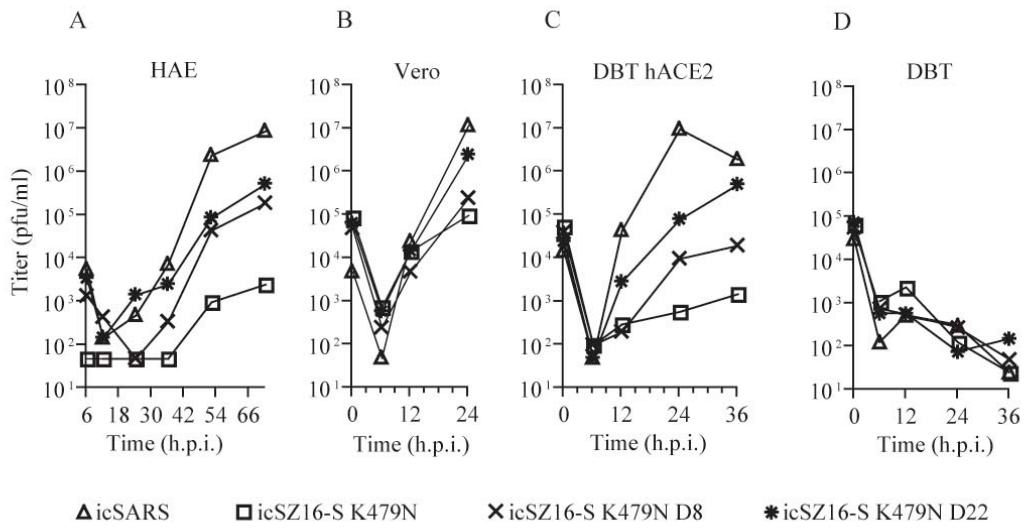

Figure 3: Growth curve analysis of the mutant virus panel in HAE, Vero E6, DBT-hACE2 and DBT cells. (A) HAE cultures were infected with $4.4x10^4$pfu/200µl of with the indicated viruses for 2hr at 37˚C, the inoculum was removed and apical surface was rinsed with DPBS. Apical washes were taken at 0, 6, 12, 24, 36, 48 and 72hr post infection. Virus titers were assessed on Vero E6 cells by standard plaque assay. (B-D) Vero E6, DBT-hACE2, or DBT cells were infected with the indicated viruses at an MOI of 0.01 for 1hr at 37˚C, the inoculum was removed, cultures were rinsed with DPBS and growth media was added. Media was sampled at 0, 6, 12, 24, and 36 hr post infection and virus titer was assessed by plaque assay on Vero-E6 cells. Data presented are representative of two separate experiments.

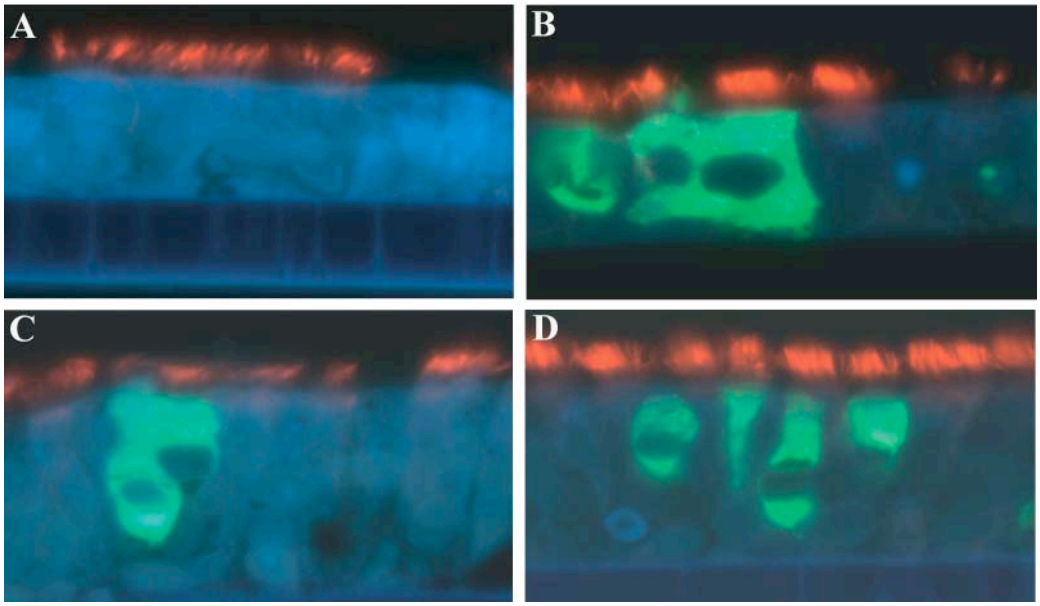

Figure 4: Immunofluorescence staining of HAE cultures infected with the mutant virus panel. At 72hr post infection, mock and infected HAE cultures were PFA fixed and paraffin embedded for tissue sectioning. Sections were stained for SARS-CoV N (FITC) and tubulin within cilia (Texas Red) and viewed by fluorescence microscopy at a magnification of 100X. Mock (A), icSARS (B), icSZ16-S K479N (C), and icSZ16-S K479N D22 (D).

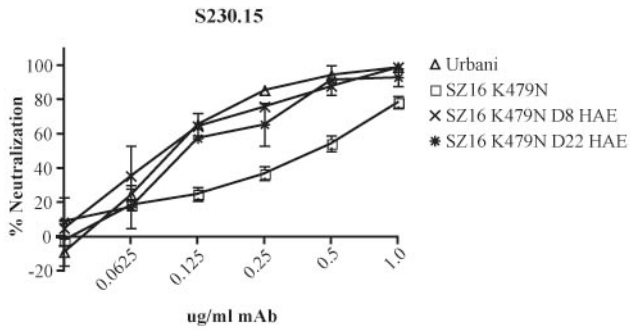

Figure 5: Plaque reduction neutralization assay of mutant panel virus using human monoclonal antibody S230.15. 100pfu of the indicated virus was incubated at 37˚C for 1 hr with 2-fold dilutions of antibody or DPBS in duplicate. After the incubation, the virus/antibody cocktails were used to infect Vero E6 cell monolayers for 1hr after which cultures were overlayed with growth media containing agarose. After 48 hr, plaques were enumerated. The percentage of neutralization was calculated as: 1-(number of plaques with antibody / number of plaques without antibody) x 100%. Error bars represent standard error of the mean.

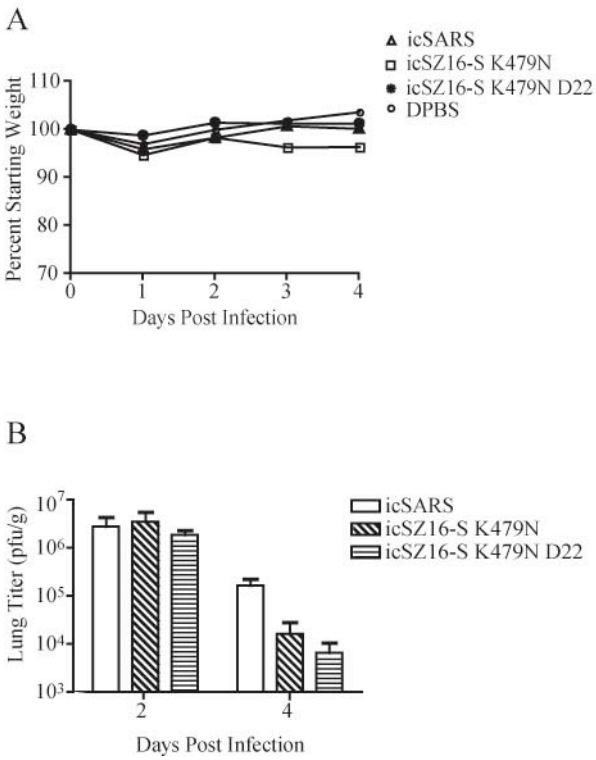

Figure 6: Clinical signs and lung titer of 6wk old BALB/c mice infected with DPBS, icSARS, icSZ16-S K479N or icSZ16-S K479N D22. (A) Mice were infected with 10^5pfu/50µl intranasally (n= 10 per virus) and weight was monitored daily. (B) Lungs were removed on days 2 and 4 post infected (n=3 mice per group per day), homogenized and centrifuged to pellet debris. Supernatants were used in a standard plaque assay to determine lung titer (pfu/g).

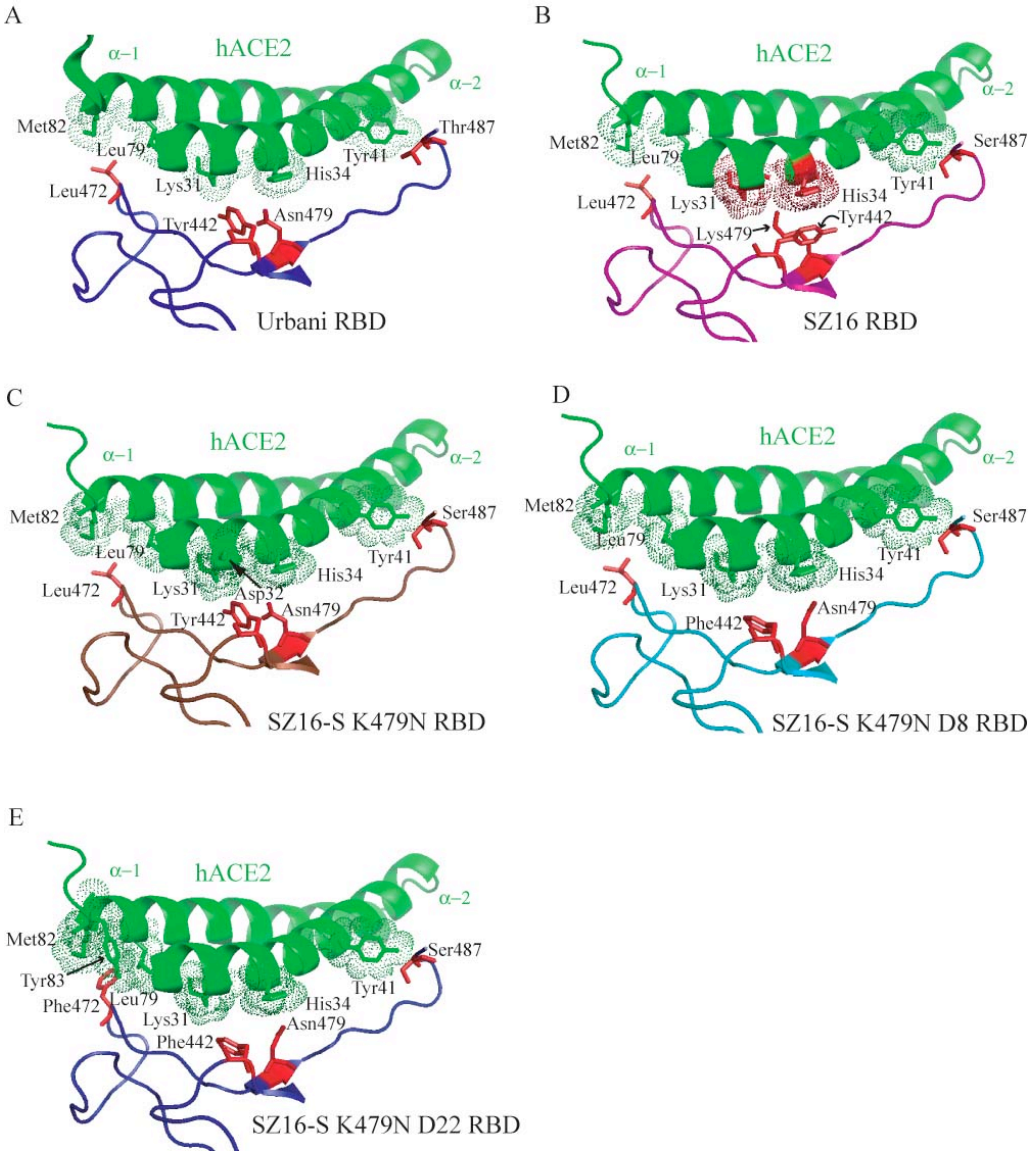

Figure 7: Rosetta Design modeling of "evolved" mutations that enhance spike binding to ACE2. Rosetta Design was used to generate structural models of SZ16 and mutant RBDs that were then superimposed onto the existing crystal structure of the SARS Urbani RBD bound to ACE2. (A) Epidemic strain and hACE2 RBD architecture (B) SZ16 and hACE2 interaction is inhibited by steric clashing, shown as red dots, of K479 of S and residues K31 and H34 of hACE2 (C) Electrostatic repulsion at residue 479 is eradicated allowing S and ACE2 binding but local remodeling within the RBD due to hydrogen bonding differences at residue 487 create cross reactions whereby residues 442 and 479 of K479N compete with each other for interaction partners H34, K31 and D32 of hACE2 (D) Y442F mutation of icSZ16-S K479N D8 restores an optimal RBD allowing for favorable packing to create an architecture similar to that of wild type (E) Leucine 472 of the icSZ16-S K479N and D8 S interacts with L79 and M82 of ACE2. The icSZ16-S K479N D22 L472F mutation is predicted to have hydrophobic interactions with three potential partners L79, M82 and Y83 of hACE2 that is predicted to increase stability of binding. Green dots on the hACE2 indicate residues which are within 4 angstroms and thus are predicted to interact with the S residues shown in red.

CHAPTER III

PATHWAYS OF CROSS SPECIES TRANSMISSION OF SYNTHETICALLY RECONSTRUCTED ZOONOTIC SARS-CoV

Abstract

Zoonotic SARS Coronavirus (SARS-CoV) likely evolved to infect humans by a series of transmission events between humans and animals for sale in markets in China. Virus sequence data suggests the palm civet served as an amplification host where civet and human interaction fostered the evolution of the epidemic strain SARS Urbani (Urbani). The prototypic civet epidemic strain of SARS-CoV, SZ16, was isolated from a palm civet but has not been successfully cultured in vitro. In order to propagate a chimeric recombinant SARS-CoV bearing an SZ16 Spike (S) glycoprotein, we constructed cell lines expressing the civet ortholog (DBT-cACE2) of the SARS-CoV receptor (hACE2). Zoonotic SARS-CoV were completely dependent on ACE2 for entry. Urbani grows with similar kinetics in both DBT-cACE2 and DBT-hACE2 cells while icSZ16-S only grows within DBT-cACE2 cells. In vitro "evolved" SZ16 S mutant viruses with enhanced affinity for hACE2 exhibited severe growth defects in DBT-cACE2 cells suggesting that evolutionary pathway that promoted efficient hACE2 interactions, simultaneously abolished efficient interactions with cACE2. Structural modeling reveals two distinct biochemical interaction networks by which zoonotic RBD architectures can productively engage hACE2. However only the Urbani mutational spectra promoted efficient usage of both hACE2 and cACE2 binding interfaces. Since dual species tropism is retained by Urbani, it is likely that it retained high affinity for cACE2/hACE2 receptors by evolving through repeated passage between human and civet hosts. Zoonotic SARS-CoV were variably neutralized by antibodies that were effective against the epidemic strain highlighting their utility to evaluate passive immunization efficacy.

Introduction

Within wet markets in China, a wide range of common and exotic food animals like bats and civets are sold live or as fresh meat for human consumption in part to improve health and sexual

performance (28, 69, 236, 238). In Southern China, the consumption of exotic animals is especially prevalent during the winter months when most respiratory tract infections are highly prevalent(236). Since many zoonotic viral pathogens are shed in stool, densely housed birds and mammals shedding excreta in the wet marketplace creates a ripe atmosphere for zoonotic virus transmission to human consumer populations(236). Most recently, wet markets in Southeast Asia have been associated with cultivating the cross species transmission of avian influenza H5N1 and the newly emerged severe acute respiratory syndrome coronavirus (SARS-CoV)(69, 108, 236).

In 2002, a novel coronavirus, SARS-CoV, emerged suddenly as the causative agent of severe acute respiratory syndrome (SARS) and spread worldwide causing about 8000 cases and >700 deaths(29, 173, 236). Viruses similar to the epidemic strain, SARS Urbani, were isolated from animals for sale within wet markets in China during the epidemic in 2003 and the reemergence in 2004(28, 69). Genome sequences of viruses isolated from bats, civets and humans suggest that viruses circulating in bats crossed the species barrier to infect civets who then served as an amplification host for yet another host range shift generating a human tropic virus(28, 69, 108, 122). Recent surveys of animal populations in North America, Africa, and China implicate bats as reservoirs of a diverse group of coronaviruses including SARS-CoV like progenitors(43, 44, 108, 109, 141, 234, 236, 237). As some bat species were found to be coinfected with more than one coronavirus lineage, recombination between and within genogoups and subsequent emergence of novel coronavirus is a real possibility(109). In 2007, surveys of wild Asian leopard cats and Chinese ferret badgers revealed the presence of yet more novel and highly divergent coronavirus circulating in animals typically sold in wet markets in China(44). Since viruses similar to the epidemic strain of SARS-CoV are currently circulating in zoonotic pools, the future emergence of a SARS-CoV like virus may occur. Therefore, it is imperative that current vaccination and passive immunization therapies be effective in protecting humans from infection by a wide range of epidemic and zoonotic SARS-CoV. Unfortunately, bat-SARS-CoV and the prototypic civet SARS-CoV strain, SZ16, have not been able to be cultured in vitro hampering our ability to evaluate their epidemic potential, pathogenesis and susceptibility to current therapeutic interventions within in vitro and in vivo models(108, 110).

SARS-CoV spike gene (S) sequences isolated from human cases during the early phase of the epidemic in 2002-2003 and during the reemergence of 2003-2004 are very similar to the SZ16 strain(28,

69, 94). SZ16 was isolated from palm civets in wet markets within Guangdong region of China during the epidemic and its S protein differs from the epidemic strain in 18 amino acids 16 of which reside in the S1 domain containing the receptor binding domain (RBD)(69). SARS GD03 was isolated from a sporadic human case during the reemergence in 2003-2004 and closely resembles those viruses isolated from civets and raccoon dogs within wet markets(28). SARS GD03 differs from the epidemic strain in 17 amino acids 16 of which reside in the S1 domain(28). Recently we have shown that a recombinant SARS-CoV bearing the SZ16 S (icSZ16-S) was capable of replication within Vero E6 cells but progeny virions were unable to infect naïve cell cultures, supporting evidence that the binding of the civet S to the human SARS-CoV receptor (angiotensin I converting enzyme 2, hACE2) was inefficient(122). Since clinical SZ16 isolates and our recombinant chimeric icSZ16-S virus could not be successfully cultured in vitro, the biology of the SZ16 S and its effect on virus growth and pathogenesis remains elusive.

In this study, we describe the recovery and growth of icSZ16-S in culture using cells stably expressing the civet ortholog (cACE2) of hACE2. Like the epidemic strain, both icSZ16-S and icGD03-S are completely dependent on ACE2 for entry. In DBT-cACE2 cells, icSZ16-S grows with similar kinetics to that of the epidemic strain but point mutations in the SZ16 S glycoprotein that enhance growth in hACE2 expressing cells abrogate growth in cACE2 expressing cells. The epidemic strain grows equally well in cACE2 or hACE2 expressing cells suggesting that epidemic strain evolution probably occurred through repeated exchange of virus between civet and human thus retaining dual host tropism. icSZ16-S and icGD03-S are moderately susceptible to neutralization by the human monoclonal antibody (mAb) S230.15. Unlike the epidemic strain, zoonotic viruses are resistant to mAb S3.1 suggesting that therapeutics successful against directed against the epidemic strain may not work as well against zoonotic viruses. These data highlight the utility of employing antigenically diverse zoonotic S panel of SARS-CoV in the study of host range expansion and antiviral therapy efficacy.

Materials and Methods

Viruses and Cells. The recombinant epidemic strain virus "icSARS" (GenBank accession no. AY278741), icSZ16-S (GenBank accession no. AY304488), icGD03-S (GenBank accession no. AY525636), icCUHK-W1 (GenBank accession no. AY278554), icGZ02 (GenBank accession no. AY390556), icSZ16-S K479N, icSZ16-S K479N D8, and icSZ16-S K479N D22 were propagated on Vero

E6 or DBT cells stably expressing cACE2 (DBT-cACE2) as described(41, 172, 179, 180, 247). icSZ16-S virus supernatant from the electroporated cell culture (passage zero), was passaged on DBT-cACE2 cells four times at 48hr intervals after which a robust cytopathic effect observed. icSZ16-S was then plaque purified on DBT-cACE2 cells and plaques were expanded in 6-well dishes of DBT-cACE2 cells. 6-well dish supernatant was used to infect a T175 flask of DBT-cACE2 cells to generate a virus stock that was harvested after 20 hours post infection (hpi). Viral RNA from the icSZ16-S virus stock was isolated using TRIzol (Invitrogen, Carlsbad, CA), cDNA was synthesized using SSII (Invitrogen, Carlsbad, CA) and amplicons spanning the S, 3a, E and M genes were generated by RT-PCR and directly sequenced. Virus stocks used throughout this study were grown and titered by plaque assay in Vero E6 and/or DBT-cACE2 cells as described(249). Vero E6 and DBT cells were grown in MEM (Invitrogen, Carlsbad, CA) supplemented with 10% FCII (Hyclone, South Logan, UT) and gentamycin/kanamycin (UNC Tissue Culture Facility). DBT-cACE2 and DBT-hACE2 were grown in Vero/DBT growth media supplemented with 700µg/ml G418 (Invitrogen, Carlsbad, CA). All virus work was performed in a Class II biological safety cabinet in a certified biosafety level 3 laboratory containing redundant exhaust fans while wearing Tyvek suits and PAPRs as described(249).

Generation of cACE2 expressing DBT cells. Plasmids encoding N-terminal myc tagged human (hACE2) and civet (cACE2) angiotensin converting enzyme-2 (ACE2) were kindly provided by M. Farzan at the New England Primate Research Center. The construction of the DBT-hACE2 cell line is described in Sheahan et al(180). The cACE2 gene was amplified by PCR using Expand High Fidelity polymerase (cACE2F 5'-caccATGTCAGGCTCTTTCTGGCTCC-3', cACE2Rh 5'-AAATGAAGTCTGAACGTCATCAG-3'). Amplicon was gel purified and cloned into pcDNA3.1/V5-His according to protocol. The cACE2 reverse primer did not contain a stop codon allowing for read through and the inclusion of a 6X his tag on the 3' end. pcDNA cACE2-His plasmids were sequenced and found to have two amino acid changes, G354D and R736Q, as compared to the published sequence (Genbank accession number AY881174) one of which (G354D) resides in a proposed interaction site with SARS S residues Y491 and G488 but these changes were also found in the parent gifted plasmid. Delayed brain tumor cells (DBT) cells were transfected with 4µg of pcDNA3.1/V5-His expressing cACE2-His or GFP-His using the Fugene reagent (Roche, Indianapolis, IN). After 24 hours, cells were placed under continuous

drug selection using 700µg/ml of G418 (Invitrogen, Carlesbad, CA). DBT-cACE2-His, DBT-hACE2, and DBT-GFP-His cells were passaged 4 times under drug selection and then sorted for high ACE2 or GFP expression and expanded for future use.

Cell sorting and FACS analysis of DBT expressing ACE2 stable cell lines. 10^6 DBT (control), DBT-hACE2, and DBT-cACE2-His cells were blocked with DPBS/5% FBS and stained with a polyclonal goat anti human ACE2 (R+D Systems, Minneapolis, MN) followed by a secondary anti-goat IgG-FITC (Invitrogen, Carlsbad, CA) antibody. Stained DBT, DBT-hACE2, DBT-cACE2-His and unstained DBT-GFP-His cells were sorted on a Cytomation Inc. MoFlo cell sorter (Dako, Denmark) for medium to high FITC or GFP expression and sorted cells were expanded in four passages after which stocks of DBT, DBT-hACE2, DBT-cACE2-His, DBT-GFP-His were cyropreserved for future experiments. To assess transgene expression in post-sorted cell stocks, $5x10^5$ DBT, DBT-hACE2, DBT-cACE2-His, DBT-GFP-His or Vero E6 cells were seeded into 6-well dishes. 24 hours later, media was removed and the cells were removed from the plate with Versene (UNC Tissue Culture Facility). Cells were stained for FACS analysis as done above and analyzed for FITC/GFP expression by FACScan (BD Biosciences, San Jose, CA).

Western blot analysis of DBT expressing ACE2 stable cell lines. To assess transgene expression in post sorted cell stocks by Western Blot, DBT, DBT-hACE2, DBT-cACE2-His, DBT-GFP-His and Vero E6 cells were seeded in 6-well dishes at $5x10^5$ cells/well. 24 hours later, cells were lysed with protein lysis buffer (1% Triton X-100, 0.5% SDS, in 1X TBS). 20µl of cell lysates were heated at 70˚C in 1X Nupage buffer/4% BME, loaded on a Nupage 12% Bis-Tris SDS PAGE gel (Invitrogen, Carlsbad, CA) and separated at 150 volts for 2 hrs. Proteins were transferred to nylon membrane using the NuPage transfer apparatus according to the manufacturers protocol. Membranes were blocked with 5% milk and probed with either polyclonal goat anti-human ACE2 (R+D Systems, Minneapolis, MN) or mouse anti-penta-His antibody (Qiagen, Valencia, CA). Membranes were washed with 1X TBS/0.1% Tween 20 and then probed with either rabbit anti-goat HRP (Invitrogen, Carlsbad, CA) or anti-mouse IgG-HRP antibody (Amersham, Piscataway, NJ). Membranes were rinsed and then treated with ECL Plus reagent (Amersham) and then exposed to radiographic film (Amersham).

RT-PCR to detect viral subgenomic leader containing transcripts, ACE2 and GAPDH transcripts. RT-PCR to detect subgenomic leader containing transcripts was performed to detect viral replication as

described in Sheahan et al(180). DBT, DBT-GFP-His, DBT-cACE2, DBT-hACE2, or Vero E6 cells were seeded at $5x10^5$ cells/well in a 24 well dish. 24hr later, cells were infected with 100µl of viral supernatant from the initial icSZ16-S transfection, icSARS supernatants or were mock infected. 24hpi, total RNA was isolated using TRIzol reagent (Invitrogen, Carlsbad, CA) according to the manufacturer's protocol. 1 µg of total RNA was used to generate cDNA by Superscript II (Invitrogen, Carlsbad, CA) using random hexamer primers (Invitrogen, Carlsbad, CA). cDNA was then used as template for PCR using Taq polymerase (NEB, Ipswich, MA). Evidence of SARS-CoV replication and subgenomic transcription (3a = 1796bp, E = 947bp, M = 666bp) was detected using a leader forward (CTCTTGTAGATCTGTTCTCTAAACGAAC) and reverse primer in the M gene (TTACTGTACTAGCAAAGCAATATTGTCG). Detection of ACE2 transcripts was performed using a conserved primer set capable of detecting primate, human and civet ACE2 (258bp) (ACE2RTF2 5'-AGCCTAAAATCAGCTCTTGG-3', ACE2RTR2 5'-CCGGGACATCCTGATGGC-3'). Detection of GAPDH (235bp) (GAPDHF 5'-CATGGGGAAGGTGAAGGTCG-3', GAPDHR 5'-TTGATGGTACATGACAAGGTGC-3') messages by RT-PCR was used as a positive control. PCR reactions were separated by gel electrophoresis on 1.8% agarose TAE gels and visualized by ethidium bromide staining.

Growth curve analysis in Vero E6, DBT-cACE2, DBT hACE2, or DBT cells. Vero E6, DBT-cACE2, DBT-hACE2 or DBT cells were infected with icCUHK-W1, icGD03-S, icGZ02, icSZ16-S K479N p6, icSZ16-S K479N D22, icSARS, or icSZ16-S, at an MOI of 0.01 for 1hr at 37˚C after which the inoculum was removed, the monolayer was rinsed with DPBS, and growth media was added. Virus stock titers generated by plaque assay in DBT-cACE2 cells were used to calculate MOI for the DBT-cACE2 growth curve. Virus stock titers generated by plaque assay in Vero E6 cells were used to calculate MOI for the Vero E6 and DBT-hACE2 growth curves. 25µl of cell media was removed at 0, 6, 12, 24 and 36 hpi and samples were stored at -80˚C until titered by plaque assay. For all growth curves except those performed within DBT cells, the cell type used for growth curve analysis was also utilized for the titration of growth curve samples by plaque assay. For example, samples generated from growth curves performed within DBT-cACE2 cells were titered on DBT-cACE2 cells. All DBT cell growth curve samples were titered on DBT-cACE2 cells. Since previous experiments suggested that Vero E6 and DBT-hACE2 cells were not permissive for icSZ16-S infection, icSZ16-S samples from DBT-hACE2 and Vero E6 growth curves were

titered on DBT-cACE2 cells. Growth curves were performed in duplicate. Growth curves were performed on two independent occasions and data shown is one representative experiment.

ACE2 blockade experiments in DBT-cACE2. DBT-cACE2 cells were seeded at $5x10^5$cells/well in 6-well dishes. The following day, cell media was removed and cells were incubated with 10, 5, 2.5, 1.25 or 0.625µg/ml polyclonal anti-ACE2 or anti-ACE antibody (R+D Systems, Minneapolis, MN) or DBPS for 1hr at 37˚C. After the 1hr pretreatment with antibody, 100pfu/50µl of icSARS, icSZ16-S, or icGD03-S, was added to the antibody mixture and incubated 1hr at 37˚C. After the infection, the inoculum was removed, the monolayer was rinsed with 2 times with 1ml DPBS then overlayed with 0.9% agarose in complete growth media. After 48hpi, plates were stained with neutral red and plaques were counted. The average percent blockade was calculated by dividing the average number of plaques per Ab dilution by the average number of plaques in the DPBS no Ab controls. Virus stock titers generated by plaque assay in DBT-cACE2 cells were used to calculate virus concentrations for the blockade experiment. Blockade experiments were performed in duplicate on two separate occasions.

Plaque reduction neutralization assay (PRNT). Neutralizing titers were determined by plaque reduction neutralization titer assay (PRNT) as described in Rockx and Sheahan et. al. (171, 172, 180). Briefly, 24hr prior to infection, 6-well plates were seeded with $5x10^5$ DBT-cACE2 cells/well. Human monoclonal antibodies (mAb) S230.15 and S3.1 directed against the SARS-CoV S and an isotype control antibody directed against cholera toxin, D2.2, were kindly provided by A. Lanzavecchia. mAbs were serially diluted two-fold, and incubated with 100 pfu of either icSARS, icSZ16-S, or icGD03-S for 1 hour at 37ºC. Virus and antibodies were then added to 6-well plates of Vero E6 cells in duplicate and incubated at 37˚C for 1 hour after which the cells were overlayed with 0.8% agarose in media. Plates were incubated for 48 hours at 37ºC, stained with neutral red for 3 hours and plaques were counted. The percentage of neutralization was calculated as: 1-(number of plaques with antibody / number of plaques without antibody) x 100%.

Computer modeling of RBD interactions with cACE2 and hACE2. Based on the reported crystal coordinates of SARS Urbani RBD interacting with the hACE2 receptor (PDB code 2AJF), we generated models of SZ16, SZ16-K479N, and SZ16 K479N D22 RBD interaction with either cACE2 or hACE2 using the Rosetta Design web server (http://rosettadesign.med.unc.edu/) as described(119, 180). Briefly, each amino acid to be altered was highlighted and all other amino acids within an interaction distance of 5

angstroms were identified. Using the Rosetta Design website, the amino acid replacements were incorporated and all amino acids within the 5 angstrom interaction distance were relaxed to allow the program to repack the side chains to an optimal energetic state. This process was repeated with each mutation and series of mutations. Ten models were generated for each set of mutations, and the best model, based on lowest energy score, was selected and further evaluated using Mac Pymol.

Results

Construction and Characterization of ACE2 expressing stable cell lines. Since previous efforts to culture either wild-type SARS-CoV SZ16 or recombinant icSZ16-S were unsuccessful, we used a cell based approach to resurrect icSZ16-S(110, 180). We constructed stable cell lines expressing cACE2-His, hACE2 and GFP-His in the DBT cell background. The gifted cACE2 gene utilized to construct our stable cells varied in two amino acids (G354D and R736Q) as compared to the published sequence. The stable cells were sorted for medium to high ACE2 or GFP expression and cultivated master cell stocks were analyzed by flow cytometry and Western Blot (Figure 1). By flow cytometry and Western Blot, hACE2 expressing cells had the highest ACE2 protein expression as compared to Vero E6 and DBT-cACE2. Contrary to the Western Blot analysis that was performed under reducing conditions, cACE2 expression by flow cytometry appears to be lower than that of Vero E6 cells although this may be mediated by less efficient interactions between polyclonal hACE2 antibody and cACE2 in its natural conformation in flow cytometry. In support of the hypothesis that polyclonal anti-hACE2 may not bind to cACE2 as efficiently in its natural conformation, the cACE2 and hACE2 proteins are only 83.5% similar. Positive control GFP-His exhibited a high level of GFP expression by flow cytometry and Western blot. ACE2 expression was not detected in untransfected DBT cells.

Resurrection of icSZ16-S in DBT-cACE2 cells. To assess virus replication and ACE2 transgene expression in our cell panel, we employed a highly sensitive RT-PCR based assay. In the coronavirus model of discontinuous transcription, subgenomic messages all contain the same 5' leader sequence(177). Thus, active SARS-CoV replication and mRNA synthesis can be detected by RT-PCR for viral subgenomic leader containing transcripts. In our assay, we use a forward primer directed against the leader sequence and a reverse primer in the M gene allowing us to preferentially detect subgenomic transcripts encoding the ORF 3a, E, and M genes. ACE2 transcripts were detected by RT-PCR in mock infected cell cultures of

DBT-hACE2, DBT-cACE2, and Vero E6 cell cultures (Figure 2). ACE2 transcripts were not detected in DBT cells corroborating our flow cytometry and Western blot results. As expected GAPDH positive control transcripts were detected at similar levels in all mock infected cell cultures while none of the mock infected cultures were positive for SARS-CoV replication (Figure 2). In the icSARS infected cell panel, DBT-cACE2, DBT-hACE2 and Vero E6 cells were clearly capable of supporting efficient SARS-CoV replication. Under identical conditions, SARS-CoV leader containing transcripts were not detected in control DBT and DBT-GFP-His cells (Figure 2). Interestingly, only cACE2 expressing cells efficiently supported the replication of icSZ16-S. Importantly, icSZ16-S was successfully passaged and maintained in DBT-cACE2 cells in vitro producing a robust cytopathic after four passages at 48hr intervals. Passage four virus was plaque purified, stocks were grown and the S, 3a, E and M genes were sequenced. Only one coding mutation (Y107H) was found in the 3a gene.

Assessment of virus growth in DBT, DBT-cACE2, DBT-hACE2, and Vero cells. Prior to this report, zoonotic SARS S and human/civet ACE2 interactions were evaluated using pseudovirus bearing GD03 and SZ16 S proteins but these assays were unable to address virus growth fitness(122, 242). Moreover, one study suggested that the GD03 S was not dependent on ACE2 for docking and entry(242). Consequently, we assessed the growth fitness of recombinant virus bearing various S glycoproteins derived from the early, middle and late phases of the SARS epidemic in China. We employed recombinant SARS-CoV bearing S genes isolated from humans during the early (icGZ02), middle (icCUHK-W1), and late (icSARS) phases of the epidemic and one isolate from a sporadic human case in early 2004 (icGD03-S). The GD03, GZ02 and CUHK-W1 S glycoproteins differ from the epidemic strain in 17, 8 and 2 amino acids, respectively (Figure 3D). We also evaluated the growth of icSZ16 parent virus and two SZ16 mutants previously described in Sheahan et al that were selected for efficient growth in human airway epithelial cells (HAE)(180). The SZ16, SZ16-K479N and SZ16-K479N D22 S glycoproteins differ from the epidemic strain in 18, 17, and 19 amino acids, respectively. The growth fitness of the virus panel was assessed within DBT, DBT-cACE2, DBT-hACE2 and Vero cell cultures (Figure 3A, B, C). Cultures were infected at an MOI of 0.01 for 1hr, subsequently washed to remove input virus, growth media was added and then sampled at various times post infection. DBT cells not transfected with the SARS receptor, ACE2, were not permissive to infection by any of the viruses tested (Data not shown). Within DBT-cACE2 cells, icSARS, icSZ16-S,

icGZ02, and icGD03-S grew to similar peak titers at 36 hpi (Figure 3A). In DBT-cACE2 cells at 12 hpi, icSZ16-S titers were approximately one log higher than all of the other viruses tested (Figure 3A). Interestingly, CUHK-W1 had severely delayed growth kinetics within the cACE2 expressing cells. Similarly, icSZ16-S K479N and icSZ16-S K479N D22 exhibited little to no growth in the DBT-cACE2 cells though their S proteins differ from SZ16 in 1 (K479N) and 3 (D22) amino acids (Figure 3A). Within DBT cells expressing the hACE2, the epidemic strain exhibited superior growth fitness as compared to the other viruses tested with a 1-2 log titer advantage at 12 hpi. Within DBT-hACE2, icSARS, icCUHK-W1, icGZ02, icGD03-S and icSZ16-K479N D22 grew to similar peak titers 36hpi while icSZ16-K479N grew more poorly reaching titers less than 10^4pfu/ml and icSZ16-S did not grow at all (Figure 3B). Vero E6 cell growth kinetics for icSARS, icCUHK-W1, icGZ02 and icSZ16-S K479N D22 were quite similar reaching titers around 10^7pfu/ml at 36hpi while icSZ16-S K479N and icGD03-S grew much more poorly (~10^5pfu/ml at 36hpi) (Figure 3C). As we had seen by RT-PCR, the Vero E6 cell was not permissive to infection by icSZ16-S (Figure 3C).

icGD03-S and icSZ16-S are dependent on ACE2 for entry. Using pseudotyped viruses, previous reports have suggested that some zoonotic SARS-CoV do not use ACE2 for entry(242). In order to assess receptor dependence of the recombinant SARS-CoV strains bearing zoonotic S proteins, we utilized a receptor antibody blockade assay (Figure 4). Two-fold dilutions of antibody (pAb anti-ACE2) or control antibody (pAb anti-ACE) were used to block ACE2 within DBT-cACE2 cells that were subsequently infected with 100pfu of icSARS, icGD03-S or icSZ16-S, rinsed and overlayed with media containing agarose. All three viruses tested were equally dependent on ACE2 for entry exhibiting a dose dependent response to anti-ACE2 receptor blocking antibody (Figure 4). Control antibody (pAB anti-ACE) was not capable of blocking entry of any of the viruses tested in a dose dependent manner firmly establishing that ACE2 is a receptor for both epidemic and civet strains of SARS-CoV (Figure 4).

mAb S230.15 and S3.1 neutralization profiles differ between epidemic, in vitro evolved and zoonotic strains of SARS-CoV. S230.15 and S3.1 are human monoclonal antibodies (hu-mAb) that were isolated from a convalescent SARS patient's B cells. In order to assess neutralization efficacy of the above hu-mAb, we employed a plaque reduction neutralization assay (PRNT) with the following challenge viruses: icSARS (epidemic strain S protein), icGD03-S (divergent human strain S protein), icSZ16-S (prototypic

civet strain), icSZ16-S K479N (SZ16 S protein mutated at residue 479 from lysine to asparagine), icSZ16-S K479N D22 (in vitro evolved mutant with enhanced growth within human cells whose S is mutated at Y442F and L472F). The broadly neutralizing hu-mAb, S230.15, was able to neutralize 50% (PRNT50) of icSARS and the evolved icSZ16-S K479N D22 virus using less than 0.03125µg/ml of antibody while icGD03-S, icSZ16-S K479N and icSZ16-S were approximately four times more resistant (PRNT50 = 0.125µg/ml) (Figure 5A). The S3.1 hu-mAb was not as effective at neutralizing the viruses tested (PRNT50: icSARS, icSZ16-S K479N = 0.25µg/ml, icSZ16-S K479N D22 = 0.625µg/ml) (Figure 5B). Unlike the S230.15, hu-mAb S3.1 was weakly efficacious against icGD03-S (PRNT50 >1µg/ml) and completely ineffective against icSZ16-S (Figure 5B).

Structure models provide insight into the retention of dual species tropism of SARS Urbani. In order to gain a better understanding of the structural changes associated with mutation of both S and ACE2 proteins, we developed predictive structure models of S and cACE2/hACE2 interactions within Rosetta Design. Our models suggest additional methyl groups in E30 and Y34 of cACE2 likely create an enhanced protrusion from the binding interface as compared to hACE2. The architecture of the Urbani RBD can accommodate this protrusion on the cACE2 binding interface thus retaining efficient binding to both cACE2 and hACE2 (Figure 6A and 6B). We and others previously have published structure models that suggest that K479 of the SZ16 S inhibits binding to hACE2 because of electrostatic clashes with hACE2 binding partners K31 and H34 but the SZ16 binding partners within cACE2 are mutated (Y34 and E30) and allow for efficient binding of SZ16 S(Figure 6C)(119, 122, 180). Interestingly, the human ACE2 adaptive mutations in SZ16 K479N and SZ16 K479N D22, that progressively remodel the RBD binding interface to enhance binding to hACE2 (Figure 6D and 6F) create a steric clash between the RBD V404/F440 and E30/Y34 of cACE2 (Figure 6E and 6G). Similar to what we had seen within in vitro growth analysis, the SZ16 K479N and D22 binding interface cannot accommodate the enhanced protrusion of cACE2 and are unable to bind efficiently.

Discussion

Recent emergence of viruses like SARS-CoV, Ebola, Influenza H5N1, Marburg, and Nipah viruses highlight the pathogenic and epidemic potential of zoonosis in human populations(63, 85, 115, 204, 236). The identification of zoonotic virus animal reservoirs are often unsuccessful hampering our ability to

understand the epidemiology of zoonotic diseases and the conditions required for zoonotic host range expansion. Extensive virus sequencing efforts allowed for the identification of palm civets as a potential amplification host for SARS-CoV and the Chinese horsehoe bat as the potential SARS-CoV animal reservoir in a short span of 2 years(28, 69). Though sequencing efforts have revealed much about the biology of zoonotic SARS-CoV, bat and civet isolates have not yet been cultured in vitro(108, 110). Using synthetic biology and reverse genetics we constructed a SARS-CoV bearing an SZ16 civet S glycoprotein. In corroboration with Lau and Peiris, we have shown that icSZ16-S could not be maintained by passage in cell cultures that normally support SARS-CoV infection(110). Without the successful cultivation of zoonotic SARS-CoV, their mechanisms of host range expansion and pathogenic potential remain elusive and the efficacy of current therapies against zoonotic strains remains unknown.

Rather than mutate the SZ16 S glycoprotein in order to promote growth in cell culture, we constructed a stable cell line expressing the civet ortholog (cACE2) of the human SARS-CoV receptor (hACE2). As compared to the published sequence, the cACE2 gene utilized to construct our stable cells differed in two residues, G354D and R736Q, but only the G354 resides in a proposed interaction site with SARS S RBD (Y491 and G488)(119). All of the viruses used within this study have the same amino acid at residues 491 (tyrosine) and 488 (glycine). In turn, if the G354D mutation in our cACE2 protein has a deleterious effect on binding and entry, we predict all viruses would be affected equally. As our data regarding Urbani and SZ16 binding to cACE2 and hACE2 is concordant with previously published data by Li et. al., we do not think the G354D mutation in cACE2 is altering our virus growth phenotypes(122). Within DBT-cACE2 cells, we have demonstrated that icSZ16-S can be grown, maintained and plaque purified. In support of Li et al, we have shown that civet SARS-CoV utilizes cACE2 but cannot utilize hACE2 or Vero E6 ACE2 confirming that the civet SZ16 virus is restricted in its host range (Figure 2B). Using pseudotyped lentivirus, Li et al showed that the SARS Urbani S is capable of utilizing both cACE2 and hACE2 and we confirmed these data showing that icSARS is capable of infecting both cACE2 and hACE2 expressing cells and replicating to high titer(Figure 2B, 3A, 3B). In support of our RT-PCR data that suggesting icSZ16-S was restricted in its host range (Figure 2B), icSZ16-S only grew within cACE2 expressing cells and grew to titers similar to the epidemic, icGD03-S and icGZ02 strains (Figure 3 A, B, and C). Interestingly, icSZ16-S exhibited a clear growth advantage at 12hpi suggesting that it gains entry

into cACE2 expressing cells more rapidly than the other viruses tested. The icSZ16-S K479N and D22 viruses were adapted for efficient growth on primary human airway epithelial cell (HAE) cultures known to be a robust and relevant model of the complex human airway epithelium. Importantly, these viruses did not grow efficiently within DBT-cACE2 cells suggesting that mutations in the civet S that enhanced growth in HAE (K479N, Y442F and L472F) diminished binding of the icSZ16-S K479N/D22 S protein to cACE2. In hACE2 expressing cells, the epidemic strain displayed a clear growth advantage at 12hpi but most all viruses tested grew to similar peak titers by 36hpi. In Vero E6 cells, the viruses bearing S proteins more similar to the epidemic strain (CUHK-W1, GZ02) grew to peak titers far greater than those viruses bearing S proteins more civet like (SZ16, GD03, SZ16 K479N). As we had expected, icSZ16-S was not capable of growth within DBT-hACE2 or Vero E6 cells but mutations in the SZ16 S at select interaction sites with ACE2 (K479N, Y442F, L472F) rescue and promote growth in hACE2 or Vero E6 cells. These data suggest the SARS-CoV S and receptor interactions are quite specific and capable of restricting host range or limiting infection efficiency. Moreover, these data also suggest that very few mutations in the civet S can enhance infection of human cells (K479N, Y442F, L472F) but simultaneously abrogate infection of cACE2 expressing cells. A corollary is seen in the more human tropic strains. icCUHK-W1, a middle phase epidemic isolate whose S differs from Urbani in 2 amino acids, is quite capable of infecting cells expressing hACE2 while it grows very poorly in cACE2 expressing cells as compared to the epidemic strain. These data suggest that G77 and/or I244 of the epidemic strain enhance growth in cACE2 expressing cells. Though G77 and I244 reside outside of the RBD (248-501aa), their close proximity to the RBD may either promote a rearrangement of the S protein subtly altering the S binding interface or somehow contribute to binding or entry by an unknown mechanism. Through passage of zoonotic S bearing SARS-CoV on Vero E6 cells, Rockx et al described mutations just outside of the RBD (HC/SZ/ 61/03, amino acid position 578, A031G, amino acid position 577) that seemed to enhance growth suggesting that mutations outside of the RBD influence the architecture of the binding interface or enhance binding and entry by an unknown mechanism(172). All together, the growth curve data highlight the plasticity of both zoonotic and human tropic SARS-CoV S proteins where the subtle remodeling RBD can both enhance and abrogate binding to ACE2.

Serological evaluation of workers in wet markets suggest that zoonotic SARS-CoV was transmitted to humans on occasion though these seropositive individuals did not clinically present with SARS(2). These data support the hypothesis that repeated transfer of zoonotic SARS-CoV from civet to human and/or from human to civet fostered the evolution of the epidemic strain. Our growth curve analysis demonstrated that the epidemic strain is equally fit at growth within cACE2 or hACE2 expressing cells. Our predictive RBD and ACE2 structure model data provide a possible explanation of how the dual host tropism of SARS Urbani is retained. The cACE2 molecule differs from hACE2 in two key residues (E30, Y34) that likely create a pronounced protrusion from the cACE2 binding interface. The Urbani RBD is able to accommodate the varied binding interfaces of both cACE2 and hACE2 thus retaining dual host tropism. These data suggest the epidemic strain's dual host tropism and RBD architecture may have evolved over time for efficient transfer of virus from civet to human and from human to civet. We also demonstrate that SZ16 lineage viruses passaged on HAE, in the absence of cACE2, evolved a mutant RBD that allowed for more efficient binding of hACE2 (icSZ16-S K479N, D22) but simultaneously lost the ability to efficiently infect cACE2 expressing cells. Our predictive structure models suggest that the human adaptive RBD mutations in icSZ16-S K479N and D22 abrogate their ability to accommodate the protrusive cACE2 binding interface. Therefore, we hypothesize that in the absence of evolutionary pressure to retain the ability to grow within both cACE2 and hACE2 expressing cells, a series of mutations are acquired to enhance binding to only one of the two receptors. We might have been able to generated a strain more similar to the dual tropic epidemic strain had we done repeated passage of icSZ16-S virus alternating between cACE2 and hACE2 expressing cells. Nevertheless, these data suggest that the natural evolution of the epidemic strain probably occurred through repeated transfer of virus from civet to human and from human to civet over a long period of time and the evolutionary pressure due to the necessity to infect human and civet hosts fostered the retention of dual ACE2 tropism. This hypothesis is supported by three serological surveys to determine the prevalence of SARS-CoV specific IgG in healthy subjects in China. First, samples collected from volunteers in Guangdong province in China in May 2003 demonstrated that SARS specific IgG was found in animal traders (13%, n= 508), hospital workers (2.9% , n = 137), Guangdong CDC workers (1.6%, n = 63), and healthy adults at the clinic (1.2%, n = 84)(2). The second study was a retrospective serological survey performed on 1,621 serum samples from March 2002 isolated

from healthy 18 year old male Chinese soldiers from 17 provinces including Guangdong(250). Of these 1,621 samples, 0.68% tested positive for SARS-CoV by ELISA though the province SARS-CoV IgG positive soldiers inhabited was not mentioned. A third study retrospectively examined 938 serum samples collected in May of 2001 from healthy adults in Hong Kong. Shockingly, 1.8% of these samples collected 2 years prior to the epidemic tested positive for SARS-CoV by immunofluorescence assay(252). These data suggest less serious or asymptomatic cases of SARS-CoV existed at least 2 years prior to the beginning of the epidemic in various geographical locations in China. If the sampled populations in the May 2003 cohort are representative of the Guandong province population (est. population of 100,000,000), there were probably many more unreported or less serious cases (>1,000,000) of SARS-CoV prior to the evolution of the highly pathogenic 2002-2003 epidemic strain.

In 2005, Yang et al reported that pseudovirus bearing zoonotic S (GD03 and SZ3) were much less dependent on ACE2 for entry in 786-O cells(242). Using 786-O cells and similar pseudoviruses bearing Tor2, GD03 or SZ3 S proteins, both Yi et al and He et al were not able to infect 786-O cells with pseudoviruses(79, 122). To reevaluate these findings in the context of live SARS-CoV infection, we constructed viruses bearing zoonotic S proteins within the natural SARS-CoV genetic background. The SZ3 S differs from SZ16 by one amino outside of the RBD (SZ3 F558, SZ16 I558). Since our molecular and growth curve data suggested that icSZ16-S only efficiently infects cACE2 expressing cells, we performed receptor blockade experiments in DBT-cACE2 cells. We found that icSARS, icSZ16-S and icGD03-S were similarly blocked from entry in a dose dependent manner using an antibody directed against ACE2 while the control antibody had little effect. Though we did not achieve 100% blockade with the highest concentration of antibody tested, we believe that polyclonal anti-hACE2 may interact less efficiently with native cACE2. Alternatively, we may not have completely saturated the available surface cACE2 which would result in an incomplete blockade. At this time, we believe it is more likely that our inability to block 100% of infection was due the technical issues discussed above and less likely that zoonotic viruses gain entry into cells via alternative receptors. However, co-receptors (L-SIGN) have been reported for SARS-CoV but to our knowledge, the ability of zoonotic SARS-CoV to engage these receptors has not been rigorously examined(90). Since the viruses we evaluated could not productively infect non-

transfected DBT cells, it is unlikely that the incomplete block in entry with Ab was due to entry via alternative receptors. We most likely did not block 20% of the surface ACE2 with 10μg/ml Ab.

Since it is impossible to predict the antigenic identity of future SARS virus emergents, the development of highly cross reactive antibody, drug or vaccination therapies would provide the greatest potential benefit to public health. Recently, we have shown that mAb S230.15 was less effective in neutralizing icSZ16-S K479N in vitro but was very effective in passive transfer studies in mice lowering viral titers of both icGD03-S and icSZ16-S K479N below the detectable limit(256). icSZ16-S and icGD03-S are also more resistant to neutralization by S230.15 as compared to the epidemic strain. Since icSZ16-S and icGD03-S are similarly neutralized by S230.15 in vitro, passive transfer studies by Zhu et al suggest that S230.15 would be effective against icSZ16-S in vivo as well(256). Yang et al described an antibody dependent enhancement (ADE) phenomenon using mAb S3.1 in neutralization assays in 786-O cells using GD03 and SZ16 pseudovirus(242). We performed PRNT assays in cACE2 cells using icSARS, icSZ16-S and icGD03-S and found that S3.1 is moderately effective against icSARS, weakly effective against icGD03-S and ineffective against icSZ16-S. Since there was such a dynamic range of neutralization efficacies using S3.1 against a panel of epidemic and zoonotic SARS-CoV, these data highlight pitfalls of using only the epidemic strain when evaluating passive immunization or vaccination therapies. Moreover, ter Meulen et al explored the possibility of ADE in human macrophages using SARS-CoV and subneutralizing concentrations of monoclonal antibodies and found that SARS-CoV is taken up by macrophages but does not productively infect the cells(200).

Coronavirus similar to SARS Urbani are currently circulating within bat species in China. Constant surveillance and biological evaluation of zoonotic pools of coronavirus is impractical making it quite difficult to predict the antigenic identity of SARS-CoV-like virus emergents in the future. Therefore, it is imperative that current antiviral therapies be broadly cross reactive against all know SARS-CoV thereby maximizing the potential public health benefit. We have constructed a SARS-CoV bearing the prototypic civet S protein from the SZ16 strain. Prior to this publication, SARS-CoV bearing the SZ16 S were not able to be propagated in vitro hampering the study of the SZ16 biology and its pathogenic potential. We have demonstrated that icSZ16-S can be propagated in vitro within DBT-cACE2 cell cultures, is dependent on ACE2 for entry and is incapable of using hACE2 for entry. We have also

demonstrated that point mutations in the SZ16 S protein that enhance virus growth in cells expressing hACE2 severely diminish growth in DBT-cACE2 cells while the epidemic strain retains dual ACE2 tropism. These data and retrospective serological surveys in China suggest that the natural evolution of the epidemic strain probably occurred through repeated transfer of virus from civet to human and from human to civet over a long period of time and the evolutionary pressure due to the necessity to infect human and civet hosts fostered the retention of dual ACE2 tropism . We have also demonstrated that both icGD03-S and icSZ16-S are neutralized by human mAb S230.15 and are more resistant to S3.1 highlighting the utility of using an antigenically diverse SARS-CoV panel to assess sero therapy efficacy. The icSZ16-S virus is yet another antigenically divergent zoonotic S bearing SARS-CoV that will prove useful in evaluating future sero or vaccination therapies.

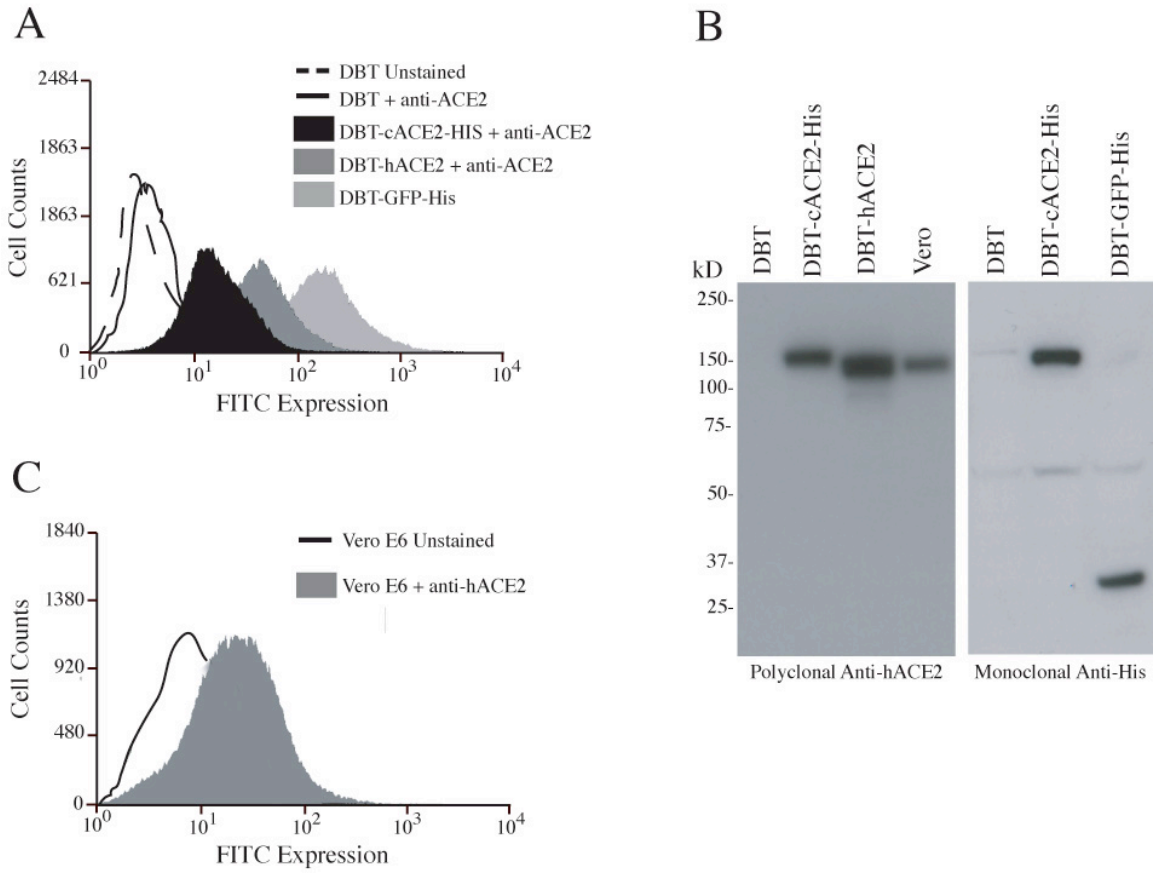

Figure 1: Characterization of cACE2 and hACE2 expressing DBT cells by flow cytometry and Western Blot. Transgene expression levels in cells stably expressing cACE2, hACE2 or GFP were assessed by flow cytometry and Western blot. DBT cells were stably transfected with plasmids encoding cACE2-HIS, hACE2, or GFP-HIS were passaged 4 times after which cells were stained for ACE2 expression (1˚ polyclonal anti-hACE2, 2˚ anti-goat-FITC) and sorted for mid/high ACE2 expression (FITC). GFP control cells were also sorted for mid/high expression. (A) To assess transgene expression in expanded post-sorted cell stocks, cells were stained as done above and analyzed for FITC/GFP expression by flow cytometry. (B) To assess transgene expression in post sorted cell stocks by Western Blot, similar numbers of DBT, DBT-hACE2, DBT-cACE2-His, DBT-GFP-His were lysed and separated on a Nupage 12% Bis-Tris SDS PAGE gel. After membrane transfer, blots were probed with either polyclonal goat anti-human ACE2 or mouse anti-penta-His antibody. After washing, membranes were probed with either rabbit anti-goat HRP or anti-mouse IgG-HRP antibody. Membranes were rinsed and then treated with ECL Plus reagent and to radiographic film.

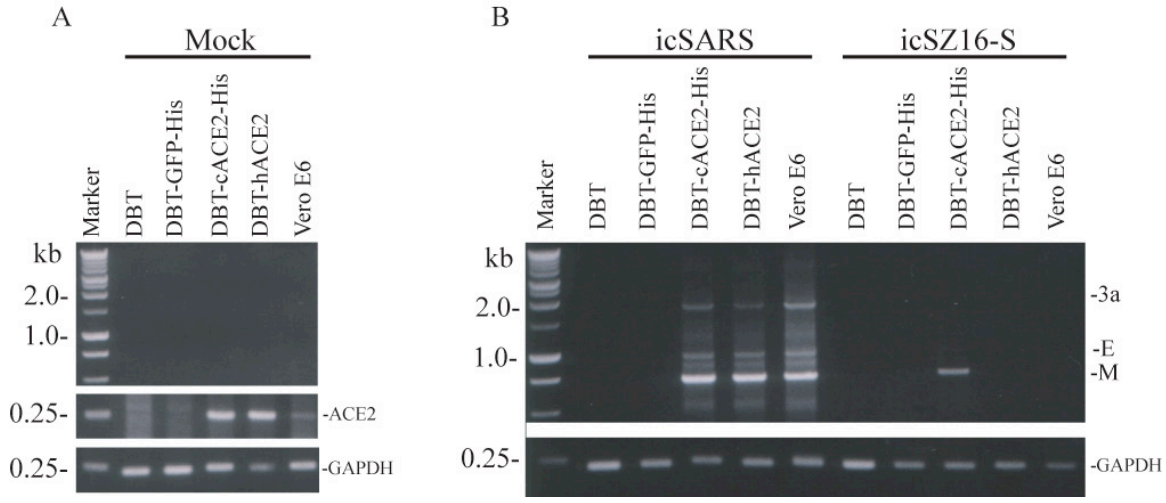

Figure 2: Resurrection of icSZ16-S with DBT-cACE2 cells. RT-PCR to detect subgenomic leader containing transcripts was performed to detect viral replication. DBT, DBT-GFP-His, DBT-cACE2, DBT-hACE2, or Vero E6 cells were infected with 100µl of viral supernatant from the initial icSZ16-S transfection, icSARS supernatants or were mock infected. 24hpi, total RNA was isolated, cDNA was generated and then used as template for PCR. Evidence of SARS-CoV replication and subgenomic transcription, ACE2 gene expression and control GAPDH gene expression was detected by the production of amplicons (SARS-CoV = 3a (1796bp), E (947bp), M(666bp), Control = 235bp GAPDH, ACE2 = 258bp) visualized through electrophoresis within a 1.8% agarose TAE gel.

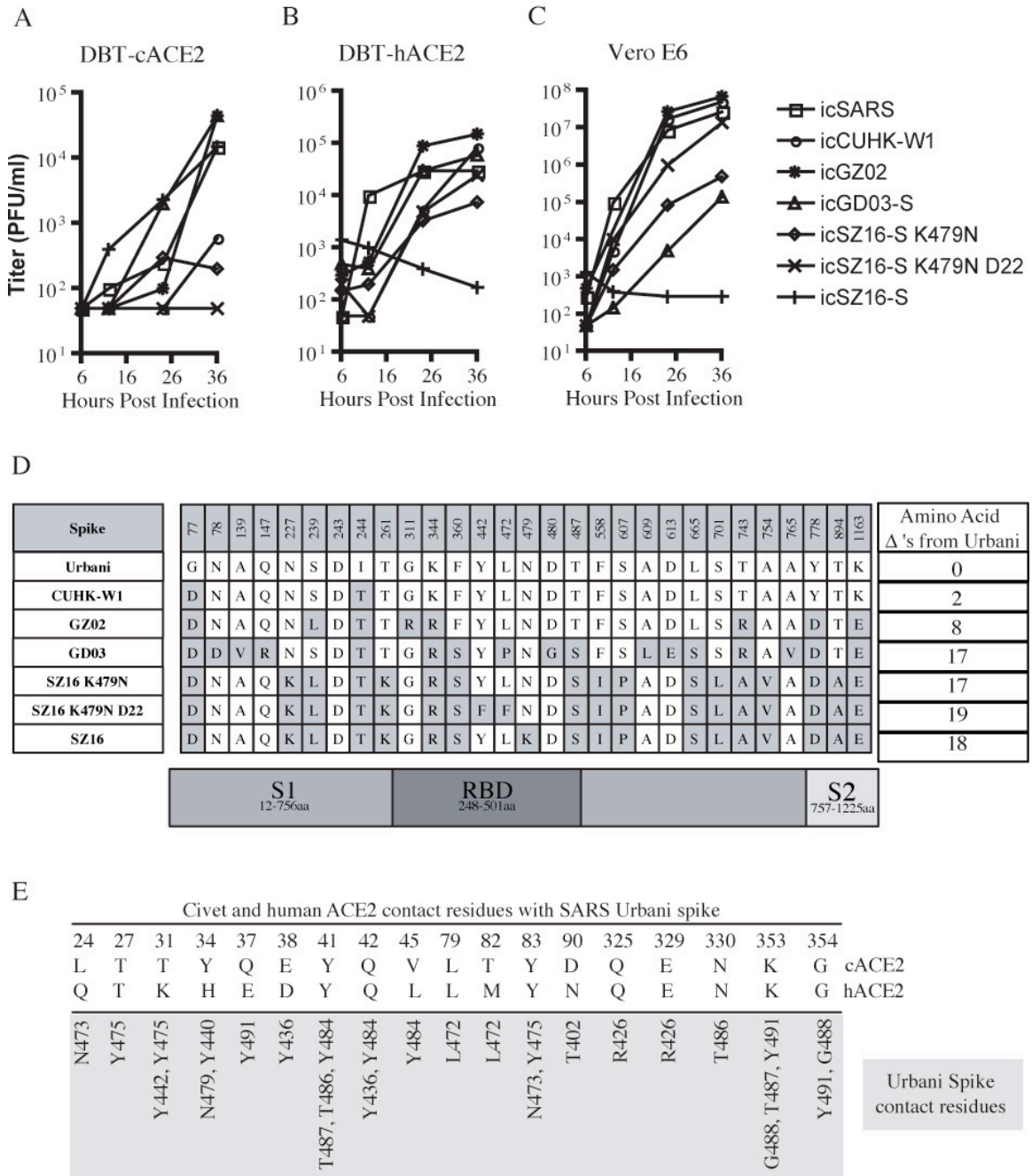

Figure 3: Assessment of virus growth in DBT, DBT-cACE2, DBT-hACE2, and Vero cells, spike variation in our recombinant virus panel, and ACE2 contact residues with the Urbani spike. (A) DBT-cACE2 (B) DBT-hACE2 (C) Vero E6 or DBT cells (data not shown) were infected with icCUHK-W1, icGD03-S, icGZ02, icSZ16-S K479N p6, icSZ16-S K479N D22, icSARS, or icSZ16-S, at an MOI of 0.01 for 1hr at 37˚C. 25µl of cell media was removed at 0, 6, 12, 24 and 36 hpi and samples were stored at -80˚C until titered by plaque assay. Growth curves were performed in duplicate. Growth curves were performed on two independent occasions and data shown is one representative experiment. (D) Location of spike amino acid differences among the recombinant virus panel. (E) Urbani, cACE2 and hACE2 contact residues adapted from the crystal structure published by Li et. al. 2005.

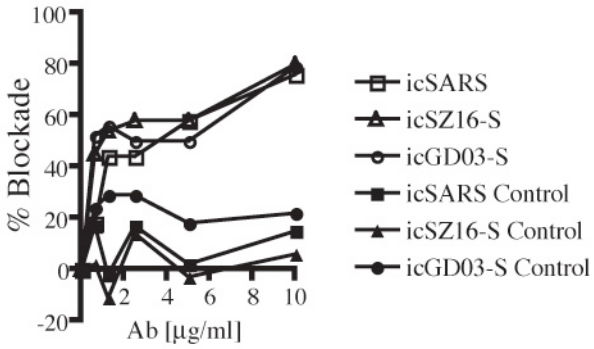

Figure 4: icGD03-S and icSZ16-S are dependent on ACE2 for entry. DBT-cACE2 cells were seeded at $5x10^5$cells/well in 6-well dishes. The following day, cell media was removed and cells were incubated with 10, 5, 2.5, 1.25 or 0.625µg/ml polyclonal anti-ACE2 or anti-ACE or DBPS for 1hr at 37˚C. After the 1hr pretreatment with antibody, 100pfu/50µl of icSARS, icSZ16-S, or icGD03-S, was added to the monolayer and incubated 1hr at 37˚C. After the infection, the inoculum was removed, the monolayer was rinsed with DPBS then overlayed with 0.9% agarose in complete growth media. After 48hpi, plates were stained with neutral red and plaques were counted. The average percent blockade was calculated by dividing the average number of plaques per Ab dilution by the average number of plaques in the DPBS no Ab controls. Blockade experiments were performed in duplicate on two separate occasions.

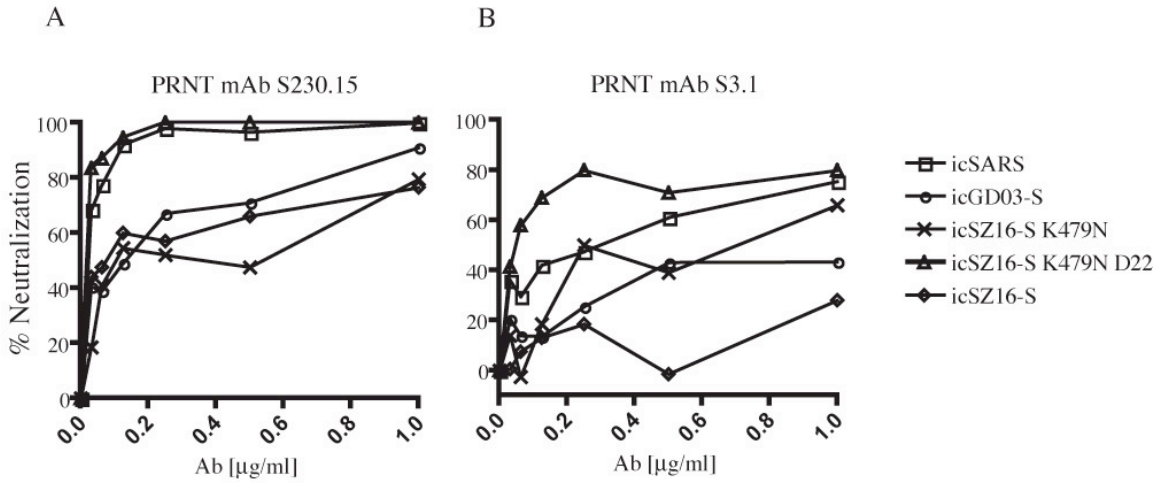

Figure 5: mAb S230.15 and S3.1 neutralization profiles differ between epidemic, in vitro evolved and zoonotic strains of SARS-CoV. Neutralizing titers were determined by plaque reduction neutralization titer assay (PRNT). 24hr prior to infection, 6-well plates were seeded with $5x10^5$ DBT-cACE2 cells/well. Human monoclonal antibodies (mAb) S230.15 and S3.1 and an isotype control antibody directed against cholera toxin, D2.2, were serially diluted two-fold, and incubated with 100 pfu of either icSARS, icSZ16-S, or icGD03-S for 1 hour at 37ºC. Virus and antibodies were then added to 6-well plates of Vero E6 cells in duplicate and incubated at 37˚C for 1 hour after which the cells were overlayed with 3ml of 0.8% agarose in media. After 48 hr, plates were stained with neutral red and plaques were counted. The percentage of neutralization was calculated as: 1-(number of plaques with antibody / number of plaques without antibody) x 100%.

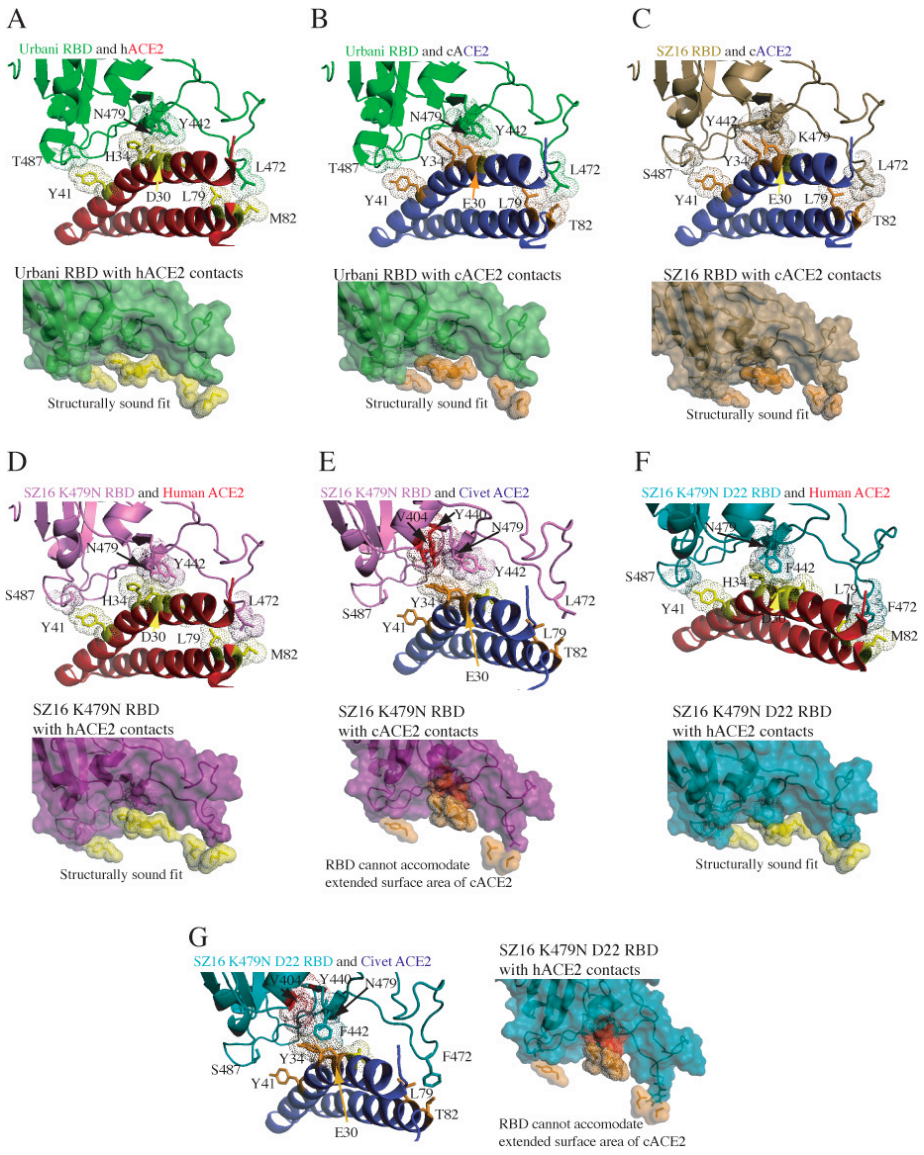

Figure 6: Rosetta Design modeling demonstrating structural mechanisms of ACE2 tropism. Based on the reported crystal coordinates of SARS Urbani RBD interacting with the hACE2 receptor, we generated models of Urbani, SZ16, SZ16-K479N, and SZ16 K479N D22 RBD interaction with either cACE2 or hACE2 using Rosetta Design. Ribbon structures and "space filling" schematics of each RBD and ACE2 combination are shown. Dotted spheres around RBD and ACE2 residues indicate they are within 4 angstroms and thus are predicted to interact. Red spheres around RBD and ACE2 residues indicate a steric clash. (A) Urbani RBD and hACE2 architecture (B) Additional methyl groups of the E30 and Y34 cACE2 mutations add a surface protrusion to the contact interface. The Urbani RBD can accommodate the increased surface protrusion of cACE2 thereby retaining an efficient binding interface. (C) Similar to the Urbani RBD, the SZ16 RBD can accommodate the increased surface protrusion of cACE2 for efficient binding (D) The N479 mutation in SZ16 K479N remodels the SZ16 binding interface to promote binding to hACE2 (E) The remodeling of the SZ16 K479N binding interface by the N479 mutation creates a clash between S residues (V404 and F440) and cACE2 residues (E30 and Y34) blocking S and ACE2 binding. The SZ16 K479N RBD cannot accommodate the extended surface protrusion of the cACE2 RBD (F) In addition to the N479 mutation, the F442 and F472 mutations further remodel the SZ16 K479N D22 RBD further enhancing binding efficiency to hACE2 (G) Similar to the SZ16 K479N RBD interaction with cACE2, the SZ16 K479N D22 RBD cannot accommodate the protrusion of cACE2 abrogating binding.

CHAPTER IV

MYD88 IS REQUIRED FOR PROTECTION FROM LETHAL INFECTION WITH A MOUSE ADAPTED SARS-CoV

Abstract

A novel human coronavirus, SARS-CoV, emerged suddenly in 2003 causing ~8000 human cases and greater than 700 deaths worldwide. Since most animal models fail to faithfully recapitulate the clinical course of SARS-CoV in humans, the virus and host factors that mediate disease pathogenesis remain unclear. Recently, our laboratory and others developed a recombinant mouse-adapted SARS-CoV (rMA15). Intranasal infection of C57BL/6 mice with rMA15 results in a nonlethal infection characterized by high titer replication within the lungs, lung inflammation, destruction of lung tissue, and loss of body weight, thus providing a useful model to identify host mediators of protection. Here, we report that mice deficient in MyD88 ($MyD88^{-/-}$), an adapter protein that mediates Toll-like receptor (TLR), IL-1R, and IL-18R signaling, are far more susceptible to rMA15 infection. The genetic absence of MyD88 resulted in greater than 90% mortality by day 7 post-infection. $MyD88^{-/-}$ mice had higher viral loads in lung tissue throughout the course of infection. Despite increased viral loads, the expression of multiple proinflammatory cytokines and chemokines within lung tissue was significantly reduced in $MyD88^{-/-}$ mice compared to wild-type mice. Furthermore, the recruitment of inflammatory monocytes/macrophages to the lung was severely impaired in $MyD88^{-/-}$ mice. These data suggest that MyD88-mediated innate immune signaling and inflammatory cell recruitment to the lung are required for protection from rMA15 infection.

Introduction

In 2003, a novel coronavirus, SARS-CoV, emerged from zoonotic pools of virus in China to cause a global outbreak of Severe and Acute Respiratory Syndrome (SARS) affecting 29 countries, causing over 8000 human cases and greater than 700 deaths(29, 103, 173). The clinical course of SARS-CoV disease in humans is characterized by fever, non-productive cough, and malaise culminating in lung infiltrates visible by x-ray and an atypical pneumonia(11, 19, 114, 124, 152). Immunologically, SARS-CoV infection of

humans generates a cytokine storm where elevated levels of IP-10, MIP1-α, and MCP-1 are detected within the blood(21). Histological examination of lung tissue in terminal SARS-CoV cases revealed SARS antigen within macrophages in the lung suggesting a role for these cells in SARS-CoV pathogenesis(68, 144).

Though clinical and epidemiological data from the epidemic and reemergence has provided insight in the molecular pathogenesis of SARS-CoV, thorough studies of virus and host interactions have been hampered by the lack of animal models that fully recapitulate human disease. C57BL/6 mice infected with the epidemic strain, SARS Urbani, do not show any overt signs of disease but there is virus replication in the lung (10^7TCID$_{50}$/g 3dpi), induction of MIP1α/MCP-1 and viral clearance even in the absence of T, B and NK cells suggesting that innate immunity alone is required for protection within this acute model of SARS-CoV replication(62). MA15 is a mouse adapted SARS-CoV strain that was generated by fifteen serial passages of the epidemic strain, SARS Urbani, in the lungs of BALB/c mice(167). Infection of young or senescent BALB/c mice with either MA15 or recombinant MA15 (rMA15) results in high virus titers in the lung, pulmonary pathology and mortality similar to those seen in severe and acute human cases of SARS-CoV disease(144, 152, 167).

Toll-like receptors (TLRs) are cellular receptors that recognize molecular signatures of pathogens and initiate an inflammatory signaling cascade that is key to the innate immune response(147). Myeloid differentiation primary response gene 88 (Myd88) is key adaptor protein within the inflammatory signaling pathways of most all TLRs as well as IL-1R, IL-18R and INFγR1(147). In animal models of viral pathogenesis, Myd88 signaling has been shown to be protective oftentimes providing instructions to innate immune cells shown to be important for viral clearance(155, 174). The role of Myd88 signaling in SARS-CoV pathogenesis has not yet been described.

In this study, we describe a C57BL/6 mouse model of recombinant mouse adapted SARS-CoV (rMA15) acute pathogenesis characterized by high titers of virus replication within the lung with a concurrent induction of inflammatory cytokines and immune cell infiltration followed by viral clearance. WT mice show clinical signs of disease as manifested in 12-15% loss of body weight by 3 dpi but fully recover initial body weight by 7dpi. We show a protective roll for Myd88 signaling events in our model of rMA15 pathogenesis. Myd88$^{-/-}$ mice infected with rMA15 have significantly higher and prolonged virus

titers in the lung, exacerbated lung pathologies, defective induction of inflammatory cytokines, fail to recruit inflammatory macrophages to the lung and ultimately succumb to infection. These data suggest that a failure or delay in Myd88 inflammatory signaling or a failure to recruit inflammatory macrophages to the lung during acute infection results in exacerbated SARS-CoV disease.

Materials and Methods

Viruses and Cells. Vero E6 cells were grown in MEM (Invitrogen, Carlsbad, CA) supplemented with 10% FCII (Hyclone, South Logan, UT) and gentamycin/kanamycin (UNC Tissue Culture Facility). Stocks of the recombinant mouse-adapted SARS-CoV (rMA15) were propagated and titered on Vero E6 cells and cryopreserved at -80˚C until use as described(247). All viral and animal experiments were performed in a Class II biological safety cabinet in a certified biosafety level 3 laboratory containing redundant exhaust fans while wearing personnel protective equipment including Tyvek suits, hoods, and HEPA-filtered powered air-purifying respirators (PAPRs) as described(247).

Mice. C57BL/6 mice were obtained from The Jackson Laboratory (Bar Harbor, Maine) and bred in house. MyD88$^{-/-}$ mice were obtained from Shizou Akira (Osaka University) and backcrossed 11 generations to the B6 background. Animal housing and care were in accordance with all UNC-Chapel Hill Institutional Animal Care and Use Committee guidelines. 10 week old WT or MyD88$^{-/-}$ mice were anaesthetized with a mixture of ketamine/xylazine and intranasally infected with 10^5pfu/50µl rMA15 in DPBS (Invitrogen, Carlsbad, CA). Mice were monitored at 24 h intervals for virus-induced morbidity and mortality.

Viral tissue titers. To quantify the amount of infectious virus in tissues, lung tissue was weighed, placed in 0.5 ml DPBS, homogenized and titered via plaque assay on Vero E6 cells as previously described(180).

In situ hybridization. ^{35}S-UTP-labeled riboprobes specific to the N gene of SARS-CoV (Urbani) or to the EBER2 gene from Epstein-Barr virus (negative control probe) were generated with an SP6-specific MAXIscript in vitro transcription kit (Ambion) and in situ hybridization was performed as described previously(41). Briefly, deparaffinized tissue sections were hybridized with 5 x 10^4 cpm/µl of ^{35}S-labeled riboprobes overnight. Tissues were washed, dehydrated through graded ethanol, coated in NTB autoradiography emulsion (Kodak), and incubated at -80°C for 7 days. Following development, sections were counterstained with hematoxylin and silver grain deposition was analyzed by light microscopy.

qRT-PCR. To determine levels of inflammatory gene transcription within the infected lung, we employed a quantitative real-time PCR (qRT-PCR) approach. Lungs from mock- or rMA15-infected mice were removed and homogenized directly in 1 ml of Trizol reagent (Invitrogen) and total RNA was isolated following the manufacturer's instructions. Complementary DNA was generated from 0.25-1 ug of total RNA using 250 ng random primers (Invitrogen) and superscript III reverse transcriptase (Invitrogen). Real-time PCR experiments were performed using Taqman© gene expression assays and an AB Prism 7300 (Applied Biosystems). 18s rRNA was used as an endogenous control to normalize for input amounts of cDNA. RNA levels of the target gene and the 18s endogenous control were quantitated by comparing the experimental signal with a standard curve generated from a DNA plasmid encoding the appropriate sequences.

Flow cytometry. Mice were inoculated as described above, sacrificed by exsanguination at 2 and 4 days post-infection, and lungs were perfused via cardiac puncture with 1X PBS. Lungs were dissected, minced, and incubated for 2 hours with vigorous shaking at 37°C in digestion buffer [RPMI, 10% FBS, 15 mM HEPES, 2.5 mg/ml collagenase A (Roche), 1.7 mg/ml DNase I (Sigma)]. Cells were passed through a 40 micron cell strainer, resuspended in RPMI media, layered on 5 ml lympholyte-M (Cedarlane), and centrifuged 30 minutes at 2500 rpm. Banded cells were collected, washed in wash buffer (1X HBSS, 15 mM HEPES), and total viable cells were determined by trypan blue exclusion. Isolated cells were incubated with anti-mouse FcγRII/III (2.4G2; BD Pharmingen) for 20 min. on ice and then stained in FACS staining buffer (1X HBSS, 1% FBS, 2% normal rabbit serum) with the following antibodies from eBioscience: anti-F4/80-FITC, anti-Gr-1-PE, anti-CD11b-APC, anti-CD3-FITC, and anti-NK1.1-PE. Cells were fixed overnight in 2% paraformaldehyde and analyzed on a Cyan cytometer (Dako) using Summit software.

Statistical analyses. Viral titers and inflammatory cell numbers were evaluated for statistically significant differences by unpaired t-tests using GraphPad InStat3 software. $P \leq 0.05$ was considered significant.

Results

MyD88$^{-/-}$ mice are highly susceptible to rMA15 infection.

To assess the contribution of MyD88 to SARS-CoV-induced disease, wild-type (WT) and congenic MyD88$^{-/-}$ mice were infected intranasally with 10^5 pfu of recombinant mouse-adapted SARS-CoV

(rMA15) and monitored for virus-induced morbidity and mortality. Infection of WT or MyD88$^{-/-}$ mice resulted in weight loss beginning at day 2 post-infection (Fig. 1A). Infected WT mice lost 14±5% of starting body weight by 3 dpi and returned to starting body weights by 5-7 dpi, indicating that the mice recovered from infection. In contrast, infected MyD88$^{-/-}$ mice continued to lose weight after 3 dpi. Additionally, 0% of WT mice succumbed to infection (n = 9) while 90% of MyD88$^{-/-}$ mice (n = 16) died as a result of rMA15 infection by 7 dpi (Fig. 1B). These results indicate that MyD88 plays an important role in protection from SARS-CoV infection.

Increased viral loads and viral spread in the lungs of MyD88$^{-/-}$ mice

To determine if lethal infection of MyD88-deficient mice to was due to increased virus replication and/or a lack of clearance, a kinetic analysis of rMA15 growth within the mouse lung was performed. Viral titers in WT mice peaked at 24 hpi ($9x10^8$pfu/g ± $7x10^8$ (standard deviation)) and diminished by 6 dpi ($5x10^5$pfu/g ± $9x10^5$) (Fig. 2). Infectious virus was not recovered from the lungs of infected WT mice by 7 dpi. Lung titers in MyD88$^{-/-}$ mice were similar to WT mice at 24 hpi. However, at 2 and 3 dpi, virus lung titers in MyD88$^{-/-}$ were significantly elevated as compared to WT mice (2 dpi, P = 0.0052; 3 dpi, P = 0.0092) and remained elevated over time as WT virus lung titers fell (Fig. 2).

To assess the distribution of virus replication within the lung tissue of WT and MyD88$^{-/-}$ mice, in situ hybridization was performed on tissue sections using an ^{35}S-labeled riboprobe complementary for the N gene of SARS-CoV. rMA15-specific signal was determined by comparing silver grain deposition on parallel sections hybridized with an ^{35}S-labeled riboprobe complementary for the EBER2 gene of Epstein-Barr virus (data not shown). As shown in Fig. 3, in situ signal was not observed in lung sections derived from mice that received intranasal administration of PBS alone. At both 24 and 48 hpi, intense rMA15-specific in situ signal was observed throughout the lung tissue, including lung airway epithelia, in rMA15-infected WT and MyD88$^{-/-}$ mice. At 72 and 96 hpi, the distribution and intensity of rMA15-specific in situ signal had greatly diminished in lung tissue of WT mice. In contrast, rMA15-specific in situ signal in lung tissue of MyD88$^{-/-}$ mice was more intense and much broader in distribution at these time points. By 6 dpi, though significantly diminished, rMA15-specific in situ signal was still readily detectable in lung tissue of MyD88$^{-/-}$ mice, whereas only very rare rMA15-specific in situ signal could be detected in lung tissue of WT mice. These findings suggest that MyD88 is required for control of SARS-CoV replication in

pulmonary tissue at early times post-infection and the inability to control early replication is associated with increased lethality.

Decreased expression of proinflammatory cytokines and chemokines in MyD88$^{-/-}$ mice. Infection of WT mice with rMA15 results in a rapid inflammatory response in the lungs. This virus-induced inflammatory response likely has both protective and pathologic consequences. To investigate the importance of MyD88 in SARS-CoV-induced lung inflammation, we employed quantitative RT-PCR (qRT-PCR) to assess levels of proinflammatory cytokine and chemokine gene expression in the infected mouse lung at various times post-infection. Infection of WT mice with rMA15 resulted in a significant induction of proinflammatory CCL2 and CCL3 transcription as compared to mock-infected control mice (Fig. 4A). In contrast, induction of CCL2 and CCL3 transcripts were dramatically reduced in rMA15-infected MyD88$^{-/-}$ mice. In addition to proinflammatory chemokines, virus-induced expression of several proinflammatory cytokines, including TNF-α, IL-1β, and IL-6, was severely impaired in rMA15-infected MyD88$^{-/-}$ mice compared to infected WT mice (Fig. 4B). Interestingly, induction if interferon-β transcripts within lung tissue of WT mice was not detected at any of the times during the course of viral infection we evaluated. These data indicate that MyD88 is required for the induction of proinflammatory chemokines and cytokines within pulmonary tissues of SARS-CoV-infected mice and suggest that some aspect(s) of this inflammatory response is required for protection from lethal disease.

Delayed recruitment of inflammatory monocytes to lungs of MyD88$^{-/-}$ mice

The expression analyses of proinflammatory chemokine and cytokines indicated that MyD88 is critical for early immune/inflammatory responses in lung tissue following SARS-CoV infection. To investigate whether the impaired chemokine and cytokine responses in MyD88$^{-/-}$ mice affected the cellular composition within the lung, total leukocytes were isolated from pulmonary tissue and analyzed by flow cytometry. At 2 dpi, no significant differences were detected in natural killer cell (NK1.1^{+}/CD3^{-}) or T lymphocyte (CD4^{+}/CD3^{+};CD8^{+}/CD3^{+}) populations isolated from the lung tissue of mock-infected or SARS-CoV infected WT mice (data not shown). In contrast, a significant increase in inflammatory monocytes/macrophages (CD11b^{+}/Gr-1^{+}/F4/80^{+}) was detected in lung tissue of SARS-CoV-infected WT mice compared to mock-infected WT control mice (Fig. 5A). These results are consistent with previous findings demonstrating that rMA15-induced pulmonary inflammation is composed of a mononuclear

inflammatory infiltrate(167). Strikingly, the $CD11b^{+}/Gr\text{-}1^{+}/F4/80^{+}$ inflammatory monocyte/macrophage population was dramatically reduced in lung tissue of SARS-CoV-infected $MyD88^{-/-}$ compared to infected WT mice. In fact, no significant increase in inflammatory monocytes/macrophages was observed in infected $MyD88^{-/-}$ mice compared to mock-infected control mice (5A). To determine if the failure to recruit inflammatory monocytes/macrophages is sustained at later times post infection in $MyD88^{-/-}$ mice, we performed similar cell isolation experiments at 4 dpi. In contrast to 2 dpi, at 4 dpi a similar percentage and total number of inflammatory monocytes/macrophages ($CD11b^{+}/Gr\text{-}1^{+}/F4/80^{+}$) were isolated from the lung tissue of WT and MyD88-/- mice. Similar to 2 dpi, there were not significant numbers of CD3+ T lymphocytes detected within the lung tissue of rMA15-infected mice compared to PBS-inoculated control mice, indicating that T lymphocytes are not a major component of the inflammatory response at these times post-infection (data not shown). These results indicate that MyD88 is critical for early host immune and inflammatory responses, which include the recruitment of inflammatory monocytes/macrophages to pulmonary sites, in response to SARS-CoV infection.

Discussion

Since human clinical SARS data is complicated by host genetic variation, disease exacerbating comorbidities, age variation, and variable drug treatment regimens, animal models provide a more homogenous and controlled environment within which to ask questions related to the mechanisms of disease pathogenesis. C57BL/6 mouse models of SARS Urbani replication demonstrated the importance of the innate response to clear virus but overt signs of disease similar to those seen in human cases of SARS-CoV were not evident within this model(62). We have developed a C57BL/6 mouse model for acute SARS-CoV disease through infection with mouse adapted SARS-CoV (rMA15). Our model faithfully recapitulates many aspects of the acute phase of non-severe human SARS-CoV disease including high titers of virus growth within the lung, a viral induced inflammatory response, recruitment of inflammatory cells to the lung and a significant weight loss associated with the manifestation of viral disease(11, 21, 152).

Serological and pathological data from the SARS-CoV epidemic suggests that the innate immune response plays a crucial role in the control of SARS-CoV infection while also potentially contributing to immune pathology. Cameron et al describe inflammatory gene expression patterns and cytokine plasma

levels in the peripheral blood of severe and non-severe SARS patients in Toronto(21). Non-severe and severe patients had similar amounts of IP-10 and MCP-1 in their serum during the early phase of infection but as disease progressed, cytokine levels in non-severe cases decreased while levels remained high in severe cases(21). In pathological evaluation of post mortem lung tissues from SARS-CoV cases, SARS antigen was frequently in macrophages suggesting an important role for these cells in SARS-CoV disease(68). In vitro data suggests that macrophages are not productively infected by SARS-CoV and instead secrete inflammatory cytokines like IP-10 and MCP-1(27). The above data suggests a dual role of inflammation and the innate immune response in both the prevention and progression of severe SARS-CoV disease. Within our model of SARS-CoV acute disease, we see a protective role for inflammatory cytokines and chemokines and their recruitment of inflammatory cells to the infected lung to help clear infection. We have yet to determine the cell type responsible for the induction of this protective inflammatory response though we have demonstrated the recruitment of inflammatory monocytes occurs even if alveolar macrophages are depleted (data not shown). In the future, bone marrow chimeras between WT and MyD88$^{-/-}$ mice may help us deduce if myeloid derived cells are responsible for the initial induction of the protective inflammatory response.

MyD88 is a key signaling adaptor protein for most all TLRs, IL-1R, IL-18R and INFγ-R1(147). Though MyD88 mediated proinflammatory signaling events have been implicated in the protection from numerous bacteria and parasitic infections, few in vivo studies have implicated MyD88 in protection from viral diseases(5, 52, 155, 174, 178, 198). Moreover, the few studies implicating a protective roll for MyD88$^{-/-}$ in the context of viral infection suggest type I interferon induction is important for protection from disease(101, 155, 255). In contrast, we show that WT C57BL/6 mice are protected from lethal SARS-CoV infection independent of type I interferon induction. It is possible that the induction of either type II interferon (interferon gamma) or type III interferon (IL-28/29, interferon lambda) may be instigating the protective signal in WT mice that seems to be absent in MyD88$^{-/-}$ mice contributing to their mortality from rMA15 infection. Within mouse models of RSV infection, MyD88 dependent induction of Th1 cytokines like INF-γ and IL-12 were demonstrated to decrease the severity of disease(174). The signaling of INFγR1 through MyD88 activates p38, a mitogen-activated protein kinase (MAPK), which is known to induce inflammatory mediators like IL-1 and TNF(106, 147). Recent mouse models of HSV-2 pathogenesis have

demonstrated that type III interferon (IL-28/29, interferon lambda) is crucial for the control of infection and complete prevention of disease(8). Furthermore, recent studies suggest that lambda interferon can be activated in a TLR/MyD88 dependent manner(148). Currently, we are investigating the mechanism of protective signal induction that is present in WT animals and absent in MyD88$^{-/-}$ mice. Our preliminary data suggests that our MyD88 lethal phenotype is not mediated by IL-1R or IL-18R and in the future we will investigate the possible roll of TLRs in protection from lethal infection of rMA15. We will also investigate the contribution of both type II and type III interferon induction in the protection from lethal rMA15 infection.

Viral pathogenesis is a complex process where the virus and host engage in an unintended collaboration to generate the clinical presentation of disease. Being a newly emerged infectious disease, many of the pathogenic mechanisms of SARS-CoV disease remain unknown. We have developed a mouse model of acute non-severe SARS-CoV pathogenesis characterized by a high titer virus replication in the lung followed by a robust innate immune response resulting in the recruitment of inflammatory macrophages to the lung that mostly likely responsible for viral clearance and convalescence. We also demonstrate a key role for MyD88 dependent signaling events and associated inflammation/cell recruitment that serves to protect WT mice from death while Myd88$^{-/-}$ mice succumb to infection. These data suggest an important role for innate immunity in the control of SARS-CoV and prevention of virus induced mortality.

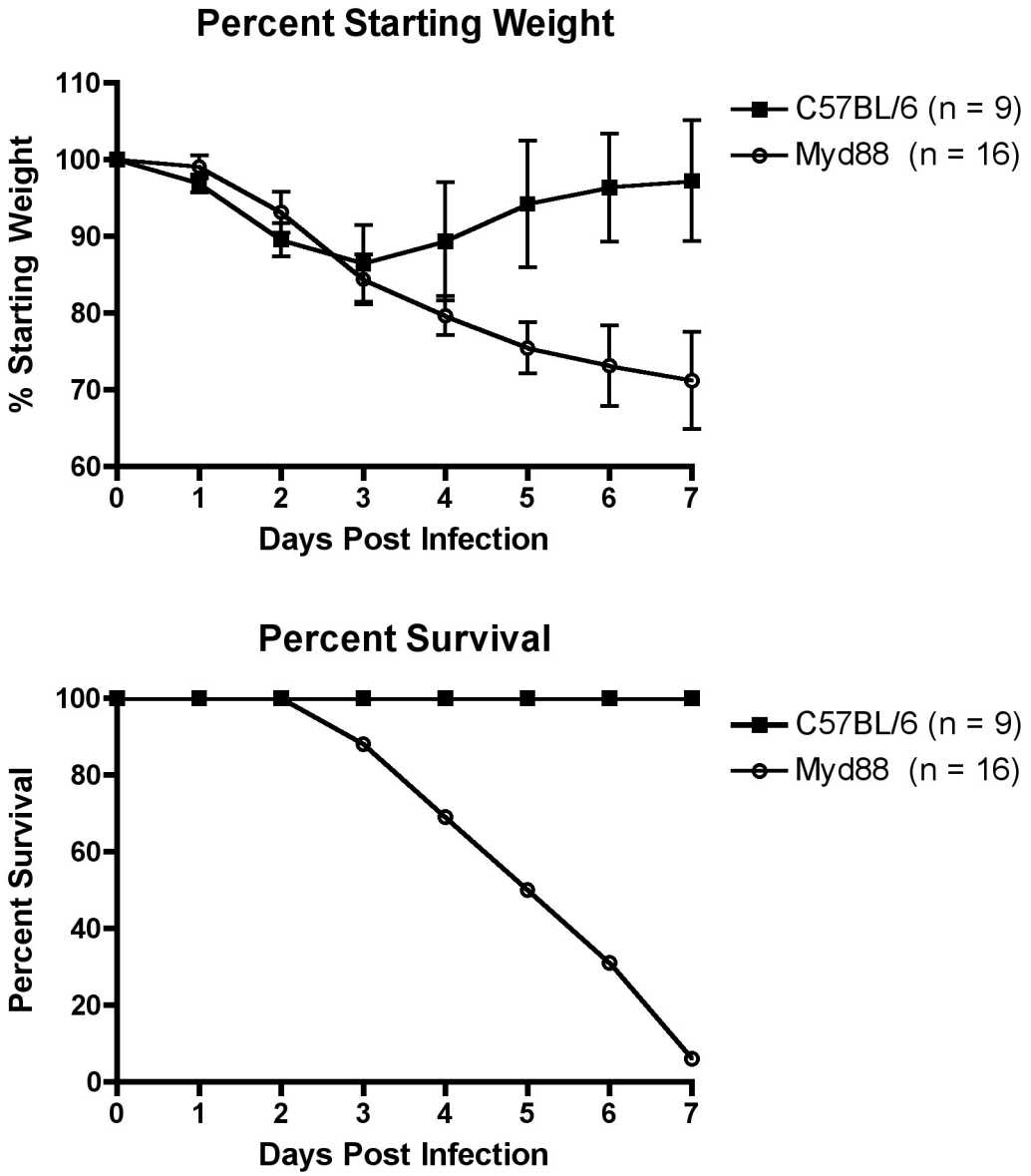

Fig. 1. MyD88$^{-/-}$ mice are highly susceptible to rMA15 infection. WT (n = 9) or MyD88$^{-/-}$ (n = 16) mice were infected intranasally with 10^5 pfu rMA15 after which virus induced morbidity and mortality was monitored every 24 hpi. Error bars represent one standard deviation.

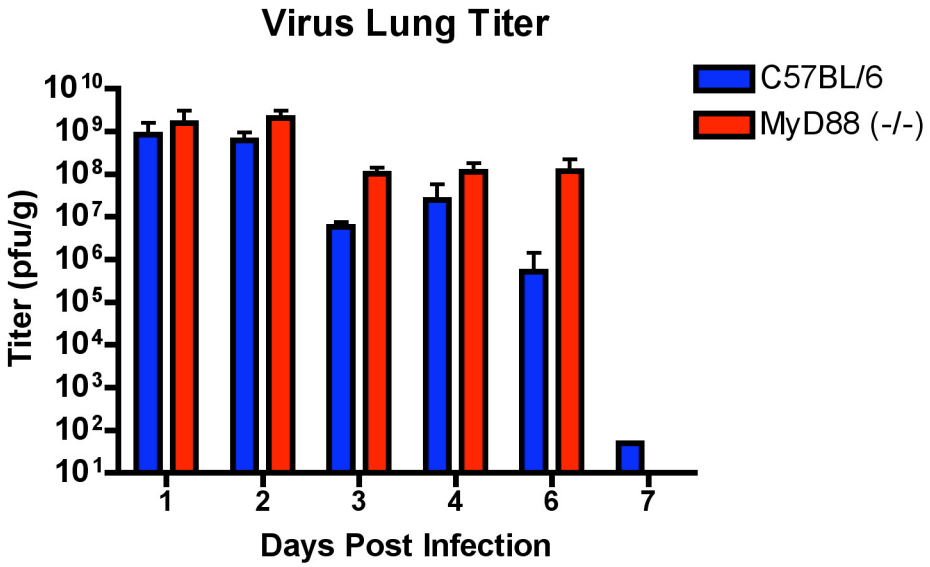

Fig. 2. rMA15 replicates to significantly higher levels in the lungs of MyD88$^{-/-}$ mice as compared to WT. WT or MyD88-/- mice were infected intranasally with 10^5 pfu rMA15. Lung tissues from 3 mice per strain were harvested on 1, 3, 4, 6, and 7 dpi, while lung tissue from 6 mice per strain were harvested on 2 dpi. Lung tissues were homogenized in DPBS and virus titer within clarified supernatants were assess by plaque assay. Mean titers are displayed and error bars represent 1 standard deviation.

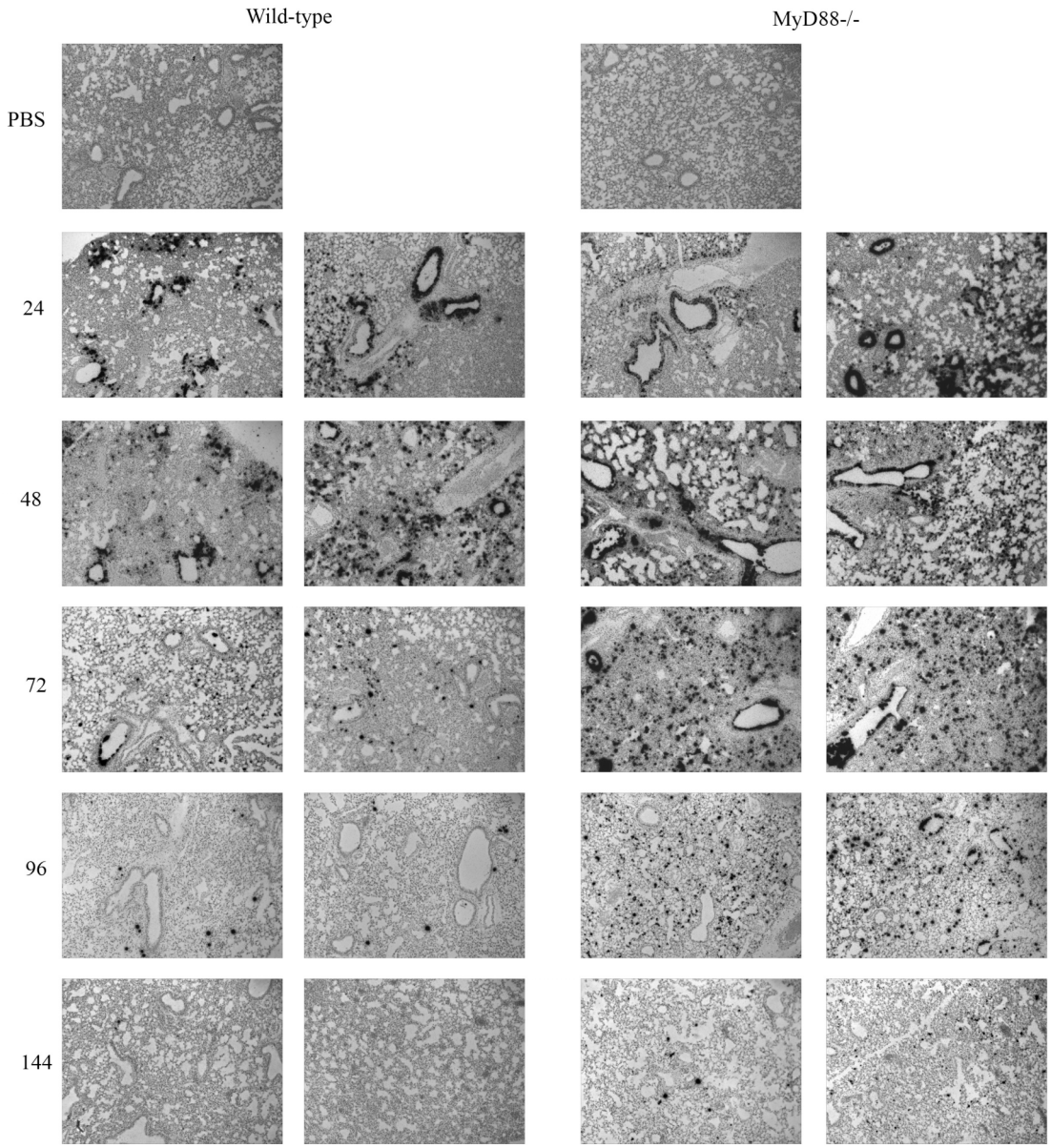

Fig. 3. Virus distribution is more widespread within the lungs of MyD88-/- mice as compared to WT mice. 5 μM paraffin-embedded sections derived from the lung tissue of WT and MyD88-/- mice were hybridized with an ^{35}S-UTP-labeled riboprobe complementary to either the N gene of SARS-CoV (Urbani) or to the EBER2 gene from Epstein-Barr virus (data not shown). Two images per strain per time point are presented (magnification, X 100) and are representative of at least three mice.

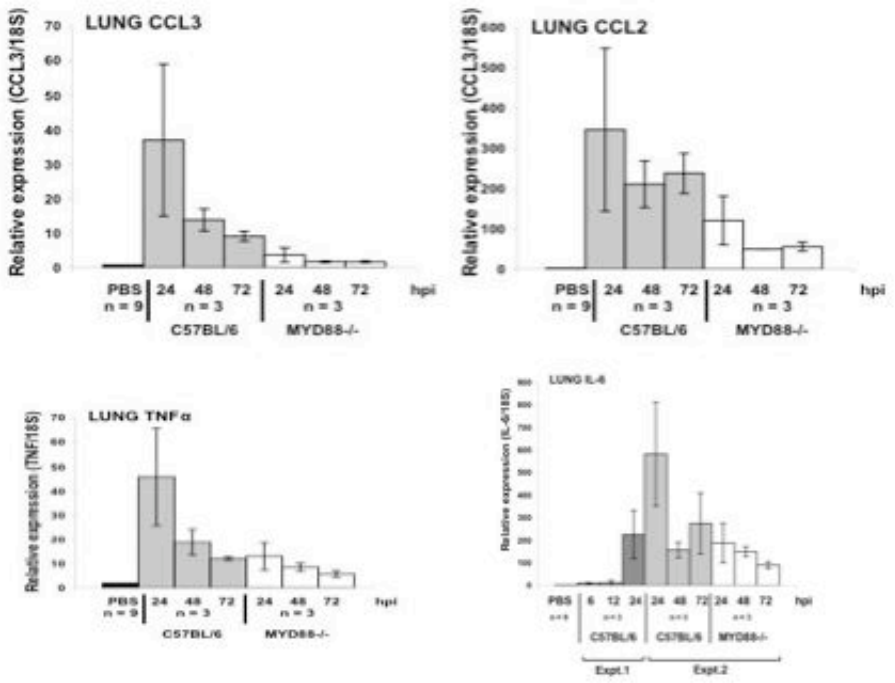

Fig. 4. Proinflammatory cytokine and chemokine transcription is depressed in MyD88$^{-/-}$ mice infected with rMA15 as compared to WT mice. To evaluate levels of proinflammatory cytokine and chemokine transcription, quantitative real-time PCR was employed. We evaluated levels of CCL3, CCL2, TNFα and IL-6 transcription. cDNA was generated from 0.25-1μg lung RNA using superscript III reverse transcriptase. Real-time PCR experiments were performed using Taqman© gene expression assays and an AB Prism 7300. 18s rRNA was used as an endogenous control to normalize for input amounts of cDNA. RNA levels of the target gene and the 18s endogenous control were quantitated by comparing the experimental signal with a standard curve generated from a DNA plasmid encoding the appropriate sequences.

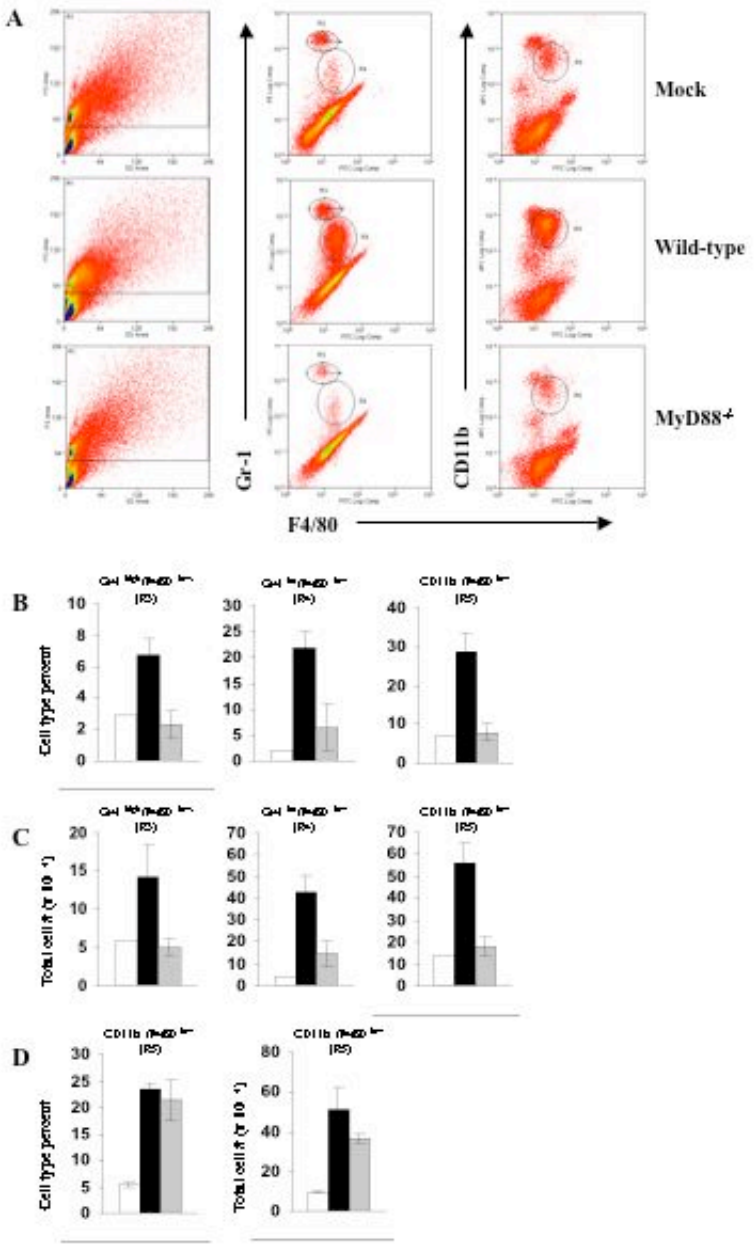

Fig. 5. Recruitment of inflammatory monocytes/macrophages to the SARS-CoV infected lung is delayed in MyD88$^{-/-}$ mice as compared to WT mice. 10 wk old B6 WT or MyD88-/- mice were inoculated intranasally with PBS or 10^5 pfu rMA15. (A) At 2 dpi, lung leukocytes were isolated as described in Materials and Methods and analyzed by flow cytometry. Histograms are representative of three mice. Two independent experiments gave similar results. (B) Percent inflammatory monocytes/macrophages of total lung leukocytes isolated from mock (□), rMA15-infected WT (■), or rMA15-infected MyD88-/-n (■) mice at 2 dpi. (C) Total numbers of inflammatory monocytes/macrophages isolated from mock (□), rMA15-infected WT (■), or rMA15-infected MyD88-/-n (■) mice at 2 dpi. (D) Percent inflammatory monocytes/macrophages of total lung leukocytes (left panel) and total numbers of inflammatory monocytes/macrophages (right panel) isolated from mock (□), rMA15-infected WT (■), or rMA15-infected MyD88-/-n (■) mice at 4 dpi.

CHAPTER V

VACCINE FAILURE IN SENESCENT BALB/C MICE CHALLENGED WITH MOUSE ADAPTED SARS-COV BEARING A ZOONOTIC SPIKE

Abstract

Severe acute respiratory syndrome coronavirus (SARS-CoV) emerged suddenly within Guangdong province of China in 2002 causing over 8000 cases and >700 deaths in 29 countries throughout the world. The disease severity associated with SARS-CoV infection of humans was directly linked to increasing age with mortality rates exceeding 50% in people over 65 years of age. The successful vaccination of elderly populations is a difficult and unpredictable task due to immunosenescence with ageing and robust models are needed to evaluate and improve vaccines targeting infections that cause a disproportionate disease burden in the elderly. In this manuscript, we have developed a senescent BABL/c mouse model of SARS-CoV pathogenesis where infection with the mouse adapted SARS-CoV bearing a GD03 S glycoprotein (rMA15 GD03-S) causes morbidity in young mice and both morbidity and mortality in senescent mice mimicking the distribution of disease seen in human populations. Our group has previously demonstrated that vaccines were inefficient at preventing SARS-CoV replication in senescent mice but it is unclear whether the vaccines protect senescent mice from lethal disease. To address this issue, we vaccinated senescent mice with Venezuelan equine encephalitis virus replicon particles (VRP) expressing Urbani-S, GD03-S, SZ16-S, or a pool of all three S expressing VRPs in a prime/boost regimen. As a control, we also vaccinated a group with VRP expressing influenza HA. Two months post boost, mice were intranasally challenged with 10^5 pfu rMA15 GD03-S after which morbidity and mortality were monitored daily. All vaccine groups experienced significant morbidity with weight loss exceeding 20% of their starting weight by 5 days post infection (dpi). All mice in the VRP HA and SZ16-S groups died while Urbani-S, GD03-S and Pool-S groups demonstrated 11, 29, 33% survival rates, respectively. GD03-S specific IgG antibody responses in the serum predicted mortality and very low neutralizing antibody titers protect against mortality. We postulate that the apparent failure to successfully vaccinate senescent mice might be due to either intrinsic vaccine or senescent immune factors or a complex mixture of the two.

Introduction

Severe acute respiratory syndrome coronavirus (SARS-CoV) emerged suddenly in Guangdong province of China in 2002 causing over 8000 cases and >700 deaths in 29 countries throughout the world(139). In 2004, SARS-CoV reemerged in the Guangdong province of China causing a more mild sporadic human disease and there were also several laboratory acquired cases and fatalities(28, 69, 146). Zoonotic SARS-CoV similar to the epidemic strain, SARS Urbani, have been found in the putative animal reservoir, the Chinese horseshoe bat, as well as in other exotic species like raccoon dogs and palm civets(108). Molecular epidemiology suggests that within wet markets in the Guangdong province, zoonotic SARS-CoV evolved to efficiently infect and transmit among humans through repeated animal to human or human to animal transmission events(28, 69, 108, 236). SARS-CoV disease is characterized by an atypical pneumonia where approximately 20% of cases progressed to acute respiratory distress syndrome (ARDS) requiring mechanical ventilation(19, 114, 124, 152, 153). The disease severity associated with SARS-CoV infection of humans was directly linked to increasing age with mortality rates exceeding 50% in people over 65 years of age(46, 73). Due to travel restrictions and associated hysteria, the SARS-CoV epidemic had a profound global economic impact with estimates between 30-100 billion dollars lost world wide(187). Given the impact of the SARS-CoV epidemic on the global economy and public health and the potential for another reemergence, the development of therapeutic vaccines and passive sero therapies to combat future SARS-CoV emergence or laboratory acquired infection is highly desirable.

The successful vaccination of elderly populations is a difficult and unpredictable task due to the senescence of the immune system associated with ageing(17, 18, 50, 53, 64, 65, 67, 77, 151, 212, 215). Current models predict that influenza vaccine efficacy in elderly populations ranges from 17-53% while the vaccine in young adults is 70-90% effective(64). Current research suggests that the senescent innate and adaptive immune system is defective on multiple levels making successful vaccination of the elderly a difficult task. Defects in antigen presenting and T cell activation/cytokine secretion affect the generation of effective adaptive immune system helper (T helper or Th) cells and effector (B cells and cytotoxic T cells) cells resulting in diminished vaccine efficacy(50, 53, 58, 64, 65, 77, 136, 212, 223). Interestingly, some of the senescent immune system deficiencies can be overcome through administration of cytokines or

adjuvants during vaccination that effectively activate APCs/Th cells thereby increasing the probability of generating appropriate amounts of effector cells required for successful vaccination(75, 76, 83, 160, 201). Since influenza, West Nile Virus and SARS-CoV infection all produce a disproportionate amount of disease burden in the elderly, the development of robust model systems for the design of successful vaccine strategies in the elderly has a broad public health application especially given the increasing age of global human populations(1, 116, 142).

Inactivated whole virus and vectored SARS-CoV vaccine trials in a number of different animals models have demonstrated that the SARS-CoV spike glycoprotein (S) is the critical component of protective immunity and the passive transfer of SARS-CoV S specific sera and select human monoclonal antibodies is sufficient to provide protection from lethal and nonlethal infection by a homologous and select heterologous SARS-CoV strains(20, 41, 78, 95, 163, 171, 190, 194, 224, 241, 253, 254, 256). Since the epidemic strain may not exist in nature, vaccination with epidemic strain antigens followed by challenge with the epidemic strain may represent a biologically irrelevant design. Unfortunately, a difficult choice is presented in choosing SARS-CoV vaccine antigens in hopes of preventing disease by future emergents whose antigenic identity is unknown. Therefore, employing an antigenically diverse panel of SARS-CoV antigens for vaccination coupled with the use of an similarly diverse lethal challenge virus panel may represent the most pertinent and relevant strategy to assess vaccine efficacy. In 2003, Deming et al demonstrated that a Venezuelan equine encephalitis virus replicon particles expressing SARS Urbani S (VRP-S) vaccine provided complete protection in young mice from replication of a SARS-CoV bearing a zoonotic heterologous GD03 S but protection was variable in senescent mice(41). Due to the lack of significant morbidity and mortality in the SARS-CoV replication models, previous vaccine studies were unable to assess protection from disease or death and could only speculate that diminishing virus replication might result in reduced disease severity.

In 2007, Subbarao et al created a mouse adapted SARS-CoV (MA15) through repeated passage of SARS Urbani in BALB/c mice(167). We then constructed a molecular clone of MA15 (rMA15) by introducing the six amino acid changes found in MA15 into the infectious clone for SARS Urbani (icSARS)(167). When administered intranasally to young BALB/c mice, rMA15 causes significant weight loss by 4 days post infection (dpi) (~20 % of starting weight) and is uniformly lethal by 5 dpi(167).

Unfortunately pathogenesis of rMA15 in senescent animals has not yet been evaluated. Nevertheless, if applied as a challenge virus in vaccine studies, the robust rMA15 lethal BALB/c model would allow for the assessment of protection from not only replication but also disease and mortality.

In this study, we have developed a lethal mouse adapted recombinant SARS-CoV bearing a zoonotic GD03 S glycoprotein (rMA15 GD03-S) testing the hypothesis that the mouse adapted gene set will universally enhance pathogenesis of variant S glycoproteins. In contrast to the parent rMA15 virus, the recombinant rMA15 GD03-S is only lethal in senescent BALB/c mice. We vaccinated senescent BALB/c mice with VRP vaccines expressing human (Urbani S), civet (SZ16 S) or zoonotic sporadic human (GD03-S) S glycoproteins or a pool or all three VRP vaccines and challenged them with the lethal rMA15 GD03-S. The homologous VRP GD03-S and pooled VRP-S cocktail provided the most robust protection from mortality(GD03-S 29% and Pool-S 33% survival) however, all vaccines failed to protect animals from morbidity and mortality. In the future, this model will be useful in evaluating the design and efficacy of vaccines targeting elderly populations and in elucidating the molecular mechanisms by which senescent immune systems attenuate vaccine efficacy.

Materials and Methods

Viruses and cells. The recombinant epidemic strain virus "icSARS" (AY278741), rMA15, icGD03-S (AY525636), and rMA15 GD03-S were titered and propagated on Vero E6 cells as described(247). Vero E6 cells were grown in MEM (Invitrogen, Carlsbad, CA) supplemented with 10% FCII (Hyclone, South Logan, UT) and gentamycin/kanamycin (UNC Tissue Culture Facility). All virus work was performed in a Class II biological safety cabinet in a certified biosafety level 3 laboratory containing redundant exhaust fans while wearing Tyvek suits and PAPRs as described(249).

Construction of rMA15 GD03-S. The SARS Urbani infectious clone genome is divided across 6 plasmids (icSARS-A to icSARS-F) and the spike gene is split between plasmids icSARS-E and icSARS F pSMART. Recently we have introduced the GD03 S into the SARS infectious clone resulting in the creation of a recombinant chimeric SARS-CoV bearing a GD03 S. Using an infectious cDNA clone for the mouse adapted SARS (MA15) genome, which contains 6 amino acid changes from the epidemic strain sequence (H133Y nsp5, E269A nsp5, T67A nsp9, A4V nsp13, Y436H Spike, E11K M protein), we used overlapping PCR to mutate the icSARS GD03-E subclone to encode the Y436H mutation. Briefly, the

icSARS-GD03-E pSMART fragment DNA was amplified by PCR using Expand High Fidelity Polymerase (Roche, Indianapolis, IN) with the following primer sets: Amplicon A (NcoIF 5'-TGTTTCTAAACCCATGGGTACACAG-3' and MA15spkR 5'-GATACCTATATTTATAATTATGATTACCAG-3') and Amplicon B(XbaIR 5'-GGGCCCTCTAGAGATCGAGC-3', and MA15spkF 5'-CTGGTAATCATAATTATAAATATAGGTATC-3'). A second round of high fidelity PCR was performed using amplicons A and B as template and the NcoIF and XbaIR primer set creating an AB amplicon containing GD03 spike sequences and the Y436 mouse adaptive mutation. The final AB amplicon was purified using a Qiagen PCR purification kit (Qiagen, Valencia, CA) and digested with NcoI and XbaI (NEB, Ipswich, MA) for 1 hour at 37˚C. The target vector, icSARS GD03-E pSMART, was digested with NcoI and XbaI (NEB, Ipswich, MA) for 1 hour at 37˚C. The digested AB amplicon (2.2KB) and vector fragments (5.3KB) were gel purified using a QIAquick gel purification kit (Qiagen, Valencia, CA), ligated to create rMA15 GD03-E pSMART and sequence verified. To generate rMA15 GD03 F pSMART, the 5' end of the GD03 spike contained in the icSARS GD03-F plasmid was shuttled into the rMA15 F TOPO-XL plasmid. icSARS GD03 F pSMART was digested with BamHI (NEB, Ipswich, MA) while rMA15-F TOPO-XL was digested with BamHI and CIP (NEB, Ipswich, MA). icSARS-GD03 F pSMART (2059bp) and rMA15-F TOPO-XL (7260bp) fragments were gel purified and ligated to create rMA15 GD03-F TOPO-XL. Full length rMA15 GD03-S cDNA was constructed, *in vitro* transcripts were generated and electroporated into Vero E6 cells to create recombinant virus as described. rMA15 GD03-S virus supernatant from the electroporated Vero E6 cell culture (passage zero), was passaged 2 times after which robust cytopathic effect was seen. rMA15 GD03-S was then plaque purified and isolated plaques were expanded in 6-well dishes. 6-well dish supernatant was used to infect a T175 flask of Vero E6 cells to generate a virus stock that was harvested after 20 hours post infection (hpi). Viral RNA from the rMA15 GD03-S virus stock was isolated using TRIzol (Invitrogen, Carlsbad, CA), cDNA was synthesized using SSII (Invitrogen, Carlsbad, CA) and amplicons spanning the S, 3a, E and M genes were generated by RT-PCR and directly sequenced. One conserved coding change was found outside of the receptor binding domain of S at residue 623 from serine to tyrosine.

Growth curve analysis. Vero E6 cells were infected with icSARS, icGD03-S, rMA15, or rMA15 GD03-S at an MOI of 0.01 for 1hr at 37˚C after which the inoculum was removed, the monolayer was rinsed with DPBS, and growth media was added. Media was sampled at 0, 6, 12, 24 and 36 hpi and samples were stored at -80˚C until titered by plaque assay as described(247).

Infection of young and senescent BALB/c mice. Animal housing and care were in accordance with all University of North Carolina Institutional Animal Care and Use Committee guidelines. All BALB/c mice were purchased from Harlan Sprague Dawley (Indianapolis, IN). Ketamine anaesthetized 10 week (n = 10/virus) or 12 month old BALB/c (n = 6/virus) mice were intranasally infected with 10^5pfu/50µl of rMA15 or rMA15 GD03-S after which clinical signs of disease (weight) were monitored every day post infection (dpi). On 2 and 4 dpi, groups of animals were sacrificed and lungs were removed for histology and virus lung titer. For virus titer, portions of the lung weighed, placed in 0.5ml DPBS, and frozen until titered via plaque assay. Briefly, lungs were homogenized, clarified by centrifugation, and virus titer within lung supernatants were assessed via plaque assay in Vero E6 cells as described(180). For lung histology, portions of the lungs were fixed in 4% PFA in PBS for 7 days before paraffin embedding, sectioning at 5 µm thickness, and hemotoxylin and eosin staining at the Histopathology Core Facility (UNC, Chapel Hill).

Vaccination and challenge of senescent BALB/c mice. 12 month old Harlan Sprague Dawley (Indianapolis, IN) BALB/c mice were vaccinated with 10^6 infectious units (IU)/10µl of either HA, SARS-S, GD03-S, SZ16-S VRP or a Pool of SARS S containing VRPs (Pool-S, 10^6 IN/antigen) in the left rear footpad. Three weeks post primary vaccination, animals were bled to assess SARS S specific serum IgG. At 13 months of age, mice received a secondary vaccination of equal dose and identity of their primary vaccination. At 15 months of age, mice were bled to assess post-boost SARS S specific serum IgG. A week later, mice were intranasally infected with 10^5pfu/50µl rMA15 GD03-S. Mice were monitored daily for clinical signs (weight). At 2 dpi, three animals per group were sacrificed to assess virus lung titer and histology as described above.

Serology of vaccinated senescent BALB/c mice by ELISA. Antibodies to the SARS S protein were quantitated by enzyme-linked immunosorbant assay (ELISA). Purified recombinant SARS S proteins (BEI Resources, Manassas VA) were coupled to high-binding plastic plates (NUNC Immunlon 4HBX) in 0.1 M carbonate buffer, pH = 9.6. Alternatively, 96 well plates were coated with cell lysates from VRP GD03-S,

VRP SZ16-S or VRP HA infected BHK cells that were used as GD03, SZ16 and HA antigen in the ELISA. Antigen-coupled plates were stored at 4ºC in a humid chamber overnight, or for up to 3 weeks. Purified antigens were coupled to plates at a concentration of 1 μg/ml (100 ng/well, 100 μL/well).

On the day of the assay, the plates were washed 4x with ELISA wash buffer (EWB – phosphate buffered saline, pH = 7.4 with 0.01% Tween-20), excess medium was removed, and serum samples (diluted in EWB with 10% Sigma-Blok (Sigma-Aldrich) were added to the plate, 100 μL/well. No pre-block step was necessary. After 2 hours of incubation at 4ºC in a humid chamber, the plates were washed as above, and 100 μL of isotype-specific horseradish peroxidase- (HRP-) conjugated goat anti-mouse immunoglobulin was added to each well. The plates were returned to the humid chamber for 2 hours.

The enzyme substrate was prepared immediately before use. For each 10 ml of substrate needed, 5 ml of 0.1 M acetic acid was mixed with 5 ml of 0.1 M sodium acetate, and 2 tablets of Sigma o-Phenylenediamine dihydrochloride (OPD) substrate (catalog number P3804-50TAB) were added and dissolved. After the OPD dissolved, 7.2 μL of 30% hydrogen peroxide was added for each 10 ml of substrate. The plates were washed, a sheet of clear adhesive film was added to the top plate on the stack, and the stack of plates was inverted, shaken several times, and then washed as done above. Extra medium was flicked off, the plates slapped onto paper towels, and 100 μL of substrate was added to each well. The plates were incubated for 30 minutes in the dark at room temperature and the reaction was stopped by the addition of 100 μL of 0.1 M sodium fluoride. The optical density of colored product was read immediately at 450 nm in an automated plate reader.

For analysis, every plate includes at least 4 wells that were antigen-coupled and received HRP-conjugate, but no serum. The average of these (background) values were subtracted from all of the OD readings, and these adjusted OD values were plotted for each serum sample *versus* the $\log_{10}$ of the serum dilution A sigmoidal curve was then fit to these values using regression analysis and the half-max titer of that sample was derived: the serum dilution at which the OD is exactly half of the plateau maximum value. Comparisons between half-max titers derived from different experimental groups were statistically evaluated using the Mann-Whitney U test, a non-parametric method.

Plaque reduction neutralization assay using post-boost sera. The percent neutralization for post boost serum samples was determined by a microneutralization assay as previously described(172). Briefly, sera

was serially diluted in twofold increments beginning at 1:25 and then mixed with 100pfu of rMA15-GD03 and incubated for 1hr at 37˚C. Virus and sera was then added to a 96-well plate of Vero E6 cells (5 x 10^3 Vero E6/well). Each dilution of sera was plated in triplicate. Wells were then assessed for the development of CPE at 4 to 5 days post infection. For each dilution of sera, the number of wells protected from CPE were scored. The greatest dilution of sera with more than 2 wells of protection is the 50% neutralization titer.

Statistical Analysis. Statistical analysis was performed using Prism (Graphpad, San Diego, CA) software. Non-parametric Mann Whitney tests were performed to generate P values noted in the text.

Results

In vitro and in vivo characterization of the mouse adapted rMA15 GD03-S virus. To increase the stringency of our senescent mouse vaccination and challenge model, we constructed a recombinant SARS-CoV bearing a GD03 spike within the mouse adapted SARS-CoV infectious cDNA clone. Recombinant rMA15 GD03-S virus was isolated, passaged twice and plaque purified. One amino acid mutation was found (S623Y) in the spike gene most likely resulting from passage while generating the virus stock. Interestingly, the recombinant icSARS GD03-S virus described in Deming et. al. developed a mutation (D613G) in a similar location of S during the process of virus stock generation(41). To assess virus growth kinetics in vitro, Vero E6 cells were infected with rMA15, rMA15 GD03-S, icGD03-S or icSARS at an MOI of 0.01. At 12 hpi, rMA15, rMA15 GD03-S and icSARS titers were 1 log superior to that of icGD03-S (Fig. 1). At 24 hpi, rMA15 GD03 and icGD03-S titers are approximately 1 log inferior to rMA15 and icSARS. Though icGD03-S and rMA15 GD03-S growth seemed to be depressed at earlier times, all viruses achieved similar peak titers (<10^8pfu/ml) at 36 hpi (Fig. 1).

Age is a critical factor in determining mortality in BALB/c mice infected with rMA15 GD03-S. After characterizing the in vitro growth kinetics of rMA15 GD03-S, we then wanted to evaluate the in vivo growth kinetics and pathogenesis of the novel virus. First, we infected 10wk old BALB/c mice with 10^5 pfu rMA15 GD03-S or rMA15. rMA15 infection was uniformly fatal with mice losing 20% of their starting weight by 4 dpi and all mice succumbing to infection by 5 dpi (Fig 2A). In contrast to rMA15 infection, rMA15 GD03-S infected mice all survived but did experience significant virus induced morbidity losing more than 10% of their starting weight by 4 dpi (Fig. 2A). Interestingly, virus titers for

rMA15 and rMA15 GD03-S were similar on both 2 (rMA15 $3.2x10^7$ pfu/g, rMA15 GD03-S $1.5x10^7$pfu/g) and 4 (rMA15 $3.6x10^5$ pfu/g, rMA15 GD03-S $9.3x10^5$pfu/g) dpi (Fig. 2A).

Unlike infection of young adult mice, rMA15 and rMA15 GD03 infection of senescent mice was uniformly lethal. Infection of 12 month old BALB/c mice with either mouse adapted strain caused rapid weight loss (~20% starting weight) and 100% mortality by 4 dpi (Fig. 2B). Mean virus lung titers in senescent mice were elevated as compared to young adult mice at early time points. On 2 dpi, rMA15 and rMA15 GD03-S achieved mean titers approximately 1 log greater (rMA15 $1.3x10^8$ pfu/g, rMA15 GD03-S $2.6x10^8$ pfu/g) than titers in young adult mice at similar times post infection (Fig. 2B). By 4 dpi, mean virus lung titers of both viruses had waned to similar levels (rMA15 $9.7x10^5$ pfu/g, rMA15 GD03-S $3.5x10^5$ pfu/g) seen in young adult mice at similar times post infection (Fig 2B).

Morbidity and mortality is seen in all experimental groups of VRP vaccinated 15 month old rMA15 GD03-S challenged BALB/c mice. The SARS-CoV epidemic was most virulent in the elderly therefore it is imperative that vaccine therapies be effective in immune senescent populations. Senescent BALB/c mice were primed at 12 and boosted at 13 months of age with VRP expressing SARS Urbani-S, GD03-S, SZ16-S or a pool of all three SARS-CoV S antigens (Pool-S). Control mice were administered VRP expressing the influenza HA glycoprotein in the same manner. At 15 months of age, mice were intranasally challenged with 10^5 pfu of rMA15 GD03-S after which morbidity and mortality were monitored daily over 13 days. All vaccination groups exhibited significant morbidity and mortality after rMA15 GD03-S infection (Fig. 3A, 3B). All groups lost more than 20% of their starting weight by 4 dpi. In addition, 100% of VRP HA and VRP SZ16-S vaccinated mice succumbed to infection by 5 and 6 dpi, respectively (Fig. 3B). The groups receiving the VRP expressing the Urbani-S, GD03-S or Pool-S demonstrated varying degrees of survival with the groups receiving the homologous antigen experiencing the most protection (Percent survival: VRP Urbani-S 11%, VRP GD03-S 29%, VRP Pool-S 33%) (Fig. 3B). Virus lung titers were very high 2 dpi (< 10^8pfu mean lung titer) in all vaccine groups (Fig. 4). Regardless of the SARS vaccine antigen, most vaccinated animals died from virus infection demonstrating difficulties in priming the adaptive immune response through vaccination in aged animals.

Levels of GD03-S specific IgG predict mortality in post boost sera. The development of an adequate antibody response against the SARS S glycoprotein through vaccination is necessary to prevent SARS-CoV

replication after challenge. To assess the SARS S specific IgG response in post prime and post boost sera, we performed several versions of ELISA. The target antigen employed in the ELISA assay was varied (Urbani-S, SZ16-S, or GD03-S proteins) in order to gauge cross reactivity of the immune responses generated by each vaccine regimen. For example, ELISA plates coated with Urbani-S antigen probed with sera from Urbani-S, SZ16-S or GD03-S vaccinated mice allow us to assess the quality of the homologous Urbani-S specific responses but also the heterologous and cross reactive SZ16-S and GD03-S specific responses. When comparing peak IgG titers in each vaccine group, the titer of the greatest magnitude was typically against the cognate vaccine antigen. Mean Log_{10} Half-Max IgG titers against the homologous vaccine antigen in the Urbani-S and GD03-S groups increased with boost while SZ16-S decreased slightly (Fig. 5A, B, C). Not surprisingly, the mean Log_{10} Half-Max IgG responses within the Pool-S group were similar for each antigen in the cocktail(Fig. 5D). Importantly, sera from control VRP HA animals did not significantly cross react with the SARS antigens and the magnitude of HA specific responses were comparable to those seen in the SARS S groups (Fig. 5E). Though the degree of mortality varied with each group, the magnitude of the mean Log_{10} Half-Max GD03 specific IgG titers in each group were similar (Fig. 5A, B, C, D). Since mean GD03 specific IgG titer in each group did not seem to correlate well with mortality, animal serology data was stratified by mortality to create two groups: "protected" from mortality (n = 7) and "not protected" from mortality (n = 26). When comparing the protected and not protected cohorts that received VRP expressing SARS antigen, there is a statistically significant difference ($p = 0.0002$) in the mean Log_{10} Half-Max GD03-S specific IgG titer (protected = 2.455, not protected = 1.233) (Fig. 5F). We performed a microneutralization assay to generate 50% neutralization titers from post boost sera for each animal in the study. One animal in the SZ16 group and one animal in the GD03 group had a reciprocal 50% neutralization titer of 25 while all other animals tested had titers below the limit of detection(Fig. 6).

Discussion

Many respiratory viruses like influenza, RSV and SARS-CoV cause disproportionate burdens of disease in the immune senescent and it is important that vaccination be successful in this most vulnerable population(116, 202). Prior to this report, most all SARS-CoV vaccine studies were performed within young animal models of SARS-CoV infection characterized by acute virus replication and deficient in

overt signs of clinical disease. In 2006, Deming et al demonstrated that VRP expressing Urbani-S provided complete protection from heterologous challenge virus (icGD03-S) replication in young adult mice but provided variable protection in the senescent model(41). However, it was not clear whether variable protection from replication in this model would correlate with protection from lethal infection. To this end, we developed a recombinant mouse adapted SARS-CoV (rMA15) through the introduction of six amino acid changes into the epidemic strain infectious cDNA clone. Within the rMA15 infectious cDNA clone, we constructed a recombinant mouse adapted virus bearing the S glycoprotein from the most divergent human strain (GD03). The rationale for the construction of this virus is three-fold: First, we sought to investigate whether the mouse adapted mutations would universally enhance disease pathogenesis of recombinant viruses bearing zoonotic spike proteins. Secondly, since the epidemic strain may no longer exist in nature and future epidemics might emerge from zoonotic pools, we sought to create a more relevant challenge virus to evaluate vaccine efficacy that was similar to the zoonotic SARS-CoV ancestors of the epidemic strain. Lastly, we wanted to determine the feasibility of using the rMA15 molecular clone as a rapid and robust platform within which to construct lethal challenge viruses bearing S genes from future emergent SARS-CoV.

To rapidly construct the rMA15-GD03-S virus, the GD03 S gene cDNA was synthetically derived, the MA mutation was introduced into the S gene, the GD03 S containing the MA mutation (Y436H) was cloned into the rMA15 infectious clone, infectious genomic viral RNA was electroporated into Vero E6 cells and recombinant virus was recovered. Though rMA15 GD03-S in vitro growth is depressed 1 log as compared to rMA15 12 hpi, rMA15 GD03-S and rMA15 replicate to similar peak titers by 36hpi in Vero E6 cells. Also, virus lung titers on 2 and 4 dpi in young BALB/c mice infected with rMA15 or rMA15 GD03-S are similar but infection with rMA15 GD03-S is attenuated while rMA15 is uniformly lethal. These data suggest GD03 S glycoprotein and receptor ACE2 interactions are not as efficient as compared to those with rMA15 resulting in GD03 S mediated attenuation of virulence. Moreover, the Y436H MA mutation may lose its effect within GD03 S receptor binding domain architecture which may also contribute to attenuation in young mice. Interestingly, virus titers in the lungs of rMA15 and rMA15 GD03-S on 2 and 4 dpi were not statistically different. Since rMA15 has a significant growth advantage over rMA15 GD03-S at early times within in vitro growth experiments, it is possible that increased

replication of rMA15 at early times during mouse infection and/or other times we did not evaluate set the stage for the lethal phenotype. Also, where rapid rMA15 growth within the lungs of young BALB/c mice most likely sets the course for lethal infection, delayed growth of rMA15 GD03-S in the lungs at early times post infection may make the virus to be more susceptible to the innate immune response contributing to virus clearance.

For the study of age related viral pathogenesis, the extreme differences seen in mortality between young and senescent BABL/c infected with rMA15 GD03-S may allow for the elucidation of age related mechanisms of severe SARS-CoV disease. As compared to young mice, rMA15 GD03-S lung titers in senescent mice are elevated 1 log 2 dpi indicating the senescent animals on some level fail to control replication. These data suggest that some protective components within young adult mice are absent in senescent mice or senescent mice are less resilient in handling acute lung damage but both scenarios could potentially explain mortality in senescent animals. The innate immune system is debilitated in the senescent mouse and may account for the elevated virus lung titers and mortality seen with rMA15-GD03-S infection. Recent reports on the senescent immune system suggest that classical innate sentinels like macrophages and dendritic cells are defective in normal cytokine secretion after pathogen sensing, phagocytosis, and migration(31, 32, 60). These defects in the innate response may have allowed for the elevated replication of the rMA15 GD03-S virus in senescent mice and resultant mortality. The aged mouse lung might also be less resilient in acute lung injury caused by virus replication and the immune response. The repair of tissue damage in the lung has been described as an inflammatory process very similar to wound healing in other tissues(66). Deficiencies in the senescent inflammatory response whose coordination and function are necessary for appropriate wound healing have been demonstrated to delay wound healing and tissue repair(87). As compared to young mice, the cytokine milieu and inflammatory cell infiltration and function at the site of tissue damage is altered possibly contributing to a delay in repair(87). Detailed experiments exploring temporal virus lung titer and the associated inflammatory response in young and aged mice may help elucidate the mechanisms of the age related mortality seen in rMA15 GD03-S infection. Moreover, it is possible that functional innate immune deficits observed in aged related mortality seen with rMA15 GD03-S infection may also mediate enhanced pathogenesis of other respiratory viruses (i.e. RSV, influenza etc.) in the immune senescent. Surprisingly, very few small animal

models exist to simultaneously study disproportionate viral disease in the immune senescent and age related effects on vaccine efficacy and to our knowledge, with rMA15 GD03-S we have developed the third SARS-CoV model with attenuated disease in young and lethal disease in old mice(172). Studies of vaccine efficacy in young adult mice using rMA15 GD03-S as a challenge virus are not as robust as senescent models due a lack of mortality though significant morbidity and replication could be used as metrics for therapeutic efficacy.

Due to the probable extinction of the epidemic strain, vaccine studies using the epidemic strain as both vaccine antigen and challenge virus most likely do not represent realistic scenarios of future SARS-CoV emergence. So, rather than use a vaccine antigen that is homologous to antigen in the challenge virus, we constructed a panel of VRP vectors expressing an array of divergent SARS-CoV S glycoprotein antigens with the goal of inducing broadly cross reactive immune responses using an antigenic cocktail of vaccines. VRP vaccines are safe replication incompetent vaccine vectors capable of inducing mucosal immunity from a peripheral route of inoculation(41, 201). Previously, we demonstrated that vaccination of young adult mice with VRP expressing Urbani S provided complete protection from icGD03-S replication upon challenge and this protection was mediated by a very robust cross neutralizing antibody response(41). Using a prime and boost regimen, we vaccinated senescent BALB/c mice with VRP expressing S glycoproteins of Urbani, GD03 or SZ16 strains or a cocktail of all three VRPs. Both the GD03 and SZ16 S glycoproteins differ from the epidemic strain in 18 amino acids 16 of which reside in the target area of most neutralizing antibodies (S1 region). Control mice were vaccinated with VRP expressing influenza HA. Our antigenically diverse SARS S expressing VRP panel coupled with our lethal rMA15 GD03-S challenge virus allows us to assess the efficacy of immune responses to both homologous (VRP GD03-S) and heterologous (VRP Urbani-S and VRP SZ16-S) antigens. Upon challenge with the rMA15 GD03-S, all groups demonstrated significant morbidity losing more than 20% of starting weight by 5 dpi and significant virus replication in the lung with mean titers exceeding 10^8 pfu/g. Assessing protection from mortality, the HA and SZ16 groups uniformly succumbed to infection, the Urbani-S group demonstrated little protection from mortality while groups that received the homologous antigen demonstrated the most protection (GD03-S 29%, Pool-S 33% survival). These data suggest that vaccination of senescent animals with VRP expressing antigens similar to the challenge virus provides the most protection against rMA15 GD03-S

infection though protecting only 30% of vaccinated animals is not an ideal outcome. Prior to Deming et. al., SARS-CoV vaccination strategies had not been evaluated in aged mice(41). Moreover, very few studies of influenza vaccine efficacy have been performed in aged mouse models. In 1993, Ben-Yehuda et al demonstrated that a recombinant vaccinia virus vaccine expressing influenza PR8 HA protected senescent mice from intranasal challenge by a homologous PR8 strain while conventional vaccines (killed virus vaccine) failed(14). Similarly, Asanuma et. al. (2001) demonstrated partial protection of various strains (BALB/c, C57BL/6, C3H) of aged mice from PR8 challenge after conventional vaccination(9). Since effective vaccination strategies in the elderly have not yet been developed for influenza, West Nile virus and SARS-CoV, the development of small animals models to study vaccine efficacy in senescent populations may have broad public health application.

Our morbidity and mortality data suggested that the immune response to VRP vaccination may not have been robust since all vaccination groups experienced both morbidity and mortality. Since the importance of an adequate IgG response has been demonstrated to be necessary for protection from SARS-CoV infection, we assessed the magnitude and cross reactivity of the SARS S specific IgG responses by ELISA. VRP vaccination of senescent animals induced robust homologous and heterologous SARS S specific serum IgG responses while sera from the HA control group did not cross react with SARS antigens. Since the development of an adequate anti GD03-S IgG response would most likely be the most important in protection against the rMA15 GD03-S challenge, we sought to compare mean anti GD03-S IgG titers between groups. Due to the variability in mean anti GD03-S IgG within each group, the means were not statistically different when comparing Urbani-S, GD03-S, SZ16-S or Pool-S groups. As a result, these data could not help to explain the differences seen in survival among the groups receiving VRP expressing SARS-CoV antigen. Since comparing mean GD03 S specific IgG among vaccine groups was not particularly informative, we stratified the serology data into two groups: those that were protected from mortality and those that were not protected from mortality. When organizing the data in this way, we now see that the animals that were protected from mortality had a superior GD03 S specific serum IgG titer as compared to those that were not protected and this difference was statistically significant. Since neutralizing antibody would most likely be responsible for this protection from mortality, we assessed sera for neutralizing antibody by microneutralization assay using the rMA15 GD03-S as challenge virus. Only

two of our samples had reciprocal 50% neutralization titers of 25 while the remaining 57 samples were below the limit of detection (l.o.d. = 25) suggesting that low titers of neutralizing antibody are sufficient to protect from rMA15 GD03-S induced mortality. Since very few sera samples had neutralization titers above the limit of detection, we could not correlate survival to neutralizing antibody titers. Nevertheless, there was a statistically significant difference in GD03 S specific IgG in comparing animals protected and not protected from mortality confirming the importance of the antibody response in protection from virus induced death.

Deming et al reported that vaccination with VRP expressing Urbani S provided complete protection from replication after a heterologous icGD03-S challenge(41). These data suggest that VRP based vaccines are quite capable of inducing an appropriate and sufficient cross protective immune response in immune competent young adult mice. Interestingly, senescent animals seem unable to generate an adequate immune response by VRP Urbani-S vaccination and as a result we detect virus replication, morbidity and mortality. Two possible explanations may help explain the differences seen in the vaccine efficacy when comparing young adult and senescent mice. The first explanation involves VRP cell tropism in vivo while the second explanation involves deficiencies in innate and adaptive immunity due to immune senescence. Since the VEE structural genes are replaced by a transgene of interest within VRP genomes, VEE structural genes provided in trans to "package" the replicon RNA and various VEE structural proteins can be utilized to enhance vector attenuation and safety(16, 41, 98, 201). While WT recombinant VEE V3000 infection is uniformly lethal in mice, VEE clones V3010, V3014, and V3533 are mutated in their viral glycoproteins and are completely attenuated in mice with all mice surviving infection(16). A VRP packaged with wild-type VEE V3000 glycoproteins is targeted to the professional antigen presenting dendritic cell (DC) while the attenuated V3014 was found to have enhanced binding of heparan sulfate altering DC targeting/spread(130). These data suggest that the alteration of the VRP coat can have profound effects on cell targeting which may affect the efficiency of antigen presentation and the resultant immune response. On their major histocompatibility complexes (MHC), DCs can present endogenous (i.e. peptides from within the infected cell) or exogenous (peptides acquired from phagocytosis) antigen to prime cognate T cells for activation(82, 165, 231). DC priming of T cells using endogenous or exogenous (cross-priming) peptides can vary in efficiency resulting in differences in the quality and magnitude of the

immune response(231). If VRP cell targeting differentially affects the pathway of antigen presentation (endogenous vs. exogenous), T cell activation may vary directly affecting the quality of the immune response.

Another possible explanation of why our vaccine failed to generate an adequate immune response in senescent animals may involve intrinsic deficiencies of the aged immune system. Functional anomalies in both antigen presenting cells (DCs) and effector cells are seen in the senescent immune system complicating the process of vaccination. As the immune system ages, DCs become less efficient at antigen sampling by phagocytosis and pinocytosis and their ability to migrate also becomes impaired(7). If the antigen presenting cell is compromised in its ability to migrate and present antigen, the generation of an adaptive immune response may be compromised. Cytokine secretion (IL-2) and key surface receptor expression (CD40L, CD28) on $CD4^+$ T_h cells declines as the immune system ages(3, 75). Appropriate and adequate cytokine secretion and surface receptor expression are required for efficient $CD8^+$ T cell and B cell activation(75). Moreover, thymic involution and oligoclonal expansion of memory cells in response to chronic antigen exposure decrease the numbers and complexity of naïve T cells in the periphery of aged individuals(75, 77, 215). The complications of the senescent immune system have plagued successful influenza vaccination of the elderly where 17- 53 % of individuals are protected(64). Several experimental adjuvants like MF59 and CpG DNA have been able to overcome the apparent deficiencies of the senescent immune system enhancing the efficacy of vaccination and may prove to be an invaluable tool in vaccination of senescent populations(83, 131). Unfortunately, our preliminary data suggest that CpG delivered with VRP-GD03 does not enhance protection from rMA15 GD03-S infection in senescent animals(Data not shown). Rather than enhance the immune response of inactivated vaccines with adjuvants, an alternative approach might be to develop live attenuated virus vaccines.

Effective SARS-CoV vaccines should protect against future emergence of zoonotic strains and be effective in the immune senescent. We have developed a senescent mouse model of SARS-CoV disease and mortality using a mouse adapted SARS-CoV bearing a zoonotic GD03 S glycoprotein. Vaccination of senescent BALB/c mice with VRP vectors expressing epidemic strain Urbani-S, GD03-S, SZ16-S or a pool of all three S expressing vaccines (Pool-S) did not protect against morbidity and provided variable protection against mortality. Serum antibody specific for GD03 S predicted survival in the GD03-S, Pool-

S and Urbani-S groups suggesting that cross reactive epitopes exist between these antigen groups. We postulate that the apparent failure to successfully vaccinate senescent mice might be due to either intrinsic vaccine or senescent immune factors or a complex mixture of the two.

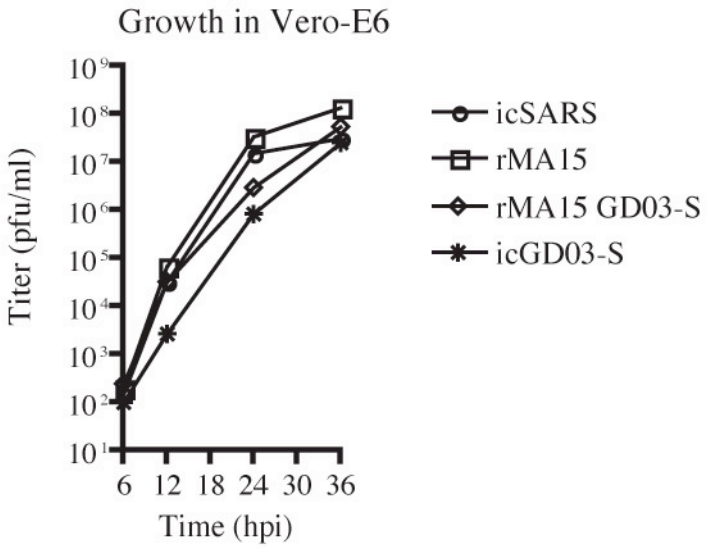

Figure 1: rMA15 GD03-S grows with slightly delayed kinetics as compared to rMA15 and icSARS in Vero E6 cells.. Vero E6 cells were infected at an MOI of 0.01 with rMA15, icSARS, or rMA15 GD03-S for 1hr at 37˚C after which monolayers were rinsed with DPBS and growth media was added. At various times post infection, cell media was sampled and frozen at -80˚C until titered by plaque assay on Vero E6 cells.

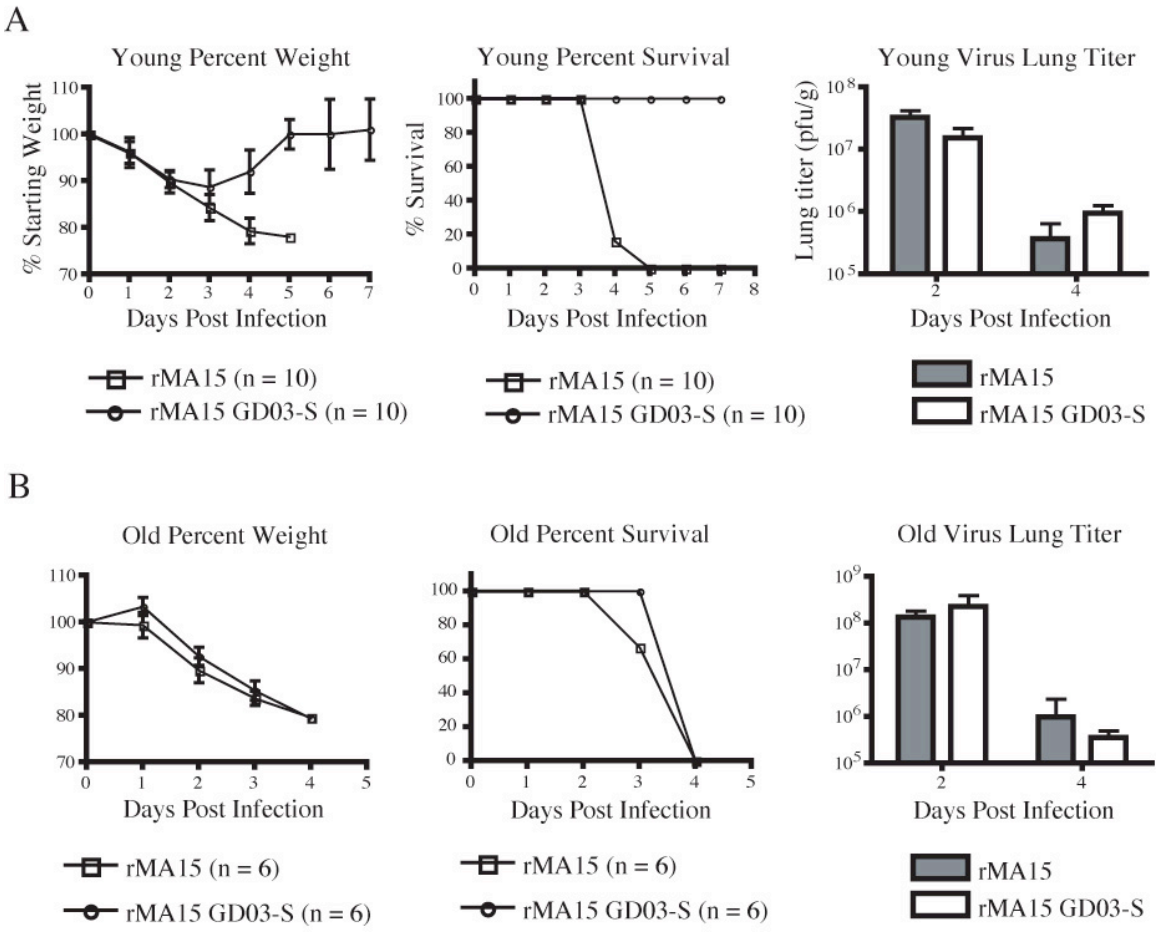

Figure 2: Age is a critical factor in determining mortality in BALB/c mice infected with rMA15 GD03-S. Ketamine anaesthetized 10wk (n = 10/virus) or 12 month old BALB/c (n = 6/virus) mice were infected with 10^5pfu/50µl of rMA15 or rMA15 GD03-S after which clinical signs of disease (weight) were monitored every dpi. Animals found dead or that were at or below 80% of starting weight were sacrificed due to IACUC protocol. On days 2 and 4 post infection, groups of animals were sacrificed and lungs were removed for histology and virus lung titer. For virus titer, lungs were homogenized, clarified by centrifugation, and virus titer within lung supernatants were assessed via plaque assay in Vero E6 cells. (A) Percent weight loss, percent mortality and virus lung titer data for young mice. (B) Percent weight loss, percent mortality and virus lung titer data for old mice.

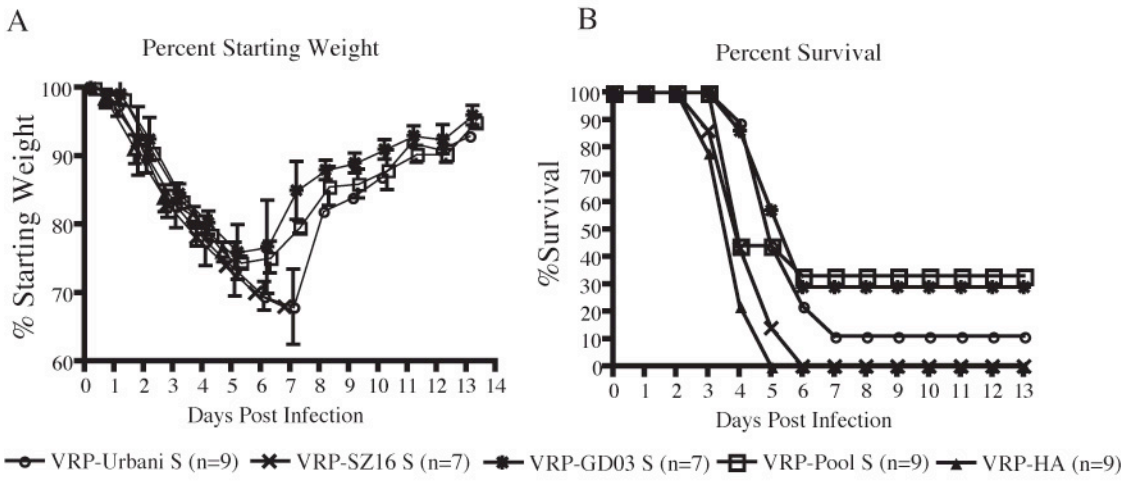

Figure 3: Morbidity and mortality is seen in all experimental groups of VRP vaccinated 15 month old rMA15 GD03-S challenged BALB/c mice. 12 month old Harlan Sprague Dawley (Indianapolis, IN) were vaccinated with 10^6 infectious units (IU)/10µl of either HA, SARS-S, GD03-S, SZ16-S VRP or a Pool of SARS S containing VRPs (Pool-S) in the left rear footpad. At 13 months of age, mice received a secondary vaccination of equal dose and identity of their primary vaccination. At 15 months of age, mice were infected with 10^5pfu/50µl rMA15 GD03-S. Mice were monitored for clinical signs (weight) every dpi. (A) Percent starting weight. (B) Percent Survival. (C) virus lung titer 2 dpi.

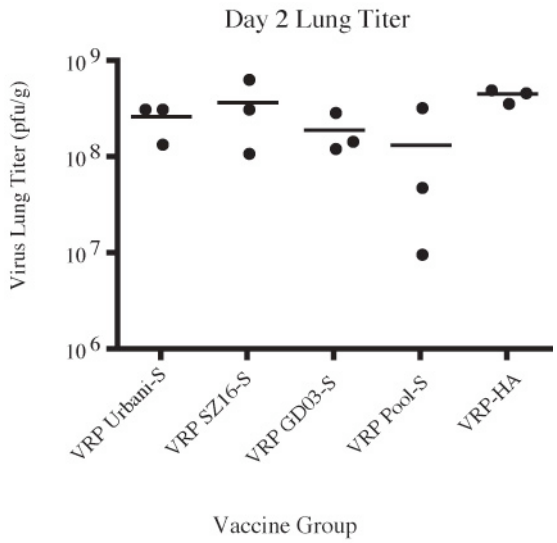

Figure 4: Virus lung titers are similar in all vaccinated groups 2 dpi. To assess the degree of protection from replication, virus lung titers were assess in 3 mice per group on 2dpi. Mean levels of replication are similar in each group.

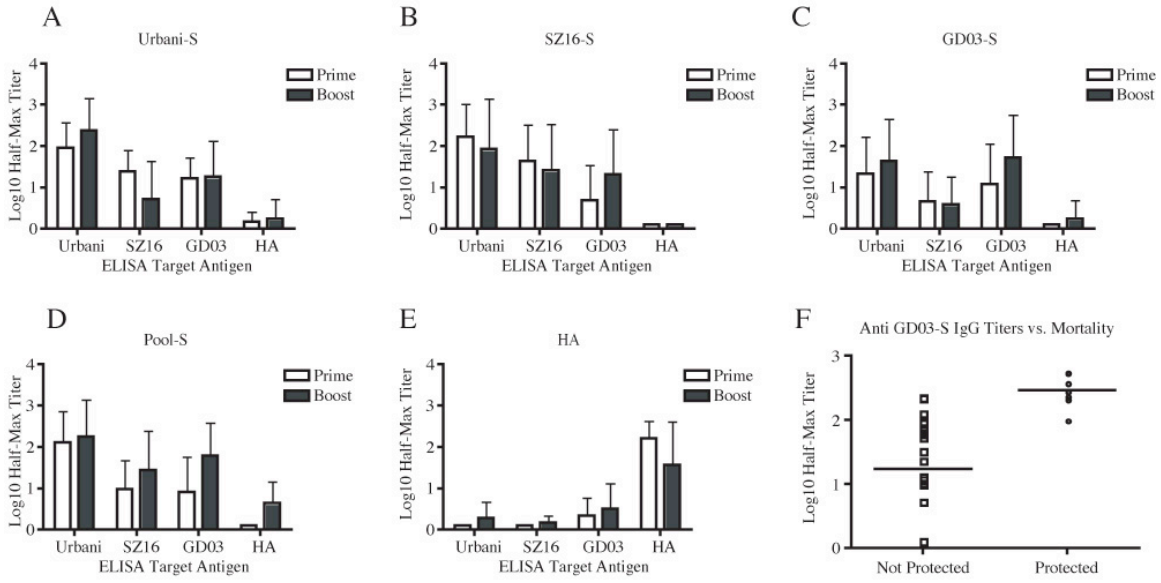

Figure 5: Levels of GD03-S specific IgG predict mortality in post boost sera. Three weeks post primary vaccination and 8 weeks post boost, animals were bled and to assess SARS S specific serum IgG by ELISA. Plates were coated with Urbani S, GD03-S, SZ16-S or HA antigen and post prime or post boost serum samples were added as primary sera in ELISA. The average of background values were subtracted from all of the OD readings, and these adjusted OD values were plotted for each serum sample *versus* the $\log_{10}$ of the serum dilution A sigmoidal curve is then fit to these values using regression analysis and the half-max titer of that sample is derived: the serum dilution at which the OD is exactly half of the plateau maximum value. (A) VRP-Urbani vaccine group responses (B) VRP-SZ16 vaccine group responses (C) VRP-GD03 vaccine group responses (D) VRP-Pool vaccine group responses (E) VRP-HA vaccine group responses (F) GD03-S specific IgG titers in animals that were protected and not protected from mortality.

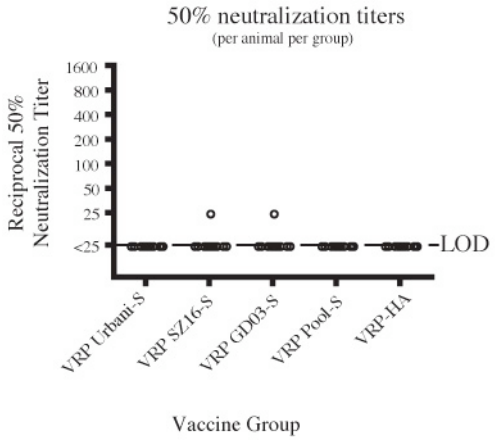

Figure 6: Very low neutralization titers are needed to protect senescent animals from mortality. The percent neutralization for post boost serum samples was determined by a microneutralization assay as previously described. Briefly, sera was serially diluted in two fold increments beginning at 1:25 and then mixed with 100pfu of rMA15-GD03 and incubated for 1hr at 37˚C. Virus and sera was then added to a 96-well plate of Vero E6 cells (5 x 10^3 Vero E6/well). Each dilution of sera was plated in triplicate. Wells were then assessed for the development of CPE at 4 to 5 days post infection. For each dilution of sera, the number of wells protected from CPE were scored. The greatest dilution of sera with more than 2 wells of protection is the 50% neutralization titer.

Chapter VI

CONCLUSION

Through the study of viral pathogenesis, the mechanisms of disease can be elucidated providing specific targets for therapeutic intervention intended to prevent the development of disease. We conducted four studies to gain a better understanding of SARS-CoV disease pathogenesis and therapeutic design. First, we two conducted studies to investigate SARS-CoV evolution and adaptation to the human host. Since efficient infection of a given host is necessary for virus propagation and the presentation of disease, host range expansion towards infection of a new host are integrative components of emerging disease pathogenesis. Second, we have investigated the importance of innate immune adaptor protein (MyD88) signaling in protection from SARS-CoV disease. Within a C57BL/6 model of SARS-CoV pathogenesis, we demonstrated that MyD88 is required for protection from lethal infection by recombinant mouse adapted SARS-CoV (rMA15). Infection of mice deficient in MyD88 with rMA15 resulted in a delay in the lung inflammatory response (i.e. deficient cytokine response, delay in macrophage recruitment) ultimately resulting in mortality. Lastly, we evaluated the protective efficacy of VRP vaccination in senescent mice challenged with a recombinant mouse adapted virus bearing a zoonotic GD03 S glycoprotein (rMA15 GD03-S). In order to induce broad cross neutralizing antibody responses, we vaccinated mice with VRP expressing three antigenically diverse SARS S glycoproteins (Urbani-S, GD03-S or SZ16-S) or a mixture of all three (Pool-S). VRP vaccination provided little protection from lethal rMA15 GD03-S infection. We postulate that the apparent failure to successfully vaccinate senescent mice might be due to either intrinsic vaccine or senescent immune factors or a complex mixture of the two.

The plasticity of SARS-CoV S in host range expansion and a putative mechanism of epidemic strain evolution. Despite initial reports that civet strains SZ16 and SZ3 could be propagated in cell culture, subsequent studies have indicated that these viruses could not be successfully maintained in culture thereby hampering our understanding of their pathogenicity and mechanisms of cross species

transmission in humans. Within the past four years, multiple newly emerging coronaviruses of human relevance have been identified highlighting the emerging disease potential of the coronavirus family. Moreover, viruses related to the SARS-CoV epidemic strain have recently been found in Chinese horseshoe bats during surveillance of wild animals in Hong Kong and as such, there is the potential for yet another reemergence. Since it is impossible to predict the antigenic identity of future SARS virus emergents, the development of highly cross reactive antibody, drug or vaccination therapies would provide the greatest potential benefit to public health. Employing a panel of all known zoonotic and human tropic SARS-CoV strains may provide the most thorough and pertinent evaluation of antiviral therapies.

The prototypic civet SZ16 spike (S) gene was engineered into our epidemic strain infectious clone (icSARS) to create the recombinant icSZ16-S virus which could not be maintained through passage in Vero E6 cell cultures. In order to promote the growth of icSZ16-S in vitro, we introduced a single point mutation in the RBD (K479N) which allowed for inefficient growth of the resultant recombinant virus (icSZ16-S K479N) in Vero E6 cells and in human airway epithelial cells (HAE). Due to the poor growth fitness of icSZ16-S K479N, we postulated that we might enhance growth fitness through passage in HAE. Moreover, we hypothesized that enhanced growth fitness through passage in HAE might be mediated by mutation in the S glycoprotein that enhanced receptor binding. After icSZ16-S K479N passage in HAE, resultant "evolved" viruses (icSZ16-S K479N D8 and D22) were mutated in S enhancing interactions with the receptor (hACE2) thereby increasing their growth fitness in HAE. Interestingly, the "evolved" virus mutations in S differed from those seen during the evolution of the epidemic strain. The in vitro growth analysis of the "evolved" viruses was supported by predictive structural models which suggested that mutations acquired through passage in HAE remodeled the RBD architecture enhancing interactions with ACE2. These data demonstrate the plasticity of the RBD contact interface and its affinity for subtle remodeling to promote efficient entry and growth. Clearly, multiple genetic pathways likely exist to allow for zoonotic SARS-CoV host range expansion and it will be interesting to determine if other mutations within the contact interface can enhance zoonotic virus infection of HAE cultures. Moreover, it will be interesting to test the limits of this S plasticity through passage in HAE. icSZ16-S K479N HAE passage experiments could be set up in parallel resulting in the isolation of several "evolved" viral clones. Through sequencing of isolated evolved clones, we could elucidate the genetic pathways that result in enhanced

infection of HAE. These pathways may be similar to those seen in the past or may be completely novel. Regardless of which outcome proves to be true, the resultant data regarding the degree of S plasticity in adaptation to the human host will be invaluable. Also, if future zoonotic SARS-CoV passage experiments in HAE produce several antigenically unique isolates, these viruses could be utilized to assess passive immunization and vaccine efficacy in current in vitro and in vivo models. Previously, we have demonstrated that the mutations acquired that enhance growth of zoonotic viruses in HAE simultaneously make them more susceptible to neutralization by human monoclonal antibody(hu-mAb) S230.15. Similar experiments could be performed with new in vitro evolved zoonotic SARS-CoV to assess their susceptibility to neutralization by hu-mAb. Since it is impossible to predict the antigenic identity of future SARS-CoV like emergents, a panel of experimentally evolved zoonotic SARS-CoV could serve as a surrogate and provide insight in the potential protective efficacy of current passive immunization and vaccination therapies.

The prototypic civet epidemic strain of SARS-CoV, SZ16, was isolated from a palm civet but has not been successfully cultured in vitro. To promote the in vitro growth of the wild type icSZ16-S virus, we constructed cell lines expressing the civet ortholog (DBT-cACE2) of the SARS-CoV receptor (hACE2). Within in vitro growth assays, we demonstrated that SARS Urbani grows with similar kinetics in both DBT-cACE2 and DBT-hACE2 cells while icSZ16-S only grows within DBT-cACE2 cells. Within predictive structure models, we provide a structural explanation as to why the epidemic strain has retained dual species tropism. Interestingly, in vitro "evolved" SZ16 S mutant viruses (icSZ16-S K479N and D22) with enhanced affinity for hACE2 exhibited severe growth defects in DBT-cACE2 cells suggesting that their mutational spectra promoting efficient hACE2 interactions, simultaneously abolished efficient interactions with cACE2. These data suggest that zoonotic viruses that evolved to more efficiently infect human cells in the absence of cACE2 lost their ability to efficient bind their native host receptor. It is hypothesized that zoonotic SARS Coronavirus (SARS-CoV) likely evolved to infect humans by a series of transmission events between humans and animals for sale in markets in China. Since dual species tropism is retained by the epidemic strain, it is likely that the 2003 epidemic virus retained high affinity interactions with cACE2/hACE2 receptors by evolving through repeated passage between human and civet hosts. This hypothesis is supported by serological surveys in Guangdong province in China where of SARS-CoV

specific IgG was found in animal traders (13%, n= 508), hospital workers (2.9% , n = 137), Guangdong CDC workers (1.6%, n = 63, and healthy adults at the clinic (1.2%, n = 84). None of the subjects tested presented with symptomatic SARS. If the subjects within the serological survey represent the population of Guangdong (est. population 100,000,000), there may have been many more subclinical cases of SARS-CoV prior to the evolution of the more virulent human adaptive strains. These data are supported by other retrospective serological surveys in China which suggest that less serious or asymptomatic cases of SARS-CoV existed at least 2 years prior to the beginning of the epidemic in various geographical locations in China. Importantly, we demonstrated that icSZ16-S is susceptible to neutralization by hu-mAb S230.15 providing further evidence of its efficacy and utility as a passive immunization therapy. We have also demonstrated that both icGD03-S and icSZ16-S are more resistant to S3.1 highlighting the utility of using an antigenically diverse SARS-CoV panel to assess sero therapy efficacy. The icSZ16-S virus is yet another antigenically divergent zoonotic S bearing SARS-CoV that will prove useful in evaluating future sero or vaccination therapies.

The innate immune response in SARS-CoV infection. The clinical course of SARS-CoV disease in humans is characterized by fever, non-productive cough, and malaise culminating in lung infiltrates visible by x-ray and an atypical pneumonia. Immunologically, SARS-CoV infection of humans generates a cytokine storm where elevated levels of IP-10, MIP1-α, and MCP-1 are detected within the blood. Histological examination of lung tissue in terminal SARS-CoV cases revealed SARS antigen within macrophages in the lung suggesting a role for these cells in SARS-CoV pathogenesis. Though clinical and epidemiological data from the epidemic and reemergence has provided insight into the molecular pathogenesis of SARS-CoV, thorough studies of virus and host interactions have been hampered by the lack of animal models that fully recapitulate human disease. C57BL/6 mice infected with the epidemic strain, SARS Urbani, do not show any overt signs of disease but there is virus replication in the lung ($10^7 TCID_{50}$/g 3dpi), induction of MIP1α/MCP-1 and viral clearance even in the absence of T, B and NK cells suggesting that innate immunity alone is required for protection within this acute model of SARS-CoV replication. MA15 is a mouse adapted SARS-CoV strain that was generated by fifteen serial passages of the epidemic strain, SARS Urbani, in the lungs of BALB/c mice. Infection of young or senescent BALB/c mice with either MA15 or recombinant MA15 (rMA15) results in high virus titers in the lung,

pulmonary pathology and mortality similar to those seen in severe and acute human cases of SARS-CoV disease. Toll-like receptors (TLRs) are cellular receptors that recognize molecular signatures of pathogens and initiate an inflammatory signaling cascade that is key to the innate immune response. Myeloid differentiation primary response gene 88 (Myd88) is key adaptor protein within the inflammatory signaling pathways of most all TLRs as well as IL-1R, IL-18R and INFγR1. In animal models of viral pathogenesis, Myd88 signaling has been shown to be protective oftentimes providing instructions to innate immune cells shown to be important for viral clearance. The role of Myd88 signaling in SARS-CoV pathogenesis has not yet been described.

We have demonstrated that mice deficient in MyD88 ($MyD88^{-/-}$), an adapter protein that mediates Toll-like receptor (TLR), IL-1R, and IL-18R signaling, are far more susceptible to mouse adapted SARS-CoV (rMA15) infection. We find overwhelming evidence that suggests that mice deficient in Myd88 are unable to control virus replication early within the course of infection. Compared to WT mice, virus titers are elevated in $Myd88^{-/-}$ mice at early times post infection and remain elevated until virus induced death. Despite increased viral loads, the expression of multiple proinflammatory cytokine and chemokine (e.g. MIP1α and MCP-1) genes within lung tissue was significantly reduced in $MyD88^{-/-}$ mice compared to wild-type mice. The recruitment of inflammatory monocytes into the infected lungs of WT mice is coincident with a reduction of virus replication as seen by in situ hybridization. The recruitment of these cells is severely delayed in $MyD88^{-/-}$ mice suggesting that MyD88-mediated innate immune signaling and inflammatory cell recruitment to the lung are required for protection from lethal rMA15 infection.

To further understand the mechanism of MyD88-mediated protection in rMA15 infection of C57BL/6 mice, the molecules mediating the induction of the initial inflammatory response to virus infection should be elucidated. We hypothesize that early inflammatory signaling events in WT mice recruit inflammatory macrophages to the lung resulting in a control of virus replication and survival. To this end, we first set out to determine the contribution of alveolar macrophages in the recruitment of the inflammatory macrophages we hypothesize are important in controlling virus replication. The depletion of alveolar macrophages did not affect the kinetics or magnitude of inflammatory macrophage recruitment during rMA15 infection of WT mice. These data suggest that alveolar macrophages are probably not the sentinel in the lung which initiate the inflammatory signaling cascade that ultimately controls virus

replication. An alternative approach may be to create bone marrow chimeras between WT and MyD88$^{-/-}$ mice. By lethal irradiation, myeloid cells are depleted from WT and MyD88$^{-/-}$ mice and mice are subsequently injected with bone marrow cells (BM) derived from either WT or MyD88$^{-/-}$ mice creating WT and MyD88$^{-/-}$ mice that have been repopulated with either WT or MyD88$^{-/-}$ derived BM. Infection of these bone marrow chimeras will allow us to deduce if myeloid or non-myeloid cells (i.e. ciliated epithelial cells in the lung) initiate the protective signal during rMA15 infection of WT mice. If myeloid cells are the sentinel in the lung that signal through MyD88 to promote protection of WT mice, MyD88$^{-/-}$ mice repopulated with WT derived BM should survive the infection similar to WT mice. If non-myeloid cells are the functional sentinel in the lung that promote protective MyD88 mediated inflammatory signaling events, WT mice repopulated with MyD88$^{-/-}$ derived BM infected with rMA15 should phenotypically look like WT mice.

MyD88 is a key signaling adaptor protein for most all TLRs, IL-1R, IL-18R and INFγ-R1. As such, we will infect TLR, IL-1R, IL-18R and INFγR1deficient mice in hopes of recapitulating the MyD88 phenotype. Our preliminary data suggests that infection of IL-1R$^{-/-}$ and IL-18R$^{-/-}$ mice fail to reproduce the MyD88 phenotype suggesting that IL1-R and IL18-R signaling through MyD88 does not provide the protective signal during rMA15 infection. Several TLR and intracellular PRRs have been shown to recognize viral RNA (TLR7, TLR8, RIG-I, MDA-5) and infection of mice deficient in these PRRs may demonstrate a MyD88$^{-/-}$ like phenotype. If we are able to demonstrate a MyD88$^{-/-}$ like phenotype through the infection PRR deficient mice, it would suggest that that the PRR is responsible for the recognition of SARS-CoV and its signaling through MyD88 is protective during rMA15 infection of WT mice.

Viral pathogenesis is a complex process where the virus and host engage in a unintended collaboration to generate the clinical presentation of disease. Being a newly emerged infectious disease, the pathogenic mechanisms of SARS-CoV disease remain unknown. We have developed a mouse model of acute non-severe SARS-CoV pathogenesis characterized by a high titer virus replication in the lung followed by a robust innate immune response resulting in the recruitment of inflammatory macrophages to the lung that mostly likely responsible for viral clearance and convalescence. We also demonstrate a key role for MyD88 dependent signaling events and associated inflammation/cell recruitment that serves to

protect WT mice from death while Myd88$^{-/-}$ mice succumb to infection. These data suggest an important role for innate immunity in the control of SARS-CoV and prevention of virus induced mortality.

Models of age related susceptibility to SARS-CoV and vaccine efficacy in senescent populations. SARS-CoV disease is characterized by an atypical pneumonia where approximately 20% of cases progressed to acute respiratory distress syndrome (ARDS) requiring mechanical ventilation. The disease severity associated with SARS-CoV infection of humans was directly linked to increasing age with mortality rates exceeding 50% in people over 65 years of age. The successful vaccination of elderly populations is a difficult task due to the immunosenescence associated with ageing. Current models predict that influenza vaccine efficacy in elderly populations ranges from 17-53% while the vaccine in young adults is 70-90% effective. Since influenza, West Nile Virus and SARS-CoV infection all produce a disproportionate amount of disease burden in the elderly, the development of robust model systems for the design of successful vaccine strategies in the elderly has a broad public health application especially given the increasing age of global human populations. Besides vaccination of immune senescent populations, vaccine induced immunopotentiation of disease and antigen selection complicate the development of successful and safe SARS-CoV vaccines.

The successful vaccination of elderly populations is a difficult and unpredictable task due to immunosenescence with ageing and robust models are needed to evaluate and improve vaccines targeting infections that cause a disproportionate disease burden in the elderly. A mouse adapted SARS-CoV was created (MA15) through repeated passage of SARS Urbani in BALB/c mice. We then constructed a molecular clone of MA15 (rMA15) by introducing the six amino acid changes found in MA15 into the infectious clone for SARS Urbani (icSARS). When administered intranasally to young BALB/c mice, rMA15 causes significant weight loss by 4 days post infection (dpi) (~20 % of starting weight) infection is uniformly lethal by 5 dpi. Infection of young adult mice with a recombinant mouse adapted SARS-CoV bearing a GD03 S glycoprotein (rMA15 GD03-S) attenuates the rMA15 lethal phenotype but rMA15 GD03-S infection of senescent mice is uniformly lethal. The age related mortality seen in BALB/c mice infected with rMA15 GD03-S mirrors the age related trends in SARS-CoV disease severity making it an attractive model within which to study age related susceptibility to SARS-CoV. Future efforts will characterize the differences seen in infection of young adult and senescent BALB/c with rMA15 GD03-S.

Initially, a comprehensive evaluation of virus growth kinetics will be performed in order to elucidate the magnitude and spread of virus throughout the course infection of young and senescent animals. Since previous experiments focused on virus replication and host pathology on 2 and 4 dpi, lungs of infected mice in future experiments will be harvested for virus titer, q-PCR, pathology and in situ hybridization every 24 hours post infection until senescent animals succumb to infection (~5 dpi). These data will allow for the assessment of virus titer/spread, inflammatory gene transcription, and pathology in young and senescent mice. Since rMA15 GD03-S lung titers in senescent mice are approximately one log greater than those in young mice on 2 dpi, the assessment of inflammatory gene transcription may suggest a defect in innate immune sensing rendering the aged mice less capable of controlling virus replication which ultimately results in their demise. As we had done for our MyD88 experiments, we will also assess the kinetics of inflammatory cell recruitment in young and old mice infected with rMA15 GD03-S. These data will allow us to determine if senescent mice are defective in inflammatory cell recruitment to the lung which may be necessary for protection in young mice.

Regardless of the mechanism of susceptibility in the aged mice, the rMA15 GD03-S BALB/c model of age related pathogenesis is a relevant model within which to study vaccine efficacy. Inactivated whole virus and vectored SARS-CoV vaccine trials in a number of different animals models have demonstrated that the SARS-CoV spike glycoprotein (S) is the critical component of protective immunity and the passive transfer of SARS-CoV S specific sera and select human monoclonal antibodies is sufficient to provide protection from lethal and nonlethal infection by a homologous and select heterologous SARS-CoV strains. Since the epidemic strain may not exist in nature, vaccination with epidemic strain antigens followed by challenge with the epidemic strain may represent a biologically irrelevant design. Unfortunately, a difficult choice is presented in choosing SARS-CoV vaccine antigens in hopes of preventing disease by future emergents whose antigenic identity is unknown. Therefore, employing an antigenically diverse panel SARS-CoV antigens for vaccination coupled with the use of an similarly diverse lethal challenge virus panel may represent the most pertinent and relevant strategy to assess vaccine efficacy. In 2003, Deming et al demonstrated that Venezuelan equine encephalitis virus replicon particles expressing SARS Urbani S (VRP-S) vaccine provided complete protection in young mice from replication of a SARS-CoV bearing a zoonotic heterologous GD03 S but protection was variable in senescent mice.

Due to the lack of significant morbidity and mortality in the SARS-CoV replication models, previous vaccine studies were unable to assess protection from disease or death and could only speculate that diminishing virus replication might result in reduced disease severity. We vaccinated senescent mice with Venezuelan equine encephalitis virus replicon particles (VRP) expressing Urbani-S, GD03-S, SZ16-S, a pool of all three S expressing VRPs or control VRPs in a prime/boost regimen and all mice were subsequently infected with rMA15 GD03-S. Our antigenically diverse SARS S expressing VRP panel coupled with our lethal rMA15 GD03-S challenge virus allowed us to assess the efficacy of immune responses to both homologous (VRP GD03-S) and heterologous (VRP Urbani-S and VRP SZ16-S) antigens. Upon challenge with the rMA15 GD03-S, all groups demonstrated significant morbidity losing more than 20% of starting weight by 5 dpi. Assessing protection from mortality, the HA and SZ16 groups uniformly succumbed to infection, the Urbani-S group demonstrated little protection from mortality while groups that received the homologous antigen demonstrated the most protection (GD03-S 29%, Pool-S 33% survival). These data suggest that vaccination of senescent animals with VRP expressing antigens similar to the challenge virus provides the most protection. Through serological evaluation of post-boost sera from vaccinated mice, we deduced that levels of GD03-S specific sera predicted mortality. Though our study outcome was not ideal, it provided us with a senescent animal vaccination and challenge model with much room for improvement.

Perhaps the most attractive aspect of viral vectored vaccine technology is that the same vaccine platform can be utilized to deliver a wide array of vaccine antigens. In theory, the same vector platform could be harnessed to deliver Influenza, SARS-CoV, or West Nile virus vaccine antigens. Therefore, improving VRP efficacy in senescent animals could potentially lead to the development of successful vaccination strategies for multiple pathogens with disproportionate disease in the elderly. To this end, future experiments will focus on increasing the protective efficacy of VRP vaccines in senescent mouse models. Previous pilot experiments suggest that delivering the TLR agonist, CpG DNA, with the VRP GD03-S vaccine does not improve its protective efficacy with rMA15 GD03-S challenge. Rather than enhance vaccine efficacy through supplemental adjuvants like CpG DNA, we looked for alternative means of improving vaccine efficacy in the immune senescent. This led us to hypothesize that the VEE glycoproteins coating the VRP vaccine may influence the quality of the immune response. Since the VEE

structural genes are replaced by a transgene of interest within VRP genomes, VEE structural genes provided in trans to "package" the replicon RNA and various VEE structural proteins can be utilized to enhance vector attenuation and safety. While WT recombinant VEE V3000 infection is uniformly lethal in mice, VEE clones V3010, V3014, and V3533 are mutated in their viral glycoproteins and are completely attenuated in mice with all mice surviving infection. A VRP packaged with wild-type VEE V3000 glycoproteins is targeted to the professional antigen presenting dendritic cell (DC) while the attenuated V3014 was found to have enhanced binding of heparan sulfate altering DC targeting/spread. These data suggest that the alteration of the VRP coat can have profound effects on cell targeting which may affect the efficiency of antigen presentation and the resultant immune response. On their major histocompatibility complexes (MHC), DCs can present endogenous (i.e. peptides from within the infected cell) or exogenous (peptides acquired from phagocytosis) antigen to prime cognate T cells for activation. DC priming of T cells using endogenous or exogenous (cross-priming) peptides can vary in efficiency resulting in differences in the quality and magnitude of the immune response. If VRP cell targeting differentially affects the pathway of antigen presentation (endogenous vs. exogenous), T cell activation may vary directly affecting the quality of the immune response. To address these concerns, we will vaccinate young adult and senescent mice with VRP GD03-S or influenza HA that have been packaged with either V3000 or V3014 glycoproteins. Post prime and boost sera will be harvested for to assess the magnitude of the SARS and HA specific antibody responses prior to challenge. Mice will receive a lethal rMA15 or rMA15 GD03-S challenge which will allow us to look at homologous and heterologous immune protection. Though infection of young mice with rMA15 GD03-S is not lethal, animals do experience a significant weight loss and this will be our metric in assessing protection. Young animals vaccinated with HA should succumb to infection by rMA15 while rMA15 GD03-S infection will most likely experience weight loss and recover. Differences in morbidity or mortality between V3000 and V3014 vaccine groups would suggest that the VEE glycoproteins affect the quality of the immune response. If we are capable of increasing the efficacy of VRP vaccination in senescent populations, this improved vaccine platform technology might be adapted to develop vaccines for other disease with disproportionate disease in the elderly like influenza and West Nile virus.

SARS-CoV pathogenesis is a complex process whose underlying mechanisms are not fully understood. Through the study of viral pathogenesis, the mechanisms of disease can be elucidated providing specific targets for therapeutic intervention intended to prevent the development of disease. We have developed models for various aspects of SARS-CoV pathogenesis including virus evolution and host range expansion, innate immune regulation to protect from lethal disease, and age-related susceptibility to lethal disease. Within these robust models of SARS-CoV pathogenesis, we assessed the protective efficacy of both passive immunization therapies and vaccination. The models and molecular tools developed for this work will hopefully continue to advance the study of SARS-CoV pathogenesis and therapeutic design. Moreover, the improvement of platform vaccine technologies in senescent populations may promote the development of effective vaccines to treat multiple diseases currently causing disproportionate disease burdens in the elderly.

REFERENCES

1. 1995. From the Centers for Disease Control and Prevention. Pneumonia and influenza death rates--United States, 1979-1994. Jama **274:**532.

2. 2003. Prevalence of IgG antibody to SARS-associated coronavirus in animal traders--Guangdong Province, China, 2003. MMWR Morb Mortal Wkly Rep **52:**986-7.

3. **Abedin, S., J. J. Michel, B. Lemster, and A. N. Vallejo.** 2005. Diversity of NKR expression in aging T cells and in T cells of the aged: the new frontier into the exploration of protective immunity in the elderly. Exp Gerontol **40:**537-48.

4. **Achtman, M., K. Zurth, G. Morelli, G. Torrea, A. Guiyoule, and E. Carniel.** 1999. Yersinia pestis, the cause of plague, is a recently emerged clone of Yersinia pseudotuberculosis. Proc Natl Acad Sci U S A **96:**14043-8.

5. **Adachi, K., H. Tsutsui, S. Kashiwamura, E. Seki, H. Nakano, O. Takeuchi, K. Takeda, K. Okumura, L. Van Kaer, H. Okamura, S. Akira, and K. Nakanishi.** 2001. Plasmodium berghei infection in mice induces liver injury by an IL-12- and toll-like receptor/myeloid differentiation factor 88-dependent mechanism. J Immunol **167:**5928-34.

6. **Agrawal, A., S. Agrawal, J. N. Cao, H. Su, K. Osann, and S. Gupta.** 2007. Altered innate immune functioning of dendritic cells in elderly humans: a role of phosphoinositide 3-kinase-signaling pathway. J Immunol **178:**6912-22.

7. **Agrawal, A., S. Agrawal, J. Tay, and S. Gupta.** 2008. Biology of dendritic cells in aging. J Clin Immunol **28:**14-20.

8. **Ank, N., H. West, C. Bartholdy, K. Eriksson, A. R. Thomsen, and S. R. Paludan.** 2006. Lambda interferon (IFN-lambda), a type III IFN, is induced by viruses and IFNs and displays potent antiviral activity against select virus infections in vivo. J Virol **80:**4501-9.

9. **Asanuma, H., K. Hirokawa, M. Uchiyama, Y. Suzuki, C. Aizawa, T. Kurata, T. Sata, and S. Tamura.** 2001. Immune responses and protection in different strains of aged mice immunized intranasally with an adjuvant-combined influenza vaccine. Vaccine **19:**3981-9.

10. **Asselin-Paturel, C., A. Boonstra, M. Dalod, I. Durand, N. Yessaad, C. Dezutter-Dambuyant, A. Vicari, A. O'Garra, C. Biron, F. Briere, and G. Trinchieri.** 2001. Mouse type I IFN-producing cells are immature APCs with plasmacytoid morphology. Nat Immunol **2:**1144-50.

11. **Avendano, M., P. Derkach, and S. Swan.** 2003. Clinical course and management of SARS in health care workers in Toronto: a case series. Cmaj **168:**1649-60.

12. **Bai, B., X. Lu, J. Meng, Q. Hu, P. Mao, B. Lu, Z. Chen, Z. Yuan, and H. Wang.** 2008. Vaccination of mice with recombinant baculovirus expressing spike or nucleocapsid protein of SARS-like coronavirus generates humoral and cellular immune responses. Mol Immunol **45:**868-75.

13. **Bauer, T. T., S. Ewig, A. C. Rodloff, and E. E. Muller.** 2006. Acute respiratory distress syndrome and pneumonia: a comprehensive review of clinical data. Clin Infect Dis **43:**748-56.

14. **Ben-Yehuda, A., D. Ehleiter, A. R. Hu, and M. E. Weksler.** 1993. Recombinant vaccinia virus expressing the PR/8 influenza hemagglutinin gene overcomes the impaired immune response and increased susceptibility of old mice to influenza infection. J Infect Dis **168:**352-7.

15. **Bender, B. S., T. Croghan, L. Zhang, and P. A. Small, Jr.** 1992. Transgenic mice lacking class I major histocompatibility complex-restricted T cells have delayed viral clearance and increased mortality after influenza virus challenge. J Exp Med **175:**1143-5.

16. **Bernard, K. A., W. B. Klimstra, and R. E. Johnston.** 2000. Mutations in the E2 glycoprotein of Venezuelan equine encephalitis virus confer heparan sulfate interaction, low morbidity, and rapid clearance from blood of mice. Virology **276:**93-103.

17. **Bernstein, E., D. Kaye, E. Abrutyn, P. Gross, M. Dorfman, and D. M. Murasko.** 1999. Immune response to influenza vaccination in a large healthy elderly population. Vaccine **17:**82-94.

18. **Bernstein, E. D., E. M. Gardner, E. Abrutyn, P. Gross, and D. M. Murasko.** 1998. Cytokine production after influenza vaccination in a healthy elderly population. Vaccine **16:**1722-31.

19. **Booth, C. M., L. M. Matukas, G. A. Tomlinson, A. R. Rachlis, D. B. Rose, H. A. Dwosh, S. L. Walmsley, T. Mazzulli, M. Avendano, P. Derkach, I. E. Ephtimios, I. Kitai, B. D. Mederski, S. B. Shadowitz, W. L. Gold, L. A. Hawryluck, E. Rea, J. S. Chenkin, D. W. Cescon, S. M. Poutanen, and A. S. Detsky.** 2003. Clinical features and short-term outcomes of 144 patients with SARS in the greater Toronto area. Jama **289:**2801-9.

20. **Buchholz, U. J., A. Bukreyev, L. Yang, E. W. Lamirande, B. R. Murphy, K. Subbarao, and P. L. Collins.** 2004. Contributions of the structural proteins of severe acute respiratory syndrome coronavirus to protective immunity. Proc Natl Acad Sci U S A **101:**9804-9.

21. **Cameron, M. J., L. Ran, L. Xu, A. Danesh, J. F. Bermejo-Martin, C. M. Cameron, M. P. Muller, W. L. Gold, S. E. Richardson, S. M. Poutanen, B. M. Willey, M. E. DeVries, Y. Fang, C. Seneviratne, S. E. Bosinger, D. Persad, P. Wilkinson, L. D. Greller, R. Somogyi, A. Humar, S. Keshavjee, M. Louie, M. B. Loeb, J. Brunton, A. J. McGeer, and D. J. Kelvin.** 2007. Interferon-mediated immunopathological events are associated with atypical innate and adaptive immune responses in patients with severe acute respiratory syndrome. J Virol **81:**8692-706.

22. **Cantor, J., and K. Haskins.** 2007. Recruitment and activation of macrophages by pathogenic CD4 T cells in type 1 diabetes: evidence for involvement of CCR8 and CCL1. J Immunol **179:**5760-7.

23. **Cella, M., D. Jarrossay, F. Facchetti, O. Alebardi, H. Nakajima, A. Lanzavecchia, and M. Colonna.** 1999. Plasmacytoid monocytes migrate to inflamed lymph nodes and produce large amounts of type I interferon. Nat Med **5:**919-23.

24. **Cello, J., A. V. Paul, and E. Wimmer.** 2002. Chemical synthesis of poliovirus cDNA: generation of infectious virus in the absence of natural template. Science **297:**1016-8.

25. **Cervantes-Barragan, L., R. Zust, F. Weber, M. Spiegel, K. S. Lang, S. Akira, V. Thiel, and B. Ludewig.** 2007. Control of coronavirus infection through plasmacytoid dendritic-cell-derived type I interferon. Blood **109:**1131-7.

26. **Chen, Y., V. S. Chan, B. Zheng, K. Y. Chan, X. Xu, L. Y. To, F. P. Huang, U. S. Khoo, and C. L. Lin.** 2007. A novel subset of putative stem/progenitor CD34+Oct-4+ cells is the major target for SARS coronavirus in human lung. J Exp Med **204:**2529-36.

27. **Cheung, C. Y., L. L. Poon, I. H. Ng, W. Luk, S. F. Sia, M. H. Wu, K. H. Chan, K. Y. Yuen, S. Gordon, Y. Guan, and J. S. Peiris.** 2005. Cytokine responses in severe acute respiratory syndrome coronavirus-infected macrophages in vitro: possible relevance to pathogenesis. J Virol **79:**7819-26.

28. **Chinese, S. M. E. C.** 2004. Molecular evolution of the SARS coronavirus during the course of the SARS epidemic in China. Science **303:**1666-9.

29. **Christian, M. D., S. M. Poutanen, M. R. Loutfy, M. P. Muller, and D. E. Low.** 2004. Severe acute respiratory syndrome. Clin Infect Dis **38:**1420-7.

30. **Chu, Y. K., G. D. Ali, F. Jia, Q. Li, D. Kelvin, R. C. Couch, K. S. Harrod, J. A. Hutt, C. Cameron, S. R. Weiss, and C. B. Jonsson.** 2008. The SARS-CoV ferret model in an infection-challenge study. Virology.

31. **Clark, J. A., and T. C. Peterson.** 1994. Cytokine production and aging: overproduction of IL-8 in elderly males in response to lipopolysaccharide. Mech Ageing Dev **77:**127-39.

32. **Cumberbatch, M., M. Singh, R. J. Dearman, H. S. Young, I. Kimber, and C. E. Griffiths.** 2006. Impaired Langerhans cell migration in psoriasis. J Exp Med **203:**953-60.

33. **Dahlem, P., W. M. van Aalderen, and A. P. Bos.** 2007. Pediatric acute lung injury. Paediatr Respir Rev **8:**348-62.

34. **de Haan, C. A., Z. Li, E. te Lintelo, B. J. Bosch, B. J. Haijema, and P. J. Rottier.** 2005. Murine coronavirus with an extended host range uses heparan sulfate as an entry receptor. J Virol **79:**14451-6.

35. **de Haan, C. A., and P. J. Rottier.** 2006. Hosting the severe acute respiratory syndrome coronavirus: specific cell factors required for infection. Cell Microbiol **8:**1211-8.

36. **de Lang, A., T. Baas, T. Teal, L. M. Leijten, B. Rain, A. D. Osterhaus, B. L. Haagmans, and M. G. Katze.** 2007. Functional genomics highlights differential induction of antiviral pathways in the lungs of SARS-CoV-infected macaques. PLoS Pathog **3:**e112.

37. **De Swart, R. L., T. Kuiken, H. H. Timmerman, G. van Amerongen, B. G. Van Den Hoogen, H. W. Vos, H. J. Neijens, A. C. Andeweg, and A. D. Osterhaus.** 2002. Immunization of macaques with formalin-inactivated respiratory syncytial virus (RSV) induces interleukin-13-associated hypersensitivity to subsequent RSV infection. J Virol **76:**11561-9.

38. **de Swart, R. L., B. G. van den Hoogen, T. Kuiken, S. Herfst, G. van Amerongen, S. Yuksel, L. Sprong, and A. D. Osterhaus.** 2007. Immunization of macaques with formalin-inactivated human metapneumovirus induces hypersensitivity to hMPV infection. Vaccine **25:**8518-28.

39. **Decaro, N., V. Martella, G. Elia, M. Campolo, V. Mari, C. Desario, M. S. Lucente, A. Lorusso, G. Greco, M. Corrente, M. Tempesta, and C. Buonavoglia.** 2008. Biological and genetic analysis of a bovine-like coronavirus isolated from water buffalo (Bubalus bubalis) calves. Virology **370:**213-22.

40. **Della Bella, S., L. Bierti, P. Presicce, R. Arienti, M. Valenti, M. Saresella, C. Vergani, and M. L. Villa.** 2007. Peripheral blood dendritic cells and monocytes are differently regulated in the elderly. Clin Immunol **122:**220-8.

41. **Deming, D., T. Sheahan, M. Heise, B. Yount, N. Davis, A. Sims, M. Suthar, J. Harkema, A. Whitmore, R. Pickles, A. West, E. Donaldson, K. Curtis, R. Johnston, and R. Baric.** 2006. Vaccine efficacy in senescent mice challenged

with recombinant SARS-CoV bearing epidemic and zoonotic spike variants. PLoS Med **3:**e525.

42. **Domingo, E., and J. J. Holland.** 1997. RNA virus mutations and fitness for survival. Annu Rev Microbiol **51:**151-78.

43. **Dominguez, S. R., O. S. T.J., O. L.M., and H. K.V.** 2007. Detection of group 1 coronaviruses in bats in North America. Emerg Infect Dis **13**.

44. **Dong, B. Q., W. Liu, X. H. Fan, D. Vijaykrishna, X. C. Tang, F. Gao, L. F. Li, G. J. Li, J. X. Zhang, L. Q. Yang, L. L. Poon, S. Y. Zhang, J. S. Peiris, G. J. Smith, H. Chen, and Y. Guan.** 2007. Detection of a novel and highly divergent coronavirus from asian leopard cats and Chinese ferret badgers in Southern China. J Virol **81:**6920-6.

45. **Donnelly, C. A., M. C. Fisher, C. Fraser, A. C. Ghani, S. Riley, N. M. Ferguson, and R. M. Anderson.** 2004. Epidemiological and genetic analysis of severe acute respiratory syndrome. Lancet Infect Dis **4:**672-83.

46. **Donnelly, C. A., A. C. Ghani, G. M. Leung, A. J. Hedley, C. Fraser, S. Riley, L. J. Abu-Raddad, L. M. Ho, T. Q. Thach, P. Chau, K. P. Chan, T. H. Lam, L. Y. Tse, T. Tsang, S. H. Liu, J. H. Kong, E. M. Lau, N. M. Ferguson, and R. M. Anderson.** 2003. Epidemiological determinants of spread of causal agent of severe acute respiratory syndrome in Hong Kong. Lancet **361:**1761-6.

47. **Donoghue, M., F. Hsieh, E. Baronas, K. Godbout, M. Gosselin, N. Stagliano, M. Donovan, B. Woolf, K. Robison, R. Jeyaseelan, R. E. Breitbart, and S. Acton.** 2000. A novel angiotensin-converting enzyme-related carboxypeptidase (ACE2) converts angiotensin I to angiotensin 1-9. Circ Res **87:**E1-9.

48. **Drosten, C., S. Gunther, W. Preiser, S. van der Werf, H. R. Brodt, S. Becker, H. Rabenau, M. Panning, L. Kolesnikova, R. A. Fouchier, A. Berger, A. M. Burguiere, J. Cinatl, M. Eickmann, N. Escriou, K. Grywna, S. Kramme, J. C. Manuguerra, S. Muller, V. Rickerts, M. Sturmer, S. Vieth, H. D. Klenk, A. D. Osterhaus, H. Schmitz, and H. W. Doerr.** 2003. Identification of a novel coronavirus in patients with severe acute respiratory syndrome. N Engl J Med **348:**1967-76.

49. **Durbin, J. E., and R. K. Durbin.** 2004. Respiratory syncytial virus-induced immunoprotection and immunopathology. Viral Immunol **17:**370-80.

50. **Eaton, S. M., E. M. Burns, K. Kusser, T. D. Randall, and L. Haynes.** 2004. Age-related defects in CD4 T cell cognate helper function lead to reductions in humoral responses. J Exp Med **200:**1613-22.

51. **Eckerle, L. D., X. Lu, S. M. Sperry, L. Choi, and M. R. Denison.** 2007. High fidelity of murine hepatitis virus replication is decreased in nsp14 exoribonuclease mutants. J Virol **81:**12135-44.

52. **Edelson, B. T., and E. R. Unanue.** 2002. MyD88-dependent but Toll-like receptor 2-independent innate immunity to Listeria: no role for either in macrophage listericidal activity. J Immunol **169:**3869-75.

53. **Effros, R. B.** 2007. Role of T lymphocyte replicative senescence in vaccine efficacy. Vaccine **25:**599-604.

54. **Falsey, A. R.** 2007. Community-acquired viral pneumonia. Clin Geriatr Med **23:**535-52, vi.

55. **Franceschi, C., D. Monti, P. Sansoni, and A. Cossarizza.** 1995. The immunology of exceptional individuals: the lesson of centenarians. Immunol Today **16:**12-6.

56. **Fraser, C., S. Riley, R. M. Anderson, and N. M. Ferguson.** 2004. Factors that make an infectious disease outbreak controllable. Proc Natl Acad Sci U S A **101:**6146-51.

57. **Frieman, M., B. Yount, M. Heise, S. A. Kopecky-Bromberg, P. Palese, and R. S. Baric.** 2007. Severe acute respiratory syndrome coronavirus ORF6 antagonizes STAT1 function by sequestering nuclear import factors on the rough endoplasmic reticulum/Golgi membrane. J Virol **81:**9812-24.

58. **Fujihashi, K., T. Koga, and J. R. McGhee.** 2000. Mucosal vaccination and immune responses in the elderly. Vaccine **18:**1675-80.

59. **Fulcher, M. L., S. Gabriel, K. A. Burns, J. R. Yankaskas, and S. H. Randell.** 2005. Well-differentiated human airway epithelial cell cultures. Methods Mol Med **107:**183-206.

60. **Ginaldi, L., M. De Martinis, A. D'Ostilio, L. Marini, M. F. Loreto, and D. Quaglino.** 1999. Immunological changes in the elderly. Aging (Milano) **11:**281-6.

61. **Ginaldi, L., M. F. Loreto, M. P. Corsi, M. Modesti, and M. De Martinis.** 2001. Immunosenescence and infectious diseases. Microbes Infect **3:**851-7.

62. **Glass, W. G., K. Subbarao, B. Murphy, and P. M. Murphy.** 2004. Mechanisms of host defense following severe acute respiratory syndrome-coronavirus (SARS-CoV) pulmonary infection of mice. J Immunol **173:**4030-9.

63. **Gonzalez, J. P., X. Pourrut, and E. Leroy.** 2007. Ebolavirus and other filoviruses. Curr Top Microbiol Immunol **315:**363-87.

64. **Goodwin, K., C. Viboud, and L. Simonsen.** 2006. Antibody response to influenza vaccination in the elderly: a quantitative review. Vaccine **24:**1159-69.

65. **Goronzy, J. J., J. W. Fulbright, C. S. Crowson, G. A. Poland, W. M. O'Fallon, and C. M. Weyand.** 2001. Value of immunological markers in predicting responsiveness to influenza vaccination in elderly individuals. J Virol **75:**12182-7.

66. **Gross, T. J., and G. W. Hunninghake.** 2001. Idiopathic pulmonary fibrosis. N Engl J Med **345:**517-25.

67. **Gruver, A. L., L. L. Hudson, and G. D. Sempowski.** 2007. Immunosenescence of ageing. J Pathol **211:**144-56.

68. **Gu, J., E. Gong, B. Zhang, J. Zheng, Z. Gao, Y. Zhong, W. Zou, J. Zhan, S. Wang, Z. Xie, H. Zhuang, B. Wu, H. Zhong, H. Shao, W. Fang, D. Gao, F. Pei, X. Li, Z. He, D. Xu, X. Shi, V. M. Anderson, and A. S. Leong.** 2005. Multiple organ infection and the pathogenesis of SARS. J Exp Med **202:**415-24.

69. **Guan, Y., B. J. Zheng, Y. Q. He, X. L. Liu, Z. X. Zhuang, C. L. Cheung, S. W. Luo, P. H. Li, L. J. Zhang, Y. J. Guan, K. M. Butt, K. L. Wong, K. W. Chan, W. Lim, K. F. Shortridge, K. Y. Yuen, J. S. Peiris, and L. L. Poon.** 2003. Isolation and characterization of viruses related to the SARS coronavirus from animals in southern China. Science **302:**276-8.

70. **Haagmans, B. L., T. Kuiken, B. E. Martina, R. A. Fouchier, G. F. Rimmelzwaan, G. van Amerongen, D. van Riel, T. de Jong, S. Itamura, K. H. Chan, M. Tashiro, and A. D. Osterhaus.** 2004. Pegylated interferon-alpha protects type 1 pneumocytes against SARS coronavirus infection in macaques. Nat Med **10:**290-3.

71. **Haagmans, B. L., and A. D. Osterhaus.** 2006. Nonhuman primate models for SARS. PLoS Med **3:**e194.

72. **Hamming, I., W. Timens, M. L. Bulthuis, A. T. Lely, G. J. Navis, and H. van Goor.** 2004. Tissue distribution of ACE2 protein, the functional receptor for SARS coronavirus. A first step in understanding SARS pathogenesis. J Pathol **203:**631-7.

73. **Han, Y., H. Geng, W. Feng, X. Tang, A. Ou, Y. Lao, Y. Xu, H. Lin, H. Liu, and Y. Li.** 2003. A follow-up study of 69 discharged SARS patients. J Tradit Chin Med **23:**214-7.

74. **Hasoksuz, M., S. Sreevatsan, K. O. Cho, A. E. Hoet, and L. J. Saif.** 2002. Molecular analysis of the S1 subunit of the spike glycoprotein of respiratory and enteric bovine coronavirus isolates. Virus Res **84:**101-9.

75. **Haynes, L., S. M. Eaton, E. M. Burns, M. Rincon, and S. L. Swain.** 2004. Inflammatory cytokines overcome age-related defects in CD4 T cell responses in vivo. J Immunol **172:**5194-9.

76. **Haynes, L., P. J. Linton, S. M. Eaton, S. L. Tonkonogy, and S. L. Swain.** 1999. Interleukin 2, but not other common gamma chain-binding cytokines, can reverse the defect in generation of CD4 effector T cells from naive T cells of aged mice. J Exp Med **190:**1013-24.

77. **Haynes, L., and S. L. Swain.** 2006. Why aging T cells fail: implications for vaccination. Immunity **24:**663-6.

78. **He, Y., J. Li, S. Heck, S. Lustigman, and S. Jiang.** 2006. Antigenic and immunogenic characterization of recombinant baculovirus-expressed severe acute respiratory syndrome coronavirus spike protein: implication for vaccine design. J Virol **80:**5757-67.

79. **He, Y., J. Li, W. Li, S. Lustigman, M. Farzan, and S. Jiang.** 2006. Cross-neutralization of human and palm civet severe acute respiratory syndrome coronaviruses by antibodies targeting the receptor-binding domain of spike protein. J Immunol **176:**6085-92.

80. **Hedlund, M., E. Ng, A. Varki, and N. M. Varki.** 2008. alpha 2-6-Linked sialic acids on N-glycans modulate carcinoma differentiation in vivo. Cancer Res **68:**388-94.

81. **Herath, C. B., F. J. Warner, J. S. Lubel, R. G. Dean, Z. Jia, R. A. Lew, A. I. Smith, L. M. Burrell, and P. W. Angus.** 2007. Upregulation of hepatic angiotensin-converting enzyme 2 (ACE2) and angiotensin-(1-7) levels in experimental biliary fibrosis. J Hepatol **47:**387-95.

82. **Hickman-Miller, H. D., and J. W. Yewdell.** 2006. Youth has its privileges: maturation inhibits DC cross-priming. Nat Immunol **7:**125-6.

83. **Higgins, D. A., J. R. Carlson, and G. Van Nest.** 1996. MF59 adjuvant enhances the immunogenicity of influenza vaccine in both young and old mice. Vaccine **14:**478-84.

84. **Hogan, R. J., G. Gao, T. Rowe, P. Bell, D. Flieder, J. Paragas, G. P. Kobinger, N. A. Wivel, R. G. Crystal, J. Boyer, H. Feldmann, T. G. Voss, and J. M. Wilson.** 2004. Resolution of primary severe acute respiratory syndrome-associated coronavirus infection requires Stat1. J Virol **78:**11416-21.

85. **Hsu, V. P., M. J. Hossain, U. D. Parashar, M. M. Ali, T. G. Ksiazek, I. Kuzmin, M. Niezgoda, C. Rupprecht, J. Bresee, and R. F. Breiman.** 2004. Nipah virus encephalitis reemergence, Bangladesh. Emerg Infect Dis **10:**2082-7.

86. **Hueffer, K., J. S. Parker, W. S. Weichert, R. E. Geisel, J. Y. Sgro, and C. R. Parrish.** 2003. The natural host range shift and subsequent evolution of canine parvovirus resulted from virus-specific binding to the canine transferrin receptor. J Virol **77:**1718-26.

87. **Hunninghake, G. W., M. B. Zimmerman, D. A. Schwartz, T. E. King, Jr., J. Lynch, R. Hegele, J. Waldron, T. Colby, N. Muller, D. Lynch, J. Galvin, B. Gross, J. Hogg, G. Toews, R. Helmers, J. A. Cooper, Jr., R. Baughman, C. Strange, and M. Millard.** 2001. Utility of a lung biopsy for the diagnosis of idiopathic pulmonary fibrosis. Am J Respir Crit Care Med **164:**193-6.

88. **Hwang, D. M., D. W. Chamberlain, S. M. Poutanen, D. E. Low, S. L. Asa, and J. Butany.** 2005. Pulmonary pathology of severe acute respiratory syndrome in Toronto. Mod Pathol **18:**1-10.

89. **Imai, Y., K. Kuba, S. Rao, Y. Huan, F. Guo, B. Guan, P. Yang, R. Sarao, T. Wada, H. Leong-Poi, M. A. Crackower, A. Fukamizu, C. C. Hui, L. Hein, S. Uhlig, A. S. Slutsky, C. Jiang, and J. M. Penninger.** 2005. Angiotensin-converting enzyme 2 protects from severe acute lung failure. Nature **436:**112-6.

90. **Jeffers, S. A., S. M. Tusell, L. Gillim-Ross, E. M. Hemmila, J. E. Achenbach, G. J. Babcock, W. D. Thomas, Jr., L. B. Thackray, M. D. Young, R. J. Mason, D. M. Ambrosino, D. E. Wentworth, J. C. Demartini, and K. V. Holmes.** 2004. CD209L (L-SIGN) is a receptor for severe acute respiratory syndrome coronavirus. Proc Natl Acad Sci U S A **101:**15748-53.

91. **Jin, H., C. Xiao, Z. Chen, Y. Kang, Y. Ma, K. Zhu, Q. Xie, Y. Tu, Y. Yu, and B. Wang.** 2005. Induction of Th1 type response by DNA vaccinations with N, M, and E genes against SARS-CoV in mice. Biochem Biophys Res Commun **328:**979-86.

92. **Jung, K., K. P. Alekseev, X. Zhang, D. S. Cheon, A. N. Vlasova, and L. J. Saif.** 2007. Altered pathogenesis of porcine respiratory coronavirus in pigs due to immunosuppressive effects of dexamethasone: implications for corticosteroid use in treatment of severe acute respiratory syndrome coronavirus. J Virol **81:**13681-93.

93. **Kahn, J. S.** 2006. Epidemiology of human metapneumovirus. Clin Microbiol Rev **19:**546-57.

94. **Kan, B., M. Wang, H. Jing, H. Xu, X. Jiang, M. Yan, W. Liang, H. Zheng, K. Wan, Q. Liu, B. Cui, Y. Xu, E. Zhang, H. Wang, J. Ye, G. Li, M. Li, Z. Cui, X. Qi, K. Chen, L. Du, K. Gao, Y. T. Zhao, X. Z. Zou, Y. J. Feng, Y. F. Gao, R. Hai, D. Yu, Y. Guan, and J. Xu.** 2005. Molecular evolution analysis and geographic investigation of severe acute respiratory syndrome coronavirus-like virus in palm civets at an animal market and on farms. J Virol **79:**11892-900.

95. **Kapadia, S. U., J. K. Rose, E. Lamirande, L. Vogel, K. Subbarao, and A. Roberts.** 2005. Long-term protection from SARS coronavirus infection conferred by a single immunization with an attenuated VSV-based vaccine. Virology **340:**174-82.

96. **Kato, H., O. Takeuchi, S. Sato, M. Yoneyama, M. Yamamoto, K. Matsui, S. Uematsu, A. Jung, T. Kawai, K. J. Ishii, O. Yamaguchi, K. Otsu, T. Tsujimura, C. S. Koh, C. Reis e Sousa, Y. Matsuura, T. Fujita, and S. Akira.** 2006. Differential roles of MDA5 and RIG-I helicases in the recognition of RNA viruses. Nature **441:**101-5.

97. **Kesson, A. M.** 2007. Respiratory virus infections. Paediatr Respir Rev **8:**240-8.

98. **Klimstra, W. B., K. D. Ryman, and R. E. Johnston.** 1998. Adaptation of Sindbis virus to BHK cells selects for use of heparan sulfate as an attachment receptor. J Virol **72:**7357-66.

99. **Kobasa, D., S. M. Jones, K. Shinya, J. C. Kash, J. Copps, H. Ebihara, Y. Hatta, J. H. Kim, P. Halfmann, M. Hatta, F. Feldmann, J. B. Alimonti, L. Fernando, Y. Li, M. G. Katze, H. Feldmann, and Y. Kawaoka.** 2007. Aberrant innate immune response in lethal infection of macaques with the 1918 influenza virus. Nature **445:**319-23.

100. **Kopecky-Bromberg, S. A., L. Martinez-Sobrido, M. Frieman, R. A. Baric, and P. Palese.** 2007. Severe acute respiratory syndrome coronavirus open reading frame (ORF) 3b, ORF 6, and nucleocapsid proteins function as interferon antagonists. J Virol **81:**548-57.

101. **Koyama, S., K. J. Ishii, H. Kumar, T. Tanimoto, C. Coban, S. Uematsu, T. Kawai, and S. Akira.** 2007. Differential role of TLR- and RLR-signaling in the immune responses to influenza A virus infection and vaccination. J Immunol **179:**4711-20.

102. **Krishnaraj, R.** 1997. Senescence and cytokines modulate the NK cell expression. Mech Ageing Dev **96:**89-101.

103. **Ksiazek, T. G., D. Erdman, C. S. Goldsmith, S. R. Zaki, T. Peret, S. Emery, S. Tong, C. Urbani, J. A. Comer, W. Lim, P. E. Rollin, S. F. Dowell, A. E. Ling, C. D. Humphrey, W. J. Shieh, J. Guarner, C. D. Paddock, P. Rota, B. Fields, J. DeRisi, J. Y. Yang, N. Cox, J. M. Hughes, J. W. LeDuc, W. J. Bellini, and L. J. Anderson.** 2003. A novel coronavirus associated with severe acute respiratory syndrome. N Engl J Med **348:**1953-66.

104. **Kuba, K., Y. Imai, S. Rao, H. Gao, F. Guo, B. Guan, Y. Huan, P. Yang, Y. Zhang, W. Deng, L. Bao, B. Zhang, G. Liu, Z. Wang, M. Chappell, Y. Liu, D. Zheng, A. Leibbrandt, T. Wada, A. S. Slutsky, D. Liu, C. Qin, C. Jiang, and J. M. Penninger.** 2005. A crucial role of angiotensin converting enzyme 2 (ACE2) in SARS coronavirus-induced lung injury. Nat Med **11:**875-9.

105. **Kuba, K., Y. Imai, S. Rao, C. Jiang, and J. M. Penninger.** 2006. Lessons from SARS: control of acute lung failure by the SARS receptor ACE2. J Mol Med **84:**814-20.

106. **Kumar, S., J. Boehm, and J. C. Lee.** 2003. p38 MAP kinases: key signalling molecules as therapeutic targets for inflammatory diseases. Nat Rev Drug Discov **2:**717-26.

107. **Kuo, L., G. J. Godeke, M. J. Raamsman, P. S. Masters, and P. J. Rottier.** 2000. Retargeting of coronavirus by substitution of the spike glycoprotein ectodomain: crossing the host cell species barrier. J Virol **74:**1393-406.

108. **Lau, S. K., P. C. Woo, K. S. Li, Y. Huang, H. W. Tsoi, B. H. Wong, S. S. Wong, S. Y. Leung, K. H. Chan, and K. Y. Yuen.** 2005. Severe acute respiratory syndrome coronavirus-like virus in Chinese horseshoe bats. Proc Natl Acad Sci U S A **102:**14040-5.

109. **Lau, S. K., P. C. Woo, K. S. Li, Y. Huang, M. Wang, C. S. Lam, H. Xu, R. Guo, K. H. Chan, B. J. Zheng, and K. Y. Yuen.** 2007. Complete genome sequence of bat coronavirus HKU2 from Chinese horseshoe bats revealed a much smaller spike gene with a different evolutionary lineage from the rest of the genome. Virology.

110. **Lau, Y. L., and J. S. Peiris.** 2005. Pathogenesis of severe acute respiratory syndrome. Curr Opin Immunol **17:**404-10.

111. **Law, H. K., C. Y. Cheung, H. Y. Ng, S. F. Sia, Y. O. Chan, W. Luk, J. M. Nicholls, J. S. Peiris, and Y. L. Lau.** 2005. Chemokine up-regulation in SARS-coronavirus-infected, monocyte-derived human dendritic cells. Blood **106:**2366-74.

112. **Lee, M. S., R. E. Walker, and P. M. Mendelman.** 2005. Medical burden of respiratory syncytial virus and parainfluenza virus type 3 infection among US children. Implications for design of vaccine trials. Hum Vaccin **1:**6-11.

113. **Lee, N., P. K. Chan, M. Ip, E. Wong, J. Ho, C. Ho, C. S. Cockram, and D. S. Hui.** 2006. Anti-SARS-CoV IgG response in relation to disease severity of severe acute respiratory syndrome. J Clin Virol **35:**179-84.

114. **Lee, N., D. Hui, A. Wu, P. Chan, P. Cameron, G. M. Joynt, A. Ahuja, M. Y. Yung, C. B. Leung, K. F. To, S. F. Lui, C. C. Szeto, S. Chung, and J. J. Sung.** 2003. A major outbreak of severe acute respiratory syndrome in Hong Kong. N Engl J Med **348:**1986-94.

115. **Leroy, E. M., B. Kumulungui, X. Pourrut, P. Rouquet, A. Hassanin, P. Yaba, A. Delicat, J. T. Paweska, J. P. Gonzalez, and R. Swanepoel.** 2005. Fruit bats as reservoirs of Ebola virus. Nature **438:**575-6.

116. **Leung, G. M., A. J. Hedley, L. M. Ho, P. Chau, I. O. Wong, T. Q. Thach, A. C. Ghani, C. A. Donnelly, C. Fraser, S. Riley, N. M. Ferguson, R. M. Anderson, T. Tsang, P. Y. Leung, V. Wong, J. C. Chan, E. Tsui, S. V. Lo, and T. H. Lam.** 2004. The epidemiology of severe acute respiratory syndrome in the

2003 Hong Kong epidemic: an analysis of all 1755 patients. Ann Intern Med **141:**662-73.

117. **Leyssen, P., E. De Clercq, and J. Neyts.** 2008. Molecular strategies to inhibit the replication of RNA viruses. Antiviral Res.

118. **Li, F., M. Berardi, W. Li, M. Farzan, P. R. Dormitzer, and S. C. Harrison.** 2006. Conformational states of the severe acute respiratory syndrome coronavirus spike protein ectodomain. J Virol **80:**6794-800.

119. **Li, F., W. Li, M. Farzan, and S. C. Harrison.** 2005. Structure of SARS coronavirus spike receptor-binding domain complexed with receptor. Science **309:**1864-8.

120. **Li, W., M. J. Moore, N. Vasilieva, J. Sui, S. K. Wong, M. A. Berne, M. Somasundaran, J. L. Sullivan, K. Luzuriaga, T. C. Greenough, H. Choe, and M. Farzan.** 2003. Angiotensin-converting enzyme 2 is a functional receptor for the SARS coronavirus. Nature **426:**450-4.

121. **Li, W., S. K. Wong, F. Li, J. H. Kuhn, I. C. Huang, H. Choe, and M. Farzan.** 2006. Animal origins of the severe acute respiratory syndrome coronavirus: insight from ACE2-S-protein interactions. J Virol **80:**4211-9.

122. **Li, W., C. Zhang, J. Sui, J. H. Kuhn, M. J. Moore, S. Luo, S. K. Wong, I. C. Huang, K. Xu, N. Vasilieva, A. Murakami, Y. He, W. A. Marasco, Y. Guan, H. Choe, and M. Farzan.** 2005. Receptor and viral determinants of SARS-coronavirus adaptation to human ACE2. Embo J **24:**1634-43.

123. **Li, Y., D. S. Carroll, S. N. Gardner, M. C. Walsh, E. A. Vitalis, and I. K. Damon.** 2007. On the origin of smallpox: correlating variola phylogenics with historical smallpox records. Proc Natl Acad Sci U S A **104:**15787-92.

124. **Liang, W., Z. Zhu, J. Guo, Z. Liu, W. Zhou, D. P. Chin, and A. Schuchat.** 2004. Severe acute respiratory syndrome, Beijing, 2003. Emerg Infect Dis **10:**25-31.

125. **Ligon, B. L.** 2006. Reemergence of an unusual disease: the chikungunya epidemic. Semin Pediatr Infect Dis **17:**99-104.

126. **Linton, P. J., S. P. Li, Y. Zhang, B. Bautista, Q. Huynh, and T. Trinh.** 2005. Intrinsic versus environmental influences on T-cell responses in aging. Immunol Rev **205:**207-19.

127. **Lipsitch, M., T. Cohen, B. Cooper, J. M. Robins, S. Ma, L. James, G. Gopalakrishna, S. K. Chew, C. C. Tan, M. H. Samore, D. Fisman, and M. Murray.** 2003. Transmission dynamics and control of severe acute respiratory syndrome. Science **300:**1966-70.

128. **Liu, R. Y., L. Z. Wu, B. J. Huang, J. L. Huang, Y. L. Zhang, M. L. Ke, J. M. Wang, W. P. Tan, R. H. Zhang, H. K. Chen, Y. X. Zeng, and W. Huang.** 2005. Adenoviral expression of a truncated S1 subunit of SARS-CoV spike protein results in specific humoral immune responses against SARS-CoV in rats. Virus Res **112:**24-31.

129. **MacDonald, A. S., and R. M. Maizels.** 2008. Alarming dendritic cells for Th2 induction. J Exp Med **205:**13-7.

130. **MacDonald, G. H., and R. E. Johnston.** 2000. Role of dendritic cell targeting in Venezuelan equine encephalitis virus pathogenesis. J Virol **74:**914-22.

131. **Maletto, B. A., A. S. Ropolo, M. V. Liscovsky, D. O. Alignani, M. Glocker, and M. C. Pistoresi-Palencia.** 2005. CpG oligodeoxinucleotides functions as an effective adjuvant in aged BALB/c mice. Clin Immunol **117:**251-61.

132. **Marasco, W. A., and J. Sui.** 2007. The growth and potential of human antiviral monoclonal antibody therapeutics. Nat Biotechnol **25:**1421-34.

133. **Marra, M. A., S. J. Jones, C. R. Astell, R. A. Holt, A. Brooks-Wilson, Y. S. Butterfield, J. Khattra, J. K. Asano, S. A. Barber, S. Y. Chan, A. Cloutier, S. M. Coughlin, D. Freeman, N. Girn, O. L. Griffith, S. R. Leach, M. Mayo, H. McDonald, S. B. Montgomery, P. K. Pandoh, A. S. Petrescu, A. G. Robertson, J. E. Schein, A. Siddiqui, D. E. Smailus, J. M. Stott, G. S. Yang, F. Plummer, A. Andonov, H. Artsob, N. Bastien, K. Bernard, T. F. Booth, D. Bowness, M. Czub, M. Drebot, L. Fernando, R. Flick, M. Garbutt, M. Gray, A. Grolla, S. Jones, H. Feldmann, A. Meyers, A. Kabani, Y. Li, S. Normand, U. Stroher, G. A. Tipples, S. Tyler, R. Vogrig, D. Ward, B. Watson, R. C. Brunham, M. Krajden, M. Petric, D. M. Skowronski, C. Upton, and R. L. Roper.** 2003. The Genome sequence of the SARS-associated coronavirus. Science **300:**1399-404.

134. **Mayer, A. K., M. Muehmer, J. Mages, K. Gueinzius, C. Hess, K. Heeg, R. Bals, R. Lang, and A. H. Dalpke.** 2007. Differential recognition of TLR-dependent microbial ligands in human bronchial epithelial cells. J Immunol **178:**3134-42.

135. **McAllister-Lucas, L. M., J. Ruland, K. Siu, X. Jin, S. Gu, D. S. Kim, P. Kuffa, D. Kohrt, T. W. Mak, G. Nunez, and P. C. Lucas.** 2007. CARMA3/Bcl10/MALT1-dependent NF-kappaB activation mediates angiotensin II-responsive inflammatory signaling in nonimmune cells. Proc Natl Acad Sci U S A **104:**139-44.

136. **McElhaney, J. E., J. W. Hooton, N. Hooton, and R. C. Bleackley.** 2005. Comparison of single versus booster dose of influenza vaccination on humoral and cellular immune responses in older adults. Vaccine **23:**3294-300.

137. **McRoy, W. C., and R. S. Baric.** 2007. Amino Acid Substitutions in the S2 Subunit of Mouse Hepatitis Virus Variant V51 Encode Determinants of Host Range Expansion. J Virol.

138. **Monto, A. S., and R. J. Whitley.** 2008. Seasonal and Pandemic Influenza: A 2007 Update on Challenges and Solutions. CID **46:**1024-31.

139. **Morens, D. M., G. K. Folkers, and A. S. Fauci.** 2004. The challenge of emerging and re-emerging infectious diseases. Nature **430:**242-9.

140. **Morrison, T. E., A. C. Whitmore, R. S. Shabman, B. A. Lidbury, S. Mahalingam, and M. T. Heise.** 2006. Characterization of Ross River virus tropism and virus-induced inflammation in a mouse model of viral arthritis and myositis. J Virol **80:**737-49.

141. **Muller, M. A., J. T. Paweska, P. A. Leman, C. Drosten, K. Grywna, A. Kemp, L. Braack, K. Sonnenberg, M. Niedrig, and R. Swanepoel.** 2007. Coronavirus antibodies in African bat species. Emerg Infect Dis **13:**1367-70.

142. **Murray, K., S. Baraniuk, M. Resnick, R. Arafat, C. Kilborn, K. Cain, R. Shallenberger, T. L. York, D. Martinez, J. S. Hellums, D. Hellums, M. Malkoff, N. Elgawley, W. McNeely, S. A. Khuwaja, and R. B. Tesh.** 2006. Risk factors for encephalitis and death from West Nile virus infection. Epidemiol Infect **134:**1325-32.

143. **Nguyen, D. C., T. M. Uyeki, S. Jadhao, T. Maines, M. Shaw, Y. Matsuoka, C. Smith, T. Rowe, X. Lu, H. Hall, X. Xu, A. Balish, A. Klimov, T. M. Tumpey, D. E. Swayne, L. P. Huynh, H. K. Nghiem, H. H. Nguyen, L. T. Hoang, N. J. Cox, and J. M. Katz.** 2005. Isolation and characterization of avian influenza viruses, including highly pathogenic H5N1, from poultry in live bird markets in Hanoi, Vietnam, in 2001. J Virol **79:**4201-12.

144. **Nicholls, J. M., J. Butany, L. L. Poon, K. H. Chan, S. L. Beh, S. Poutanen, J. S. Peiris, and M. Wong.** 2006. Time course and cellular localization of SARS-CoV nucleoprotein and RNA in lungs from fatal cases of SARS. PLoS Med **3:**e27.

145. **Nicholls, M. G., A. M. Richards, and M. Agarwal.** 1998. The importance of the renin-angiotensin system in cardiovascular disease. J Hum Hypertens **12:**295-9.

146. **Normile, D.** 2004. Infectious diseases. Mounting lab accidents raise SARS fears. Science **304:**659-61.

147. **O'Neill, L. A., and A. G. Bowie.** 2007. The family of five: TIR-domain-containing adaptors in Toll-like receptor signalling. Nat Rev Immunol **7:**353-64.

148. **Osterlund, P. I., T. E. Pietila, V. Veckman, S. V. Kotenko, and I. Julkunen.** 2007. IFN regulatory factor family members differentially regulate the expression of type III IFN (IFN-lambda) genes. J Immunol **179:**3434-42.

149. **Page, R. D.** 1996. TreeView: an application to display phylogenetic trees on personal computers. Comput Appl Biosci **12:**357-8.

150. **Parrish, C. R., and Y. Kawaoka.** 2005. The origins of new pandemic viruses: the acquisition of new host ranges by canine parvovirus and influenza A viruses. Annu Rev Microbiol **59:**553-86.

151. **Pawelec, G., and A. Larbi.** 2008. Immunity and ageing in man: Annual review 2006/2007. Exp Gerontol **43:**34-8.

152. **Peiris, J. S., C. M. Chu, V. C. Cheng, K. S. Chan, I. F. Hung, L. L. Poon, K. I. Law, B. S. Tang, T. Y. Hon, C. S. Chan, K. H. Chan, J. S. Ng, B. J. Zheng, W. L. Ng, R. W. Lai, Y. Guan, and K. Y. Yuen.** 2003. Clinical progression and viral load in a community outbreak of coronavirus-associated SARS pneumonia: a prospective study. Lancet **361:**1767-72.

153. **Peiris, J. S., K. Y. Yuen, A. D. Osterhaus, and K. Stohr.** 2003. The severe acute respiratory syndrome. N Engl J Med **349:**2431-41.

154. **Pekosz, A., S. R. Schaecher, M. S. Diamond, D. H. Fremont, A. C. Sims, and R. S. Baric.** 2006. Structure, expression, and intracellular localization of the SARS-CoV accessory proteins 7a and 7b. Adv Exp Med Biol **581:**115-20.

155. **Phipps, S., C. E. Lam, S. Mahalingam, M. Newhouse, R. Ramirez, H. F. Rosenberg, P. S. Foster, and K. I. Matthaei.** 2007. Eosinophils contribute to innate antiviral immunity and promote clearance of respiratory syncytial virus. Blood **110:**1578-86.

156. **Pickles, R. J., D. McCarty, H. Matsui, P. J. Hart, S. H. Randell, and R. C. Boucher.** 1998. Limited entry of adenovirus vectors into well-differentiated airway epithelium is responsible for inefficient gene transfer. J Virol **72:**6014-23.

157. **Plotkin, S. A.** 1999. Vaccination against the major infectious diseases. C R Acad Sci III **322:**943-51.

158. **Polack, F. P., P. G. Auwaerter, S. H. Lee, H. C. Nousari, A. Valsamakis, K. M. Leiferman, A. Diwan, R. J. Adams, and D. E. Griffin.** 1999. Production of atypical measles in rhesus macaques: evidence for disease mediated by immune complex formation and eosinophils in the presence of fusion-inhibiting antibody. Nat Med **5:**629-34.

159. **Poon, L. L., D. K. Chu, K. H. Chan, O. K. Wong, T. M. Ellis, Y. H. Leung, S. K. Lau, P. C. Woo, K. Y. Suen, K. Y. Yuen, Y. Guan, and J. S. Peiris.** 2005. Identification of a novel coronavirus in bats. J Virol **79:**2001-9.

160. **Pulendran, B., and R. Ahmed.** 2006. Translating innate immunity into immunological memory: implications for vaccine development. Cell **124:**849-63.

161. **Pyrc, K., B. Berkhout, and L. van der Hoek.** 2006. The novel human coronaviruses NL63 and HKU1. J Virol.

162. **Pyrc, K., R. Dijkman, L. Deng, M. F. Jebbink, H. A. Ross, B. Berkhout, and L. van der Hoek.** 2006. Mosaic structure of human coronavirus NL63, one thousand years of evolution. J Mol Biol **364:**964-73.

163. **Qin, E., H. Shi, L. Tang, C. Wang, G. Chang, Z. Ding, K. Zhao, J. Wang, Z. Chen, M. Yu, B. Si, J. Liu, D. Wu, X. Cheng, B. Yang, W. Peng, Q. Meng, B. Liu, W. Han, X. Yin, H. Duan, D. Zhan, L. Tian, S. Li, J. Wu, G. Tan, Y. Li, Y. Li, Y. Liu, H. Liu, F. Lv, Y. Zhang, X. Kong, B. Fan, T. Jiang, S. Xu, X. Wang, C. Li, X. Wu, Y. Deng, M. Zhao, and Q. Zhu.** 2006. Immunogenicity and protective efficacy in monkeys of purified inactivated Vero-cell SARS vaccine. Vaccine **24:**1028-34.

164. **Ramu, C.** 2003. SIRW: A web server for the Simple Indexing and Retrieval System that combines sequence motif searches with keyword searches. Nucleic Acids Res **31:**3771-4.

165. **Randolph, G. J., C. Jakubzick, and C. Qu.** 2008. Antigen presentation by monocytes and monocyte-derived cells. Curr Opin Immunol **20:**52-60.

166. **Reghunathan, R., M. Jayapal, L. Y. Hsu, H. H. Chng, D. Tai, B. P. Leung, and A. J. Melendez.** 2005. Expression profile of immune response genes in patients with Severe Acute Respiratory Syndrome. BMC Immunol **6:**2.

167. **Roberts, A., D. Deming, C. D. Paddock, A. Cheng, B. Yount, L. Vogel, B. D. Herman, T. Sheahan, M. Heise, G. L. Genrich, S. R. Zaki, R. Baric, and K. Subbarao.** 2007. A mouse-adapted SARS-coronavirus causes disease and mortality in BALB/c mice. PLoS Pathog **3:**e5.

168. **Roberts, A., C. Paddock, L. Vogel, E. Butler, S. Zaki, and K. Subbarao.** 2005. Aged BALB/c mice as a model for increased severity of severe acute respiratory syndrome in elderly humans. J Virol **79:**5833-8.

169. **Roberts, A., and K. Subbarao.** 2006. Animal models for SARS. Adv Exp Med Biol **581:**463-71.

170. **Roberts, A., J. Wood, K. Subbarao, M. Ferguson, D. Wood, and T. Cherian.** 2006. Animal models and antibody assays for evaluating candidate SARS vaccines: summary of a technical meeting 25-26 August 2005, London, UK. Vaccine **24:**7056-65.

171. **Rockx, B., D. Corti, E. Donaldson, T. Sheahan, K. Stadler, A. Lanzavecchia, and R. Baric.** 2008. Structural Basis for Potent Cross-Neutralizing Human

Monoclonal Antibody Protection Against Lethal Human and Zoonotic SARS-CoV Challenge. J Virol.

172. **Rockx, B., T. Sheahan, E. Donaldson, J. Harkema, A. Sims, M. Heise, R. Pickles, M. Cameron, D. Kelvin, and R. Baric.** 2007. Synthetic reconstruction of zoonotic and early human severe acute respiratory syndrome coronavirus isolates that produce fatal disease in aged mice. J Virol **81:**7410-23.

173. **Rota, P. A., M. S. Oberste, S. S. Monroe, W. A. Nix, R. Campagnoli, J. P. Icenogle, S. Penaranda, B. Bankamp, K. Maher, M. H. Chen, S. Tong, A. Tamin, L. Lowe, M. Frace, J. L. DeRisi, Q. Chen, D. Wang, D. D. Erdman, T. C. Peret, C. Burns, T. G. Ksiazek, P. E. Rollin, A. Sanchez, S. Liffick, B. Holloway, J. Limor, K. McCaustland, M. Olsen-Rasmussen, R. Fouchier, S. Gunther, A. D. Osterhaus, C. Drosten, M. A. Pallansch, L. J. Anderson, and W. J. Bellini.** 2003. Characterization of a novel coronavirus associated with severe acute respiratory syndrome. Science **300:**1394-9.

174. **Rudd, B. D., M. A. Schaller, J. J. Smit, S. L. Kunkel, R. Neupane, L. Kelley, A. A. Berlin, and N. W. Lukacs.** 2007. MyD88-mediated instructive signals in dendritic cells regulate pulmonary immune responses during respiratory virus infection. J Immunol **178:**5820-7.

175. **Sansonetti, P. J.** 2006. The innate signaling of dangers and the dangers of innate signaling. Nat Immunol **7:**1237-42.

176. **Savina, A., and S. Amigorena.** 2007. Phagocytosis and antigen presentation in dendritic cells. Immunol Rev **219:**143-56.

177. **Sawicki, S. G., D. L. Sawicki, and S. G. Siddell.** 2007. A contemporary view of coronavirus transcription. J Virol **81:**20-9.

178. **Scanga, C. A., J. Aliberti, D. Jankovic, F. Tilloy, S. Bennouna, E. Y. Denkers, R. Medzhitov, and A. Sher.** 2002. Cutting edge: MyD88 is required for resistance to Toxoplasma gondii infection and regulates parasite-induced IL-12 production by dendritic cells. J Immunol **168:**5997-6001.

179. **Sheahan, T., D. Deming, E. Donaldson, R. Pickles, and R. Baric.** 2006. Resurrection of an "extinct" SARS-CoV isolate GD03 from late 2003. Adv Exp Med Biol **581:**547-50.

180. **Sheahan, T., B. Rockx, E. Donaldson, A. Sims, R. Pickles, D. Corti, and R. Baric.** 2007. Mechanisms of Zoonotic SARS-CoV Host Range Expansion in Human Airway Epithelium. J Virol.

181. **Shen, S., P. S. Lin, Y. C. Chao, A. Zhang, X. Yang, S. G. Lim, W. Hong, and Y. J. Tan.** 2005. The severe acute respiratory syndrome coronavirus 3a is a novel structural protein. Biochem Biophys Res Commun **330:**286-92.

182. **Shrestha, B., and M. S. Diamond.** 2004. Role of CD8+ T cells in control of West Nile virus infection. J Virol **78:**8312-21.

183. **Siegal, F. P., N. Kadowaki, M. Shodell, P. A. Fitzgerald-Bocarsly, K. Shah, S. Ho, S. Antonenko, and Y. J. Liu.** 1999. The nature of the principal type 1 interferon-producing cells in human blood. Science **284:**1835-7.

184. **Simmons, G., D. N. Gosalia, A. J. Rennekamp, J. D. Reeves, S. L. Diamond, and P. Bates.** 2005. Inhibitors of cathepsin L prevent severe acute respiratory syndrome coronavirus entry. Proc Natl Acad Sci U S A **102:**11876-81.

185. **Sims, A. C., R. S. Baric, B. Yount, S. E. Burkett, P. L. Collins, and R. J. Pickles.** 2005. Severe acute respiratory syndrome coronavirus infection of human ciliated airway epithelia: role of ciliated cells in viral spread in the conducting airways of the lungs. J Virol **79:**15511-24.

186. **Smith, H. O., C. A. Hutchison, 3rd, C. Pfannkoch, and J. C. Venter.** 2003. Generating a synthetic genome by whole genome assembly: phiX174 bacteriophage from synthetic oligonucleotides. Proc Natl Acad Sci U S A **100:**15440-5.

187. **Smith, R. D.** 2006. Responding to global infectious disease outbreaks: lessons from SARS on the role of risk perception, communication and management. Soc Sci Med **63:**3113-23.

188. **Snijder, E. J., P. J. Bredenbeek, J. C. Dobbe, V. Thiel, J. Ziebuhr, L. L. Poon, Y. Guan, M. Rozanov, W. J. Spaan, and A. E. Gorbalenya.** 2003. Unique and conserved features of genome and proteome of SARS-coronavirus, an early split-off from the coronavirus group 2 lineage. J Mol Biol **331:**991-1004.

189. **Song, H. D., C. C. Tu, G. W. Zhang, S. Y. Wang, K. Zheng, L. C. Lei, Q. X. Chen, Y. W. Gao, H. Q. Zhou, H. Xiang, H. J. Zheng, S. W. Chern, F. Cheng, C. M. Pan, H. Xuan, S. J. Chen, H. M. Luo, D. H. Zhou, Y. F. Liu, J. F. He, P. Z. Qin, L. H. Li, Y. Q. Ren, W. J. Liang, Y. D. Yu, L. Anderson, M. Wang, R. H. Xu, X. W. Wu, H. Y. Zheng, J. D. Chen, G. Liang, Y. Gao, M. Liao, L. Fang, L. Y. Jiang, H. Li, F. Chen, B. Di, L. J. He, J. Y. Lin, S. Tong, X. Kong, L. Du, P. Hao, H. Tang, A. Bernini, X. J. Yu, O. Spiga, Z. M. Guo, H. Y. Pan, W. Z. He, J. C. Manuguerra, A. Fontanet, A. Danchin, N. Niccolai, Y. X. Li, C. I. Wu, and G. P. Zhao.** 2005. Cross-host evolution of severe acute respiratory syndrome coronavirus in palm civet and human. Proc Natl Acad Sci U S A **102:**2430-5.

190. **Spruth, M., O. Kistner, H. Savidis-Dacho, E. Hitter, B. Crowe, M. Gerencer, P. Bruhl, L. Grillberger, M. Reiter, C. Tauer, W. Mundt, and P. N. Barrett.** 2006. A double-inactivated whole virus candidate SARS coronavirus vaccine stimulates neutralising and protective antibody responses. Vaccine **24:**652-61.

191. **Stevens, J., O. Blixt, T. M. Tumpey, J. K. Taubenberger, J. C. Paulson, and I. A. Wilson.** 2006. Structure and receptor specificity of the hemagglutinin from an H5N1 influenza virus. Science **312:**404-10.

192. **Stockman, L. J., R. Bellamy, and P. Garner.** 2006. SARS: systematic review of treatment effects. PLoS Med **3:**e343.

193. **Storz, J., X. Lin, C. W. Purdy, V. N. Chouljenko, K. G. Kousoulas, F. M. Enright, W. C. Gilmore, R. E. Briggs, and R. W. Loan.** 2000. Coronavirus and Pasteurella infections in bovine shipping fever pneumonia and Evans' criteria for causation. J Clin Microbiol **38:**3291-8.

194. **Subbarao, K., J. McAuliffe, L. Vogel, G. Fahle, S. Fischer, K. Tatti, M. Packard, W. J. Shieh, S. Zaki, and B. Murphy.** 2004. Prior infection and passive transfer of neutralizing antibody prevent replication of severe acute respiratory syndrome coronavirus in the respiratory tract of mice. J Virol **78:**3572-7.

195. **Subbarao, K., and A. Roberts.** 2006. Is there an ideal animal model for SARS? Trends Microbiol **14:**299-303.

196. **Sui, J., W. Li, A. Murakami, A. Tamin, L. J. Matthews, S. K. Wong, M. J. Moore, A. S. Tallarico, M. Olurinde, H. Choe, L. J. Anderson, W. J. Bellini, M. Farzan, and W. A. Marasco.** 2004. Potent neutralization of severe acute respiratory syndrome (SARS) coronavirus by a human mAb to S1 protein that blocks receptor association. Proc Natl Acad Sci U S A **101:**2536-41.

197. **Sui, J., W. Li, A. Roberts, L. J. Matthews, A. Murakami, L. Vogel, S. K. Wong, K. Subbarao, M. Farzan, and W. A. Marasco.** 2005. Evaluation of human monoclonal antibody 80R for immunoprophylaxis of severe acute respiratory syndrome by an animal study, epitope mapping, and analysis of spike variants. J Virol **79:**5900-6.

198. **Takeuchi, O., K. Hoshino, and S. Akira.** 2000. Cutting edge: TLR2-deficient and MyD88-deficient mice are highly susceptible to Staphylococcus aureus infection. J Immunol **165:**5392-6.

199. **Tang, L., Q. Zhu, E. Qin, M. Yu, Z. Ding, H. Shi, X. Cheng, C. Wang, G. Chang, Q. Zhu, F. Fang, H. Chang, S. Li, X. Zhang, X. Chen, J. Yu, J. Wang, and Z. Chen.** 2004. Inactivated SARS-CoV vaccine prepared from whole virus induces a high level of neutralizing antibodies in BALB/c mice. DNA Cell Biol **23:**391-4.

200. **ter Meulen, J., E. N. van den Brink, L. L. Poon, W. E. Marissen, C. S. Leung, F. Cox, C. Y. Cheung, A. Q. Bakker, J. A. Bogaards, E. van Deventer, W. Preiser, H. W. Doerr, V. T. Chow, J. de Kruif, J. S. Peiris, and J. Goudsmit.** 2006. Human monoclonal antibody combination against SARS coronavirus: synergy and coverage of escape mutants. PLoS Med **3:**e237.

201. **Thompson, J. M., A. C. Whitmore, J. L. Konopka, M. L. Collier, E. M. Richmond, N. L. Davis, H. F. Staats, and R. E. Johnston.** 2006. Mucosal and systemic adjuvant activity of alphavirus replicon particles. Proc Natl Acad Sci U S A **103:**3722-7.

202. **Thompson, W. W., D. K. Shay, E. Weintraub, L. Brammer, N. Cox, L. J. Anderson, and K. Fukuda.** 2003. Mortality associated with influenza and respiratory syncytial virus in the United States. Jama **289:**179-86.

203. **Tipnis, S. R., N. M. Hooper, R. Hyde, E. Karran, G. Christie, and A. J. Turner.** 2000. A human homolog of angiotensin-converting enzyme. Cloning and functional expression as a captopril-insensitive carboxypeptidase. J Biol Chem **275:**33238-43.

204. **Towner, J. S., X. Pourrut, C. G. Albarino, C. N. Nkogue, B. H. Bird, G. Grard, T. G. Ksiazek, J. P. Gonzalez, S. T. Nichol, and E. M. Leroy.** 2007. Marburg virus infection detected in a common african bat. PLoS ONE **2:**e764.

205. **Traggiai, E., S. Becker, K. Subbarao, L. Kolesnikova, Y. Uematsu, M. R. Gismondo, B. R. Murphy, R. Rappuoli, and A. Lanzavecchia.** 2004. An efficient method to make human monoclonal antibodies from memory B cells: potent neutralization of SARS coronavirus. Nat Med **10:**871-5.

206. **Tse, G. M., K. F. To, P. K. Chan, A. W. Lo, K. C. Ng, A. Wu, N. Lee, H. C. Wong, S. M. Mak, K. F. Chan, D. S. Hui, J. J. Sung, and H. K. Ng.** 2004. Pulmonary pathological features in coronavirus associated severe acute respiratory syndrome (SARS). J Clin Pathol **57:**260-5.

207. **Tseng, C. T., L. A. Perrone, H. Zhu, S. Makino, and C. J. Peters.** 2005. Severe acute respiratory syndrome and the innate immune responses: modulation of effector cell function without productive infection. J Immunol **174:**7977-85.

208. **Tsunetsugu-Yokota, Y., M. Ato, Y. Takahashi, S. Hashimoto, T. Kaji, M. Kuraoka, K. Yamamoto, Y. Y. Mitsuki, T. Yamamoto, M. Oshima, K. Ohnishi, and T. Takemori.** 2007. Formalin-treated UV-inactivated SARS coronavirus vaccine retains its immunogenicity and promotes Th2-type immune responses. Jpn J Infect Dis **60:**106-12.

209. **Tumpey, T. M., C. F. Basler, P. V. Aguilar, H. Zeng, A. Solorzano, D. E. Swayne, N. J. Cox, J. M. Katz, J. K. Taubenberger, P. Palese, and A. Garcia-Sastre.** 2005. Characterization of the reconstructed 1918 Spanish influenza pandemic virus. Science **310:**77-80.

210. **Turner, A. J., and N. M. Hooper.** 2002. The angiotensin-converting enzyme gene family: genomics and pharmacology. Trends Pharmacol Sci **23:**177-83.

211. **Uehara, A., Y. Fujimoto, K. Fukase, and H. Takada.** 2007. Various human epithelial cells express functional Toll-like receptors, NOD1 and NOD2 to

produce anti-microbial peptides, but not proinflammatory cytokines. Mol Immunol **44:**3100-11.

212. **Vallejo, A. N.** 2005. CD28 extinction in human T cells: altered functions and the program of T-cell senescence. Immunol Rev **205:**158-69.

213. **van der Hoek, L., K. Pyrc, M. F. Jebbink, W. Vermeulen-Oost, R. J. Berkhout, K. C. Wolthers, P. M. Wertheim-van Dillen, J. Kaandorp, J. Spaargaren, and B. Berkhout.** 2004. Identification of a new human coronavirus. Nat Med **10:**368-73.

214. **Varga, S. M., X. Wang, R. M. Welsh, and T. J. Braciale.** 2001. Immunopathology in RSV infection is mediated by a discrete oligoclonal subset of antigen-specific CD4(+) T cells. Immunity **15:**637-46.

215. **Vasto, S., M. Malavolta, and G. Pawelec.** 2006. Age and immunity. Immun Ageing **3:**2.

216. **Vaughn, E. M., P. G. Halbur, and P. S. Paul.** 1995. Sequence comparison of porcine respiratory coronavirus isolates reveals heterogeneity in the S, 3, and 3-1 genes. J Virol **69:**3176-84.

217. **Vennema, H., R. J. de Groot, D. A. Harbour, M. Dalderup, T. Gruffydd-Jones, M. C. Horzinek, and W. J. Spaan.** 1990. Early death after feline infectious peritonitis virus challenge due to recombinant vaccinia virus immunization. J Virol **64:**1407-9.

218. **Vickers, C., P. Hales, V. Kaushik, L. Dick, J. Gavin, J. Tang, K. Godbout, T. Parsons, E. Baronas, F. Hsieh, S. Acton, M. Patane, A. Nichols, and P. Tummino.** 2002. Hydrolysis of biological peptides by human angiotensin-converting enzyme-related carboxypeptidase. J Biol Chem **277:**14838-43.

219. **Vijgen, L., E. Keyaerts, E. Moes, I. Thoelen, E. Wollants, P. Lemey, A. M. Vandamme, and M. Van Ranst.** 2005. Complete genomic sequence of human coronavirus OC43: molecular clock analysis suggests a relatively recent zoonotic coronavirus transmission event. J Virol **79:**1595-604.

220. **Vogel, L. N., A. Roberts, C. D. Paddock, G. L. Genrich, E. W. Lamirande, S. U. Kapadia, J. K. Rose, S. R. Zaki, and K. Subbarao.** 2007. Utility of the aged BALB/c mouse model to demonstrate prevention and control strategies for severe acute respiratory syndrome coronavirus (SARS-CoV). Vaccine **25:**2173-9.

221. **Wallinga, J., and P. Teunis.** 2004. Different epidemic curves for severe acute respiratory syndrome reveal similar impacts of control measures. Am J Epidemiol **160:**509-16.

222. **Walsh, P. D., R. Biek, and L. A. Real.** 2005. Wave-like spread of Ebola Zaire. PLoS Biol **3:**e371.

223. **Wang, C. Q., K. B. Udupa, H. Xiao, and D. A. Lipschitz.** 1995. Effect of age on marrow macrophage number and function. Aging (Milano) **7:**379-84.

224. **Wang, Z., Z. Yuan, M. Matsumoto, U. R. Hengge, and Y. F. Chang.** 2005. Immune responses with DNA vaccines encoded different gene fragments of severe acute respiratory syndrome coronavirus in BALB/c mice. Biochem Biophys Res Commun **327:**130-5.

225. **Werle, B., C. Fromantin, A. Alexandre, E. Kohli, and P. Pothier.** 1999. Dose-dependent effects of IL-12 treatment to immune response induced after immunization with a recombinant respiratory syncytial virus (RSV) fusion protein fragment. Vaccine **17:**2983-90.

226. **WHO** 2008, posting date. Global Polio Eradication Initiative. [Online.]

227. **WHO.** 2008. Measles Fact Sheet.

228. **WHO** 2008, posting date. Polio Fact Sheet. [Online.]

229. **WHO.** 2002. Revised Global Burden of Disease (GBD) 2002 Estimates.

230. **Wolfe, N. D., C. P. Dunavan, and J. Diamond.** 2007. Origins of major human infectious diseases. Nature **447:**279-83.

231. **Wolkers, M. C., N. Brouwenstijn, A. H. Bakker, M. Toebes, and T. N. Schumacher.** 2004. Antigen bias in T cell cross-priming. Science **304:**1314-7.

232. **Wong, C. K., C. W. Lam, A. K. Wu, W. K. Ip, N. L. Lee, I. H. Chan, L. C. Lit, D. S. Hui, M. H. Chan, S. S. Chung, and J. J. Sung.** 2004. Plasma inflammatory cytokines and chemokines in severe acute respiratory syndrome. Clin Exp Immunol **136:**95-103.

233. **Woo, P. C., S. K. Lau, C. M. Chu, K. H. Chan, H. W. Tsoi, Y. Huang, B. H. Wong, R. W. Poon, J. J. Cai, W. K. Luk, L. L. Poon, S. S. Wong, Y. Guan, J. S. Peiris, and K. Y. Yuen.** 2005. Characterization and complete genome sequence of a novel coronavirus, coronavirus HKU1, from patients with pneumonia. J Virol **79:**884-95.

234. **Woo, P. C., S. K. Lau, K. S. Li, R. W. Poon, B. H. Wong, H. W. Tsoi, B. C. Yip, Y. Huang, K. H. Chan, and K. Y. Yuen.** 2006. Molecular diversity of coronaviruses in bats. Virology **351:**180-7.

235. **Woo, P. C., S. K. Lau, C. C. Yip, Y. Huang, H. W. Tsoi, K. H. Chan, and K. Y. Yuen.** 2006. Comparative analysis of 22 coronavirus HKU1 genomes reveals a novel genotype and evidence of natural recombination in coronavirus HKU1. J Virol **80:**7136-45.

236. **Woo, P. C., S. K. Lau, and K. Y. Yuen.** 2006. Infectious diseases emerging from Chinese wet-markets: zoonotic origins of severe respiratory viral infections. Curr Opin Infect Dis **19:**401-7.

237. **Woo, P. C., M. Wang, S. K. Lau, H. Xu, R. W. Poon, R. Guo, B. H. Wong, K. Gao, H. W. Tsoi, Y. Huang, K. S. Li, C. S. Lam, K. H. Chan, B. J. Zheng, and K. Y. Yuen.** 2006. Comparative analysis of 12 genomes of three novel group 2c and group 2d coronaviruses reveals unique group and subgroup features. J Virol.

238. **Wu, D., C. Tu, C. Xin, H. Xuan, Q. Meng, Y. Liu, Y. Yu, Y. Guan, Y. Jiang, X. Yin, G. Crameri, M. Wang, C. Li, S. Liu, M. Liao, L. Feng, H. Xiang, J. Sun, J. Chen, Y. Sun, S. Gu, N. Liu, D. Fu, B. T. Eaton, L. F. Wang, and X. Kong.** 2005. Civets are equally susceptible to experimental infection by two different severe acute respiratory syndrome coronavirus isolates. J Virol **79:**2620-5.

239. **Xiao, X., S. Chakraborti, A. S. Dimitrov, K. Gramatikoff, and D. S. Dimitrov.** 2003. The SARS-CoV S glycoprotein: expression and functional characterization. Biochem Biophys Res Commun **312:**1159-64.

240. **Xu, Y., Z. Lou, Y. Liu, H. Pang, P. Tien, G. F. Gao, and Z. Rao.** 2004. Crystal structure of severe acute respiratory syndrome coronavirus spike protein fusion core. J Biol Chem **279:**49414-9.

241. **Yang, Z. Y., W. P. Kong, Y. Huang, A. Roberts, B. R. Murphy, K. Subbarao, and G. J. Nabel.** 2004. A DNA vaccine induces SARS coronavirus neutralization and protective immunity in mice. Nature **428:**561-4.

242. **Yang, Z. Y., H. C. Werner, W. P. Kong, K. Leung, E. Traggiai, A. Lanzavecchia, and G. J. Nabel.** 2005. Evasion of antibody neutralization in emerging severe acute respiratory syndrome coronaviruses. Proc Natl Acad Sci U S A **102:**797-801.

243. **Yano, Y., M. Kaneniwa, M. Satomi, H. Oikawa, and S. S. Chen.** 2006. Occurrence and density of vibrio parahaemolyticus in live edible crustaceans from markets in China. J Food Prot **69:**2742-6.

244. **Yano, Y., M. Yokoyama, M. Satomi, H. Oikawa, and S. S. Chen.** 2004. Occurrence of Vibrio vulnificus in fish and shellfish available from markets in China. J Food Prot **67:**1617-23.

245. **Ye, J., B. Zhang, J. Xu, Q. Chang, M. A. McNutt, C. Korteweg, E. Gong, and J. Gu.** 2007. Molecular pathology in the lungs of severe acute respiratory syndrome patients. Am J Pathol **170:**538-45.

246. **Yi, G.** 2003. SARS coronavirus HC/SZ/61/03, complete genome.

247. **Yount, B., K. M. Curtis, E. A. Fritz, L. E. Hensley, P. B. Jahrling, E. Prentice, M. R. Denison, T. W. Geisbert, and R. S. Baric.** 2003. Reverse genetics with a full-length infectious cDNA of severe acute respiratory syndrome coronavirus. Proc Natl Acad Sci U S A **100:**12995-3000.

248. **Yount, B., R. S. Roberts, L. Lindesmith, and R. S. Baric.** 2006. Rewiring the severe acute respiratory syndrome coronavirus (SARS-CoV) transcription circuit: engineering a recombination-resistant genome. Proc Natl Acad Sci U S A **103:**12546-51.

249. **Yount, B., R. S. Roberts, A. C. Sims, D. Deming, M. B. Frieman, J. Sparks, M. R. Denison, N. Davis, and R. S. Baric.** 2005. Severe acute respiratory syndrome coronavirus group-specific open reading frames encode nonessential functions for replication in cell cultures and mice. J Virol **79:**14909-22.

250. **Yu, S., M. Qiu, Z. Chen, X. Ye, Y. Gao, A. Wei, X. Wang, L. Yang, J. Wang, J. Wen, Y. Song, D. Pei, E. Dai, Z. Guo, C. Cao, J. Wang, and R. Yang.** 2005. Retrospective serological investigation of severe acute respiratory syndrome coronavirus antibodies in recruits from mainland China. Clin Diagn Lab Immunol **12:**552-4.

251. **Zhang, C. H., J. H. Lu, Y. F. Wang, H. Y. Zheng, S. Xiong, M. Y. Zhang, X. J. Liu, J. X. Li, Z. Y. Wan, X. G. Yan, S. Y. Qi, Z. Cui, and B. Zhang.** 2005. Immune responses in Balb/c mice induced by a candidate SARS-CoV inactivated vaccine prepared from F69 strain. Vaccine **23:**3196-201.

252. **Zheng, B. J., K. H. Wong, J. Zhou, K. L. Wong, B. W. Young, L. W. Lu, and S. S. Lee.** 2004. SARS-related virus predating SARS outbreak, Hong Kong. Emerg Infect Dis **10:**176-8.

253. **Zhou, J., W. Wang, Q. Zhong, W. Hou, Z. Yang, S. Y. Xiao, R. Zhu, Z. Tang, Y. Wang, Q. Xian, H. Tang, and L. Wen.** 2005. Immunogenicity, safety, and protective efficacy of an inactivated SARS-associated coronavirus vaccine in rhesus monkeys. Vaccine **23:**3202-9.

254. **Zhou, L., B. Ni, D. Luo, G. Zhao, Z. Jia, L. Zhang, Z. Lin, L. Wang, S. Zhang, L. Xing, J. Li, Y. Liang, X. Shi, T. Zhao, L. Zhou, Y. Wu, and X. Wang.** 2007. Inhibition of infection caused by severe acute respiratory syndrome-associated coronavirus by equine neutralizing antibody in aged mice. Int Immunopharmacol **7:**392-400.

255. **Zhou, S., E. A. Kurt-Jones, K. A. Fitzgerald, J. P. Wang, A. M. Cerny, M. Chan, and R. W. Finberg.** 2007. Role of MyD88 in route-dependent susceptibility to vesicular stomatitis virus infection. J Immunol **178:**5173-81.

256. **Zhu, Z., S. Chakraborti, Y. He, A. Roberts, T. Sheahan, X. Xiao, L. E. Hensley, P. Prabakaran, B. Rockx, I. A. Sidorov, D. Corti, L. Vogel, Y. Feng, J. O. Kim, L. F. Wang, R. Baric, A. Lanzavecchia, K. M. Curtis, G. J. Nabel,**

K. Subbarao, S. Jiang, and D. S. Dimitrov. 2007. Potent cross-reactive neutralization of SARS coronavirus isolates by human monoclonal antibodies. Proc Natl Acad Sci U S A **104:**12123-8.

257. **Zust, R., L. Cervantes-Barragan, T. Kuri, G. Blakqori, F. Weber, B. Ludewig, and V. Thiel.** 2007. Coronavirus non-structural protein 1 is a major pathogenicity factor: implications for the rational design of coronavirus vaccines. PLoS Pathog **3:**e109.